

**High-Frequency Self-Modulation in
External-Cavity VCSELs**
(外部共振器 VCSEL の高速自己変調)

Tao Liu

劉 濤

September 2015

Graduate School of Materials Science

Nara Institute of Science and Technology

Contents

List of Abbreviations	iii
List of Symbols	iv
Chapter 1 Introduction	1
1.1 Backgrounds	1
1.2 Aim of this research	4
1.3 Thesis outline	5
1.4 References	6
Chapter 2 Pulse Generation by Polarization Self-Modulation	11
2.1 Introduction	11
2.2 Polarization self-modulation	11
2.2.1 Principle of polarization self-modulation	11
2.2.2 Polarization-rotated feedback scheme	13
2.2.3 Crossed-polarization reinjection scheme	15
2.3 Conclusion	19
2.4 References	20
Chapter 3 Pulse Generation in External-Cavity VCSEL with Planar Mirror	24
3.1 Introduction	24
3.2 Experimental setup	24
3.3 Experimental results	31
3.3.1 For longer external cavity	31
3.3.2 For medium length external cavity	36
3.3.3 For shorter external cavity	39
3.4 Relationship between EC length and modulation mechanism	42
3.5 Conclusion	44
3.6 References	44
Chapter 4 High-Frequency Self-Modulation in External-Cavity VCSEL with Concave Mirror and Semi-Spherical Mirror	46
4.1 Introduction	46

4.2	Experiment using concave mirror	47
4.2.1	20 mm radius concave mirror	47
4.2.2	5.08 mm radius concave mirror	51
4.3	Experiment using semi-spherical mirror	64
4.3.1	Fabrication of semi-spherical mirror	64
4.3.2	4 mm radius semi-spherical mirror	67
4.3.3	3 mm radius semi-spherical mirror	74
4.4	Conclusion	81
4.5	References	82
Chapter 5 Simulation of Pulse Generation using EC-VCSEL		83
5.1	Introduction	83
5.2	EC-VCSEL model	84
5.2.1	Model conception	84
5.2.2	Rate equations	86
5.3	Solitary VCSEL operation	92
5.4	EC-VCSEL operation	96
5.4.1	Effect of gain saturation coefficient of the VCSEL	96
5.4.2	Effect of optical feedback intensity	101
5.4.3	Effect of carrier pump rate	106
5.5	Comparison with experimental results	113
5.6	Conclusion	122
5.7	References	123
Chapter 6 Summary and Outlook		126
6.1	Summary	126
6.2	Outlook	128
6.3	References	132
Acknowledgment		133
List of Publications		135

List of Abbreviations

Abbreviation	Phrase
APD	Avalanche photodiode
BS	Beam splitter
CM	Concave partial reflection mirror
CW	Continuous wave
DBR	Distributed Bragg reflector
EC	External cavity
EC-VCSEL	External-cavity VCSEL
EEL	Edge emitting semiconductor laser
FFP	Far-field pattern
FR	Faraday rotator
FSR	Free spectral range
FWHM	Full width at half maximum
High f	High frequency modulation
HWP	Half-wave plate
ISO	Polarization-independent isolator
Low f	Low frequency modulation
MQW	Multiple quantum well
PBS	Polarization beam splitter
PD	Photodiode
PR	Partial reflector
PSF	Polarization-selective feedback
QWP	Quarter-wave plate
RF	Radio frequency
SNR	Signal to noise ratio
SOA	Semiconductor optical amplifier
VCSEL	Vertical-cavity surface-emitting laser
XPR	Crossed-polarization reinjection

List of Symbols

Symbol	Phrase
f	Frequency or repetition rate
f_r	Relaxation oscillation frequency
I_2/I_3	Intensity of peak 2/Intensity of peak 3
I_{th}	Lasing threshold current of VCSEL
L	Length of external cavity
r	Curvature radius of concave or semi-spherical mirror

Chapter 1 Introduction

1.1 Backgrounds

Lasers with multi-gigahertz repetition rates are key components of many applications. They are used in high-capacity telecommunication systems, photonic switching devices and optical interconnections. Applications of the future such as clocks for large scale integrated microprocessors, polarized electron beams for electron accelerators and high speed electro-optic sampling techniques will rely on multi-gigahertz pulse trains with short pulses, low timing jitter and low amplitude noise [1]. Thanks to the fast temporal resolution, ultrashort optical pulses can be used for time-resolved spectroscopy to analyze the dynamics of fast moving objects, for example, the relaxation processes of carriers in semiconductors, chemical reaction dynamics and electro-optical sampling of high-speed electronics [1]. Applications in the transmission and processing of optical signal in the optical communication network play an important role in the various application fields of optical pulses.

In the current optical communication networks, only the signal transmission is done optically. The rapid growth of internet traffic and the increasing demand for higher transmission capacity have called for the development of all-optical communication networks [2]-[4]. All-optical signal processing has been and is receiving more and more attention all over the world

because it can increase the capacity of the optical networks greatly in avoiding of the Optical-Electrical-Optical (E/O/E) conversion process, and it can also reduce the system power consumption to a great extent [5]. All-optical signal processing can be widely used in optical signal regeneration and switching in next generation optical networks, such as optical time division multiplexing, optical packet switching and so on. There are many different elemental functions in all-optical signal processing: all-optical wavelength conversion, all-optical sampling, all-optical logic operation, all-optical 3R regeneration, all-optical format conversion, and all-optical buffering [5]. All-optical signal regeneration is a key technology for future all-optical networking. “3R” regeneration, which performs the full functions of Reamplification, Reshaping, and Retiming, is particularly attractive, because it can improve signal quality in both the amplitude and time domains [6]. Researches using different devices have been carried out for the realization of all-optical signal processing. Semiconductor optical amplifiers (SOAs) [7]-[11] and vertical-cavity surface-emitting lasers (VCSELs) [12]-[15] are two typical examples. For the realization of all-optical communication system, all-optical pulse generation, which supplies the essential clock signal for signal processing, has attracted the interest of researchers.

VCSEL was invented by Prof. Kenichi Iga of Tokyo Institute of Technology in 1977 [16]. As one of the microchip lasers, VCSELs exhibit many advantages over the conventional edge-emitting semiconductor lasers (EELs), such as single longitudinal-mode operation, low

threshold current, circular output beam with narrow divergence, low cost and easy large-scale integration into two-dimensional arrays [17] [18]. With these advantages, VCSELs have been widely used in various applications including datacom, sensors, optical interconnects, spectroscopy, optical storages, printers, laser displays, laser radar, atomic clock, and optical signal processing [19].

Bistable laser diodes (BLDs) are expected to be the key components in future optical communication and switching systems because of their inherent advantages such as optical gain, low optical switching power, a high on-off ratio, and a large fanout [20]. A VCSEL is one of the major representatives of bistable lasers [21]. The polarization-bistable operation in a VCSEL is shown schematically in Fig. 1.1 [22]. The VCSEL with a square mesa structure exhibited polarization bistable switching between 0° and 90° polarization. The VCSEL initially oscillated with 0° linear polarization, but switched permanently to 90° linear polarization upon injection of a 90° polarized optical pulse. The polarization switch was reversible upon injection of a suitable 0° polarization pulse. All-optical signal processing, including format conversion [23], signal regeneration [24], and optical buffer memory [22], using the polarization bistable VCSELs have been experimentally demonstrated by our group.

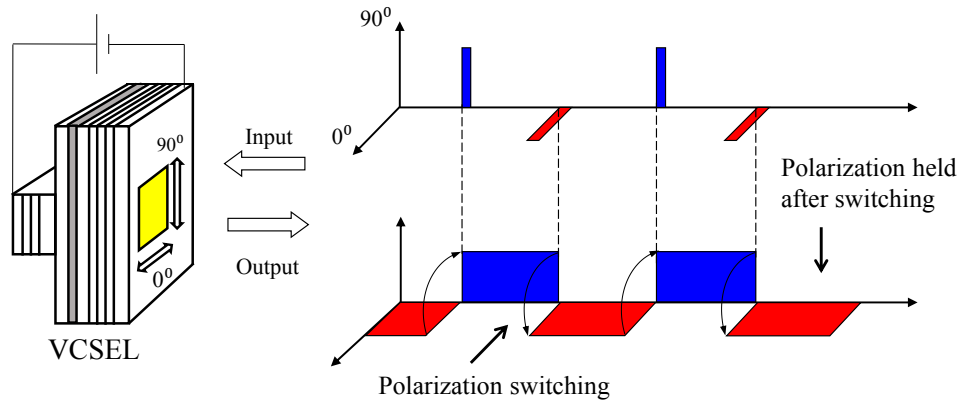


Fig. 1.1. Bistable polarization switching in a VCSEL.

In this research, polarization-rotated optical feedback is added to a polarization bistable VCSEL using an external cavity (EC). Self-modulation in the external-cavity VCSEL (EC-VCSEL) results in generation of fast and frequency-variable optical pulses, which are essential for the signal regeneration, a key-function for the whole communication system.

1.2 Aim of this research

This research aims at high-frequency optical pulse generation by self-modulation of EC-VCSEL, which has a quarter-wave plate in the EC. Firstly, we investigated the pulse generation at different frequencies by changing the EC length L . Then, to get higher frequency optical pulses, we shortened the L by using short-radius concave mirrors or semi-spherical mirrors as one end of the EC. This configuration does not need a collimation lens which limits L when planar mirror is used. The mechanism was found to have changed from polarization self-

modulation to the beat note between two EC modes with similar polarizations. Finally, simulation using two-mode rate equations was carried out to investigate the polarization self-modulation in the EC-VCSEL and gave a support to our experimental results.

1.3 Thesis outline

As shown in Fig. 1.2, this thesis consists of six chapters as follows: Chapter 1 introduces the general background and the aim of this research, and then the structure of this thesis. Chapter 2 gives a review of pulse generation by polarization self-modulation in EC laser diodes. Chapter 3 describes the results of pulse generation under different EC length using planar reflection mirrors for the EC. Chapter 4 describes the results of high-frequency self-modulation with new configurations using concave mirrors and semi-spherical mirrors for shortening the EC length. Chapter 5 presents a numerical study of the polarization self-modulation in EC-VCSEL using two-mode rate equations. We focus on the effects of the gain saturation coefficients of VCSEL, the intensity of the optical feedback, and the carrier pump rate on the polarization self-modulation in EC-VCSEL. We also compared these simulation results with those in the experiments. In Chapter 6, we conclude this research by summarizing its main results and providing an outlook to the future work.

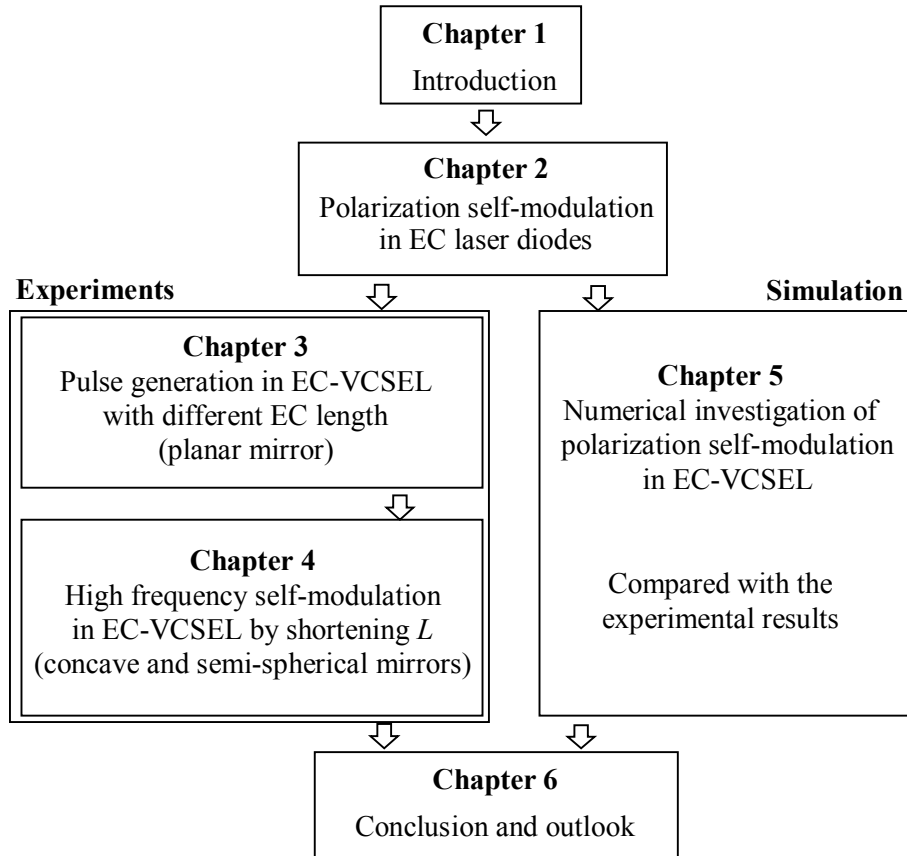


Fig. 1.2. Structure of this thesis.

1.4 References

- [1] U. Keller, "Recent developments in compact ultrafast lasers," *Nature*, vol. 424, no. 6950, pp. 831-838, 2003.
- [2] S. J. Ben Yoo, "Energy efficiency in the future internet: the role of optical packet switching and optical-label switching," *IEEE J. Selected Topics in Quantum Electronics*, vol. 17, no. 2, pp. 406-418, 2011.
- [3] L.-S. Yan, A. E. Willner, X.-X Wu, A.-L. Yi, A. Bogoni, Z.-Y Chen, and H.-Y. Jiang, "All-

- optical signal processing for ultrahigh speed optical systems and networks,” *IEEE J. Lightw. Technol.*, vol. 30, no. 24, pp. 3760-3770, 2012.
- [4] A. E. Willner, S. Khaleghi, M. R. Chitgarha, and O. F. Yilmaz, “All-optical signal processing,” *IEEE J. Lightw. Technol.*, vol. 32, no. 4, pp. 660-680, 2014.
- [5] X.-L. Zhang, X. Huang, J.-J. Dong, Y. Yu, J. Xu, and D.-X. Huang, “All-optical signal processing with semiconductor optical amplifiers and tunable Filters,” *Advances in lasers and Electro Optics*, Chap.16, pp. 337-368, 2010.
- [6] M. Funabashi, Z.-Q. Zhu, Z. Pan, L. Paraschis, and S. J. B. Yoo, “Optical clock recovery and 3R regeneration for 10-Gb/s NRZ signal to achieve 10000-hop cascability and 1000000-km Transmission,” *IEEE Photon. Technol. Lett.*, vol. 18, no. 20, pp. 2078-2080, 2006.
- [7] M. Sánchez, P.-Y. Wen, M. Gross, and S. Esener, “All-optical 2R regeneration using a non-linear vertical cavity semiconductor optical amplifier,” *Optics in Computing, OSA Digest*, vol. 90, pp. 78-81, 2003.
- [8] N. Pleros, K. Vysokinos, C. Bintjas, K. Yiannopoulos, K. Vlachos, H. Avramopoulos, and G. Guekos, “All-optical clock recovery from short asynchronous data packets at 10 Gb/s,” *IEEE Photon. Technol. Lett.*, vol. 15, no. 9, pp. 1291-1293, 2003.
- [9] Y. Liu, M.T. Hill, N. Calabretta, E. Tangdionga, R. Geldenhuys, S. Zhang, Z. Li, H. De Waardt, G.D. Khoe and H.J.S. Dorren, “All-optical signal processing for optical packet switching networks,” *Proc. of SPIE*, vol. 5907, 59070J, 2005.

- [10] Y. Liu, E. Tangdiongga, Z. Li, S. Zhang, M.T. Hill, J.H.C. van Zantvoort, F.M. Huijskens, H. de Waardt, M.K. Smit, A.M.J. Koonen, G.D. Khoe and H.J.S. Dorren, "Ultra-fast all-optical signal processing: towards optical packet switching," *Proc. of SPIE*, vol. 6353, 635312, 2006.
- [11] J. Leuthold, B. Mikkelsen, R. E. Behringer, G. Raybon, C. H. Joyner, and P. A. Besse, "Novel 3R regenerator based on semiconductor optical amplifier delayed-interference configuration," *IEEE Photon, Technol. Lett.*, vol. 13, no. 8, pp. 860-862, 2001.
- [12] S. Perrone, R. Vilaseca, and C. Masoller, "Stochastic logic gate that exploits noise and polarization bistability in an optically injected VCSEL," *Opt. Express*, vol. 20, no. 20, pp. 22692-22699, 2012.
- [13] C.-C Lin, H.-C Kuo, P.-C Peng, and G.-R Lin, "Chirp and error rate analyses of an optical-injection gain-switching VCSEL based all-optical NRZ-to-PRZ converter," *Opt. Express*, vol. 16, no. 7, pp. 4838-4847, 2008.
- [14] M. F. Salvide, C. Masoller, and M. S. Torre, "All-optical stochastic logic gate based on a VCSEL with tunable optical injection," *IEEE J. Quantum Electron.*, vol. 49, no. 10, pp. 886-893, 2013.
- [15] B. Webb, and A. Louri, "All-optical crossbar switch using wavelength division multiplexing and vertical-cavity surface-emitting lasers," *Appl. Opt.*, vol. 38, no. 29, pp. 6176-6183, 1999.

- [16] K. Iga, "Surface-emitting laser—its birth and generation of new optoelectronics field," *IEEE J. Sel. Topics Quantum Electron.*, vol. 6, no. 6, pp. 1201-1215, 2000.
- [17] J. Liu, Z.-M. Wu, and G.-Q. Xia, "Dual-channel chaos synchronization and communication based on unidirectionally coupled VCSELs with polarization-rotated optical feedback and polarization-rotated optical injection," *Opt. Express*, vol. 17, no. 15, pp. 12619-12626, 2009.
- [18] A. Scirè, J. Mulet, C. R. Mirasso, and M. S. Miguel, "Intensity and polarization self-pulsations in vertical-cavity surface-emitting lasers," *Opt. Lett.*, vol. 27, no. 6, pp. 391-393, 2002.
- [19] F. Koyama, "VCSEL photonics—advances and new changes—," *IEICE Electron. Express*, vol. 6, no. 11, pp. 651-672, 2009.
- [20] H. Kawaguchi, *Bistability and nonlinearities in laser diodes*. Norwood, MA: Artech House, 1994.
- [21] H. Kawaguchi, "Bistable laser diodes and their applications: state of the art," *IEEE J. Sel. Topics Quantum Electron.*, vol. 3, no. 5, pp. 1254-1270, 1997.
- [22] H. Kawaguchi, T. Mori, Y. Sato, and Y. Yamayoshi, "Optical buffer memory using polarization-bistable vertical-cavity surface-emitting lasers," *Jpn. J. Appl. Phys.*, vol. 45, no. 34, pp. L894-L897, 2006.
- [23] H. Kawaguchi, Y. Yamayoshi, and K. Tamura, "All-optical format conversion using an

ultrafast polarization bistable vertical-cavity surface-emitting laser,” *Proc. Conf. Lasers and Electro-Optics*, no. CWU2, pp. 379-380, 2000.

- [24] T. Mori, Y. Yamayoshi, and H. Kawaguchi, “Experimental demonstration of all-optical regeneration using a polarization bistable VCSEL,” *Proc. Conf. Lasers and Electro-Optics*, no. CThA3, 2005.

Chapter 2 Pulse Generation by Polarization Self-Modulation

2.1 Introduction

Optical pulses have been widely used in various fields such as optical communication, time-resolved spectroscopy, sensing, and metrology. Many different methods using semiconductor lasers have been investigated for pulse generation, for example, mode locking, gain switching, Q switching, and polarization self-modulation. In this chapter, we review an all-optical pulse generation method by polarization self-modulation in EELs or VCSELs with external cavities. According to the experimental setup, the pulse generations by polarization self-modulation are divided into two different schemes: polarization-rotated feedback and crossed-polarization reinjection.

2.2 Polarization self-modulation

2.2.1 Principle of polarization self-modulation

Self-modulation of polarization in a semiconductor laser is a promising technology for generating ultrahigh frequency optical pulses without requiring high-speed electronics [1]. It is an all-optical method which can be a candidate for pulse generation in the all-optical

communication system in the future. Polarization self-modulation can be performed in both the EELs and the VCSELs when polarization-rotated optical feedback is applied to them by an external partial reflector (PR). The conventional EEL structures generally have a large anisotropy between TE and TM modes because of the asymmetry of the active region. Compared with the EELs, VCSELs have small anisotropies because of the symmetry of the structure and of the gain in the plane of the active quantum wells [2]. Here, we introduce the principle of polarization self-modulation by using a VCSEL which is considered to be more suitable for polarization self-modulation due to its small gain anisotropy and small birefringence.

The principle of polarization self-modulation in a VCSEL with polarization-rotated feedback from an EC is shown in Fig. 2.1. The EC formed by the VCSEL and a PR has in it a quarter-wave plate (QWP) whose optical axis is oriented at 45° with respect to the polarization direction of the VCSEL. As shown in the top of the figure, the VCSEL is set to lase with linear polarization at 0° . Then the polarization of the VCSEL output is changed to circular polarization by the QWP. After being partially reflected by the PR, the retroreflected light goes through the QWP for the second time and its polarization is changed back to linear polarization and rotated by 90° from the initial polarization (0°). This polarization-rotated feedback changes the polarization of VCSEL lasing from 0° to 90° , the same polarization as the feedback light, which is because of all-optical polarization switching. After the second round-trip, the polarization of

VCSEL lasing will be changed back to that at the beginning of the first round-trip (0°). Thus, the lasing of the VCSEL alternately switches between 0° and 90° linear polarizations. Two round-trips in the EC become one period of the polarization self-modulation, and the repetition rate f of the polarization self-modulation is governed by the EC length L : $f = c/4L$. In every round-trip, part of the output light goes through the PR with circular polarization. The QWP#2 outside the EC changes the circular polarization back to linear polarization. As shown in the right of Fig. 2.1, two complementary modulation signals polarized at 0° and 90° can be generated [1].

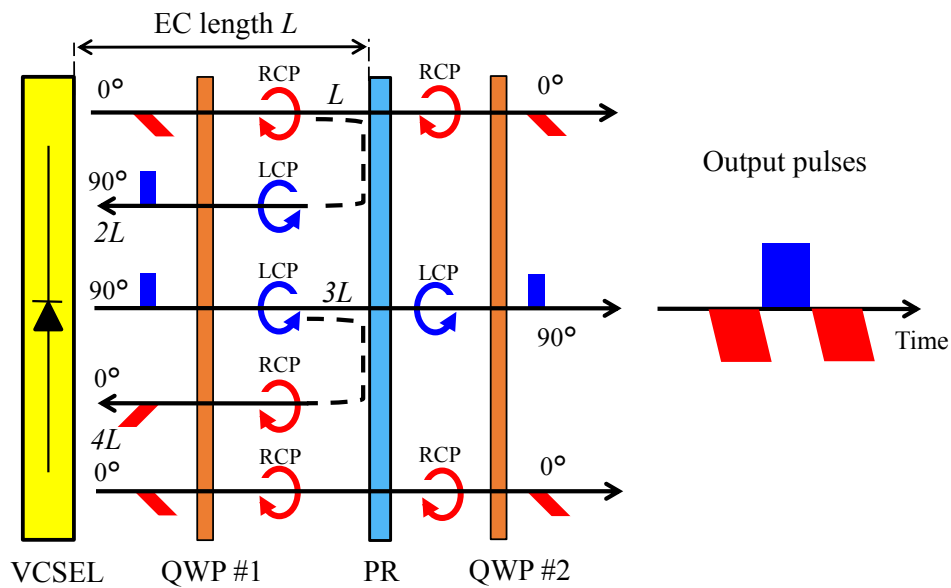


Fig. 2.1. Polarization self-modulation in an external-cavity (EC) VCSEL with a QWP. (PR: partial reflector, QWP: quarter-wave plate, L/RCP: left/right circular polarization).

2.2.2 Polarization-rotated feedback scheme

Polarization self-modulation in laser diodes has been investigated intensely in the past two

decades. Loh et al. [3] obtained optical pulses due to polarization self-modulation by inserting a QWP inside the EC of an EEL. The TE and TM pulses had different amplitudes. Jiang et al. [1] firstly demonstrated the polarization self-modulation in a VCSEL with a PR and a QWP. Polarization self-modulation frequencies of up to 6 GHz were observed. The optical pulse signals at the two orthogonal polarizations of the VCSEL had a nearly equal amplitude. The modulation frequency was claimed to be determined by the EC length. They explained this phenomenon based on the external optical feedback-induced polarization locking mechanism. Li et al. [4] added measurement of the optical spectra in their experiments to investigate the polarization self-modulation in VCSELs. They showed the results with different EC length L . At low frequency, the optical pulse was with a square waveform. In the optical spectrum, the sidebands on both sides of the main peak were nearly symmetric. As L was shortened, a larger feedback was needed and the waveform of output optical pulses turned to be sinusoidal. Polarization switching up to 9.18 GHz was obtained, which is the highest frequency in the previous researches. However, the optical spectrum in that case showed a bi-modal characteristic, which was not clarified. We also observed this phenomenon in our experiments and we clarified that the mechanism of the pulse generation changed to be the beat note of two EC modes, which was different from the polarization self-modulation [5]. Aiming at the application in atomic clock, Smith et al. [6] reduced the scale of their EC-VCSEL experimental setup by using a subwavelength grating QWP in the EC. A polarization switching frequency of

7.2 GHz with a 7 MHz full width at half maximum (FWHM) was presented.

Pulse generation by the polarization self-modulation of EELs in [3] or VCSELs in [1] [4] [6] were explained by polarization switching. However, some researchers also interpreted this phenomenon in terms of beating between two EC modes which are orthogonally polarized to each other in a new system of axes [2] [7]. The eigenaxes of the laser were considered to be changed by the intracavity QWP. The new eigenaxes were approximately along the two axes of the QWP, which were $\pm 45^\circ$ according to the lasing polarization of the VCSEL. On each of the two new axes, there were EC modes with intervals equal to the free spectral range (FSR) $c/2L$ of the EC. The modes on the two axes had a frequency difference of $c/4L$. When the output was detected along the axes of VCSEL (0° and 90°), beating between the external cavity modes on both new axes gave a modulation of the output light at $c/4L$. Robert et al. [2] [8] theoretically and numerically investigated the interpretation as spin sublevel dynamics using a Spin-Flip model [9] [10]. However, their numerical results showed that the spin relaxation introduced by them did not affect the calculation results [2]. Other groups also explained their experimental results using EELs or VCSELs with Spin-Flip model [11] [12].

2.2.3 Crossed-polarization reinjection scheme

All of those research reported in Sec. 2.2.2 used QWP in the EC to obtain polarization-rotated feedback to the laser. Vallet et al. [13] used an intracavity Faraday rotator (FR) instead

of the commonly used QWP to improve the stability of modulation. More recently, crossed-polarization reinjection (XPR) has been proposed for generating optical pulses [14]. As shown in Fig. 2.2, a FR is set to rotate the polarization of the laser output by 45° and a polarizer oriented at 45° according to the optical axes of the VCSEL is inserted after the FR. Only one polarization mode of the VCSEL output, 0° or 90° can go through both the FR and the polarizer and then reflected back to the VCSEL with its polarization rotated by 90° . The other polarization mode will be suppressed by the polarizer after the FR. Different to the polarization-rotated optical feedback using QWP in the EC, in this case, multiple round-trip reflections can be avoided [14], because only one of the linearly polarized modes can be polarization-rotated by 90° and injected back into the laser cavity [15]. The photon densities of the two modes are modified by cross saturation and eventually lead to pulsed emission.

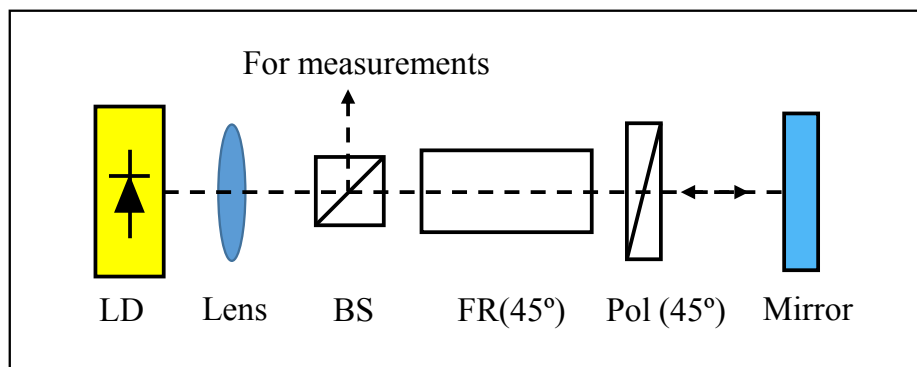


Fig. 2.2. Experimental setup of EC laser diode with crossed-polarization reinjection (XPR).

LD: laser diode, BS: beam splitter, FR: Faraday rotator, Pol: polarizer.

In recent years, high-repetition-frequency square wave has become attractive in many applications and have been studied in some optoelectronic systems [16]. EELs and VCSELs with FR in the EC were also used for the generation of square waves. Gavrielides et al. [14] [17] found square wave self-modulation experimentally in EELs and they numerically simulated the square wave modulation process. They also realized the square wave self-modulation in two orthogonally delay-coupled EELs [18] [19]. Balle et al. [15] observed square-wave oscillations for VCSEL with XPR. After that, they theoretically and experimentally studied the combined effects of weak polarization-selective optical feedback (PSF) and XPR in a VCSEL [20]. The PSF was introduced to increase the dichroism to obtain a robust square wave. Recently, with the same experimental setup applying XPR and PSF on a VCSEL, they obtained dissipative solitons, which were totally different from the output of polarization self-modulation [21].

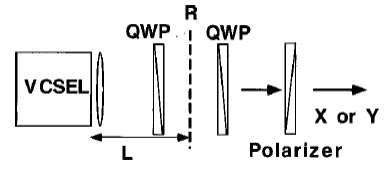
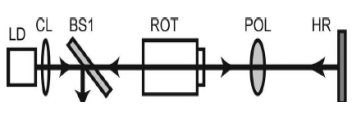
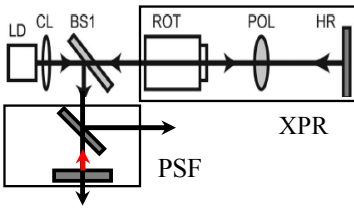
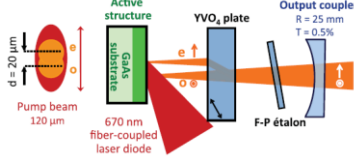
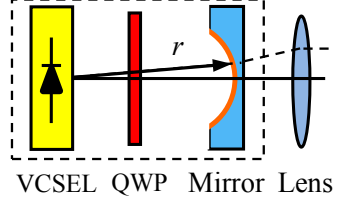
Other experimental setups were also used to obtain polarization-rotated optical feedback for polarization self-modulation, such as a half-wave plate (HWP) [11] or a HWP and an isolator with a polarization rotation function in a ring cavity [22]. Camargo et al. [23] studied the output modulations caused by the beat note in optically-pumped vertical external-cavity semiconductor lasers with a birefringent plate having dual-frequency emission.

When we use FR or HWP with isolator in the external cavity to modulate the polarization of VCSEL output, the EC becomes long. Aiming at high-frequency pulse generation with EC-

VCSEL, we insert a QWP into the EC, which could be a thin film as will be described later.

Table 2.1 gives a comparison of several schemes, with our scheme. Li et al. [4] used a QWP in the EC and obtained output modulation of 9.2 GHz, which was the fastest in the previous researches. Gavrielides et al. [14] used a FR and a polarizer to change the polarization of the feedback and obtained square wave oscillations with frequencies of about 192 MHz. Balle et al. [20] introduced a weak PSF to stabilize the pulse generation. When FR is inserted in the EC, stable square waveforms can be obtained. However, the aim of our research is to generate high-frequency optical pulse by self-modulation of the EC-VCSEL. Thus, a thin-film QWP was inserted in the EC. Moreover, besides the planar mirror, we used concave mirrors and semi-spherical mirrors for the shortening of EC length and obtained high-frequency output modulations of up to 12.6 GHz [5] and 15.3 GHz [24], respectively.

Table 2.1. Comparison between different schemes

Author	Experimental setup	Scheme	Waveform	Frequency
Li et al. [4]		Polarization rotated feedback	Sinusoidal wave	9.2 GHz
Gavrielides et al. [14]		Crossed-polarization reinjection (XPR)	Square wave	~192 MHz
Balle et al. [20]		XPR + Polarization-selective feedback (PSF)	Square wave	~230 MHz
Camargo et al. [23]		Beat note	Not shown	9.2 GHz
Liu et al. [5][24]		Polarization rotated feedback	Sinusoidal wave	12.6 GHz 15.3 GHz

2.3 Conclusion

In this chapter, we reviewed the pulse generation by polarization self-modulation in laser diodes with ECs, especially in VCSELs. The principle of polarization self-modulation was introduced and different interpretations were stated. We also divided the polarization self-

modulation operation into two schemes and discussed: polarization-rotated feedback scheme and crossed-polarization reinjection scheme.

2.4 References

- [1] S.-J. Jiang, Z.-Q. Pan, M. Dagenais, R. A. Morgan, and K. Kojima, "High-frequency polarization self-modulation in vertical-cavity surface-emitting lasers," *Appl. Phys. Lett.*, vol. 63, no. 26, pp. 3545-3547, 1993.
- [2] F. Robert, P. Besnard, M. L. Chares, and G. M. Stephan, "Polarization modulation dynamics of vertical-cavity surface-emitting lasers with an extended cavity," *IEEE J. Quantum Electron.*, vol. 33, no. 12, pp. 2231-2239, 1997.
- [3] W. H. Loh, Y. Ozeki, and C. L. Tang, "High-frequency polarization self-modulation and chaotic phenomena in external cavity semiconductor lasers," *Appl. Phys. Lett.*, vol. 56, no. 26, pp. 2613-2615, 1990.
- [4] H. Li, A. Hohl, A. Gavrielides, H. Hou, and K. D. Choquette, "Stable polarization self-modulation in vertical-cavity surface-emitting lasers," *Appl. Phys. Lett.*, vol. 72, no. 19, pp. 2355-2357, 1998.
- [5] T. Liu, T. Katayama, and H. Kawaguchi, "High-frequency self-modulation in short-external-cavity VCSEL with concave mirror," *IEEE Photon. Technol. Lett.*, vol. 27, no. 3, pp. 280-

283, 2015.

- [6] C. J. Smith, W.-D. Li, S.-F. Bai, and S. Y. Chou, "High frequency polarization switching VCSEL clock using subwavelength quarter-wave plate," OSA/CLEO/IQEC, CMP6, 2009.
- [7] G. Ropars, P. Langot, M. Brunel, M. Vallet, F. Bretenaker, A. Le Floch, and K. D. Choquette, "Experimental evidence of single round-trip oscillation in polarization self-modulated vertical-cavity surface emitting lasers," *Appl. Phys. Lett.*, vol. 70, no. 20, pp. 2661-2663, 1997.
- [8] F. Robert, P. Besnard, M.-L. Chares, and G. Stephan, "Polarization control in a vertical cavity surface emitting laser submitted to optical feedback," *ANN TELECOMMUN.*, vol. 52, no. 11-12, pp.575-587, 1997.
- [9] J. Martin-Regalado, F. Prati, M. San Miguel, and N. B. Abraham, "Polarization properties of vertical-cavity surface-emitting lasers," *IEEE J. Quantum Electron.*, vol. 33, no. 5, pp. 765-783, 1997.
- [10] M. San Miguel, Q. Feng, and J. V. Moloney, "Light-polarization dynamics in surface-emitting semiconductor lasers," *Phys. Rev. A*, vol. 52, no. 2, pp. 1728-1739, 1995.
- [11] S.-Y. Xiang, W. Pan, L.-S. Yan, B. Luo, X.-H. Zou, N. Jiang, and K.-H. Wen, "Time-delay signature of chaotic vertical-cavity surface-emitting lasers with polarization-rotated optical feedback," *Chin. Phys. Lett.*, vol. 28, no. 1, 014203, 2011.
- [12] J. Javaloyes, M. Marconi, and M. Giudici, "Phase dynamics in VCSELs with delayed

- optical feedback and cross re-injection,” *Phys. Rev. A*, vol. 90, no. 2, 023838, 2014.
- [13] M. Vallet, M. Brunel, F. Bretenaker, M. Alouini, and A. Le Floch, “Polarization self-modulated lasers with circular eigenstates,” *Appl. Phys. Lett.*, vol. 74, no. 22, pp. 3266-3268, 1999.
- [14] A. Gavrielides, T. Erneux, D.W. Sukow, G. Burner, T. McLachlan, J. Miller, and J. Amonette, “Square-wave self-modulation in diode lasers with polarization-rotated optical feedback,” *Opt. Lett.*, vol. 31, no. 13, pp. 2006-2008, 2006.
- [15] J. Mulet, M. Giudici, J. Javaloyes, and S. Balle, “Square-wave switching by crossed-polarization gain modulation in vertical-cavity semiconductor lasers,” *Phys. Rev. A*, vol. 76, no. 4, 043801, 2007.
- [16] D. W. Sukow, T. Gilfillan, B. Pope, M. S. Torre, A. Gavrielides, and C. Masoller, “Square-wave switching in vertical-cavity surface-emitting with polarization-rotated optical feedback: experiments and simulations,” *Phys. Rev. A*, vol. 86, no. 3, 033818, 2012.
- [17] A. Gavrielides, T. Erneux, D. W. Sukow, G. Burner, T. McLachlan, J. Miller, and J. Amonette, “Square-wave oscillations in edge-emitting diode lasers with polarization-rotated optical feedback,” *Opt. Lett.*, vol. 31, no. 13, pp. 2006-2008, 2006.
- [18] C. Masoller, D. Sukow, A. Gavrielides, and M. Sciamanna, “Bifurcation to square-wave switching in orthogonally delay-coupled semiconductor lasers: theory and experiment,” *Phys. Rev. A*, vol. 84, no. 2, 023838, 2011.

- [19] M. Sciamanna, M. Virte, C. Masoller, and A. Gavrielides, "Hopf bifurcation to square-wave switching in mutually coupled semiconductor lasers," *Phys. Rev. E*, vol. 86, no. 1, 016218, 2012.
- [20] M. Marconi, J. Javaloyes, S. Barland, M. Giudici, and S. Balle, "Robust square-wave polarization switching in vertical-cavity surface-emitting lasers," *Phys. Rev. A*, vol. 87, no. 1, 013827, 2013.
- [21] M. Marconi, J. Javaloyes, S. Barland, S. Balle, and M. Giudici, "Vectorial dissipative solitons in vertical-cavity surface-emitting lasers with delays," *Nature Photon.*, vol. 9, no. 7, pp. 1-7, 2015.
- [22] J. Houlihan, G. Huyet, and J.G. McInerney, "Dynamics of a semiconductor laser with incoherent optical feedback," *Opt. Commun.*, vol. 199, no. 1-4, pp. 175-179, 2001.
- [23] F. A. Camargo, J. Barrientos, G. Baili, L. Morvan, D. Dolfi, D. Holleville, S. Guerandel, I. Sagnes, P. Georges, and G. Lucas-Leclin, "Coherent dual-frequency emission of a vertical external-cavity semiconductor laser at the cesium D₂ line," *IEEE Photon. Technol. Lett.*, vol. 24, no. 14, pp. 1218-1220, 2012.
- [24] T. Liu, T. Katayama, and H. Kawaguchi, "High-frequency self-modulation in short-external-cavity VCSEL with semi-spherical mirror," *Proc. Conf. Lasers and Electro-Optics Pacific Rim*, no. T12_1016, 2015.

Chapter 3 Pulse Generation in External-Cavity VCSEL with Planar Mirror

3.1 Introduction

Self-modulation in EC-VCSEL is a promising method to generate high-repetition-frequency optical pulses without using fast electronics. Furthermore, there is another advantage that the repetition frequency of the optical pulses which is determined by the length of the EC can be variable. Here, to investigate the pulse generation at different repetition frequencies, we measured and analyzed the modulated optical output of the EC-VCSEL with different EC length. A thin-film QWP and a planar partial reflection mirror were used in the experiments for the convenience of changing the EC length.

3.2 Experimental setup

Fig. 3.1 shows the experimental setup of the EC-VCSEL using a planar mirror for the EC. A 1.55- μm polarization bistable VCSEL was used in our experiments [1]. The structure of it is schematically shown in Fig. 3.2. The VCSEL has a square mesa structure which ensures oscillation in one of the two linearly polarized modes along the edges of the mesa (0° and 90°).

The shape and sizes of the mesa-structure top Distributed Bragg Reflector (DBR) and the active layer of the VCSEL were designed by our group; the device was fabricated by RayCan Co. The VCSEL structure was monolithically grown by low-pressure metal-organic vapor phase epitaxy on an InP substrate. The active region was $0.5\text{-}\lambda$ thick and consisted of strain-compensated multiple quantum wells (MQWs). A double intracavity contact with $2.5\text{-}\lambda$ -thick n-InP cladding layers was used for highly efficient heat dispersion and low series resistance. A C-doped InAlAs tunnel junction was located at the standing-wave node position between the top n-InP layer and the active region. The top and bottom mirrors were grown as InAlAs/InAlGaAs DBRs. Current confinement was provided by an air-gap aperture formed in the selectively wet-etched $0.5\text{-}\lambda$ -thick active layer. The sides of the square mesa structure of the top DBR were aligned with the $[110]$ and $[\bar{1}\bar{1}0]$ crystal orientation directions of the InP substrate. The VCSELs exhibited continuous-wave (CW) lasing in the lowest-order transverse mode at room temperature. The lasing polarization of the VCSELs was linear and the polarization direction was 0° or 90° , corresponding to the $[\bar{1}\bar{1}0]$ and $[110]$ directions, respectively [1]. Fig. 3.3 (a) shows the polarization-resolved light output versus current (Light-I) curves of the polarization bistable VCSEL (Rev. 3.3 #932208) used in this research in CW operation at 20°C . The VCSEL lased with 90° polarization and no polarization switching occurred with increasing drive current. Fig. 3.3 (b) shows the non-polarization-resolved lasing spectra observed at 7.0 mA. The main peak shows the wavelength of 90° polarization mode and the weaker peak on the longer wavelength

side corresponds to the wavelength of the 0° mode (not lasing). The wavelength difference between the 0° and 90° modes was about 0.068 nm (8.8 GHz). Using similar polarization bistable VCSELs, we demonstrated all-optical buffer memory [2] and all-optical packet switching with header recognition [3].

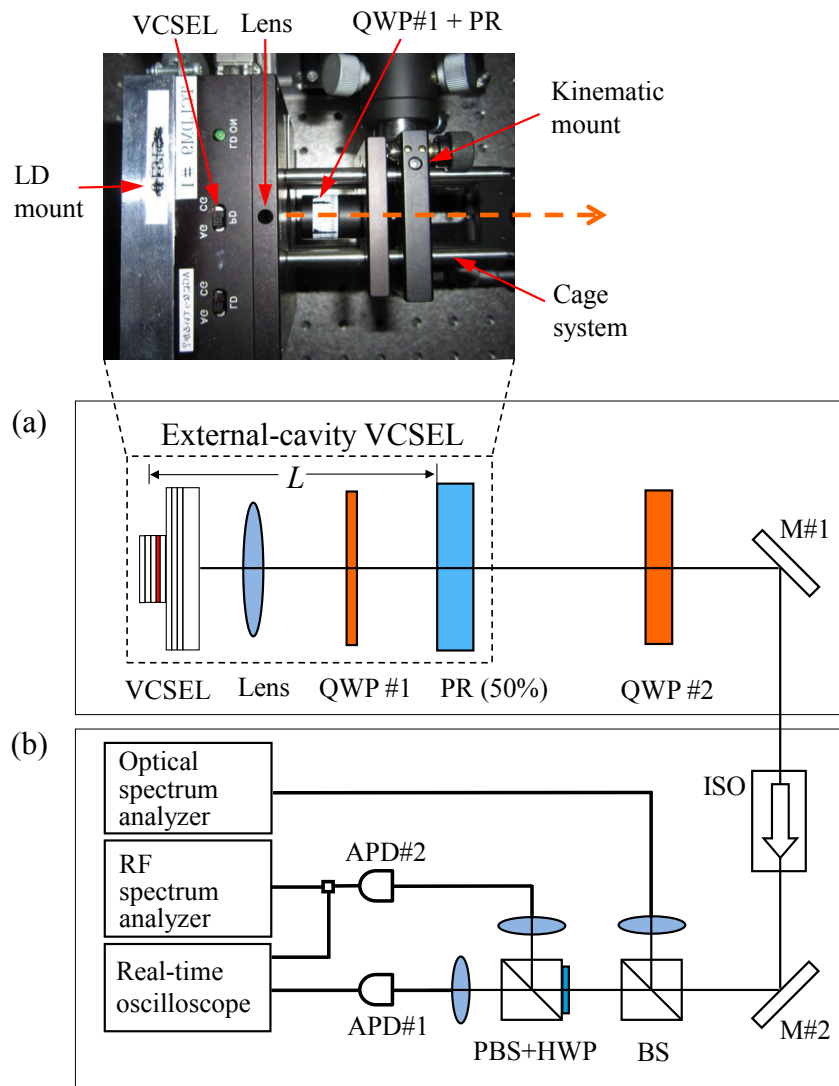


Fig. 3.1. Experimental setup for pulse generation using a planar mirror. (a) External-cavity VCSEL, (b) Measurement system. (QWP: quarter-wave plate, PR: partial reflection reflector, M: reflection mirror, ISO: polarization-independent isolator, HWP: half-wave plate, (P)BS: (polarization) beam splitter, APD: avalanche photodiode).

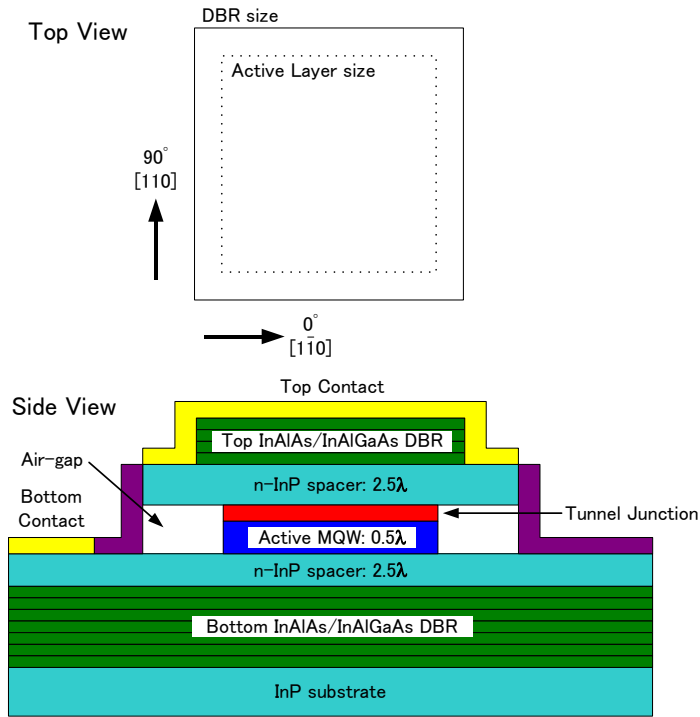


Fig. 3.2. Schematic of the VCSEL used in this research [1].

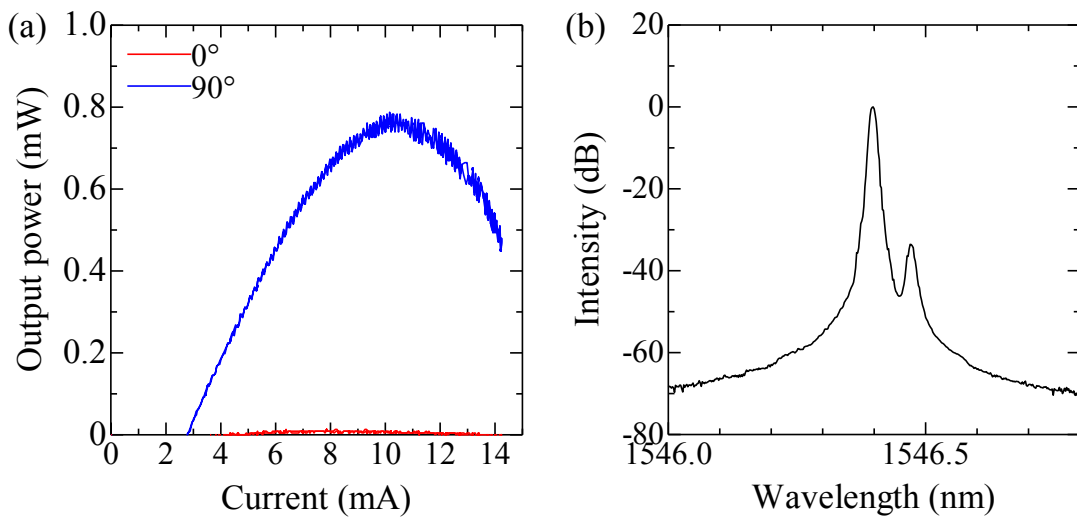


Fig. 3.3. Lasing characteristics of VCSEL (Rev. 3.3 #932208) at 20 °C.

(a) Polarization-resolved light output-current (Light-I) characteristics.

(b) Optical spectrum of the total output at 7.0 mA.

The planar partial reflection mirror PR (Lattice Electro Optics BS-1550-R50-B-0525) in Fig. 3.1 (a) had a reflectivity of 50%. To remove the limitation of L by inserting the QWP into the cavity, we used a thin-film polyimide QWP with a thickness of only $8\ \mu\text{m}$ as shown in Fig. 3.4. To be inserted in the EC, the thin-film QWP was sandwiched between two non-transparent fixing plates. The diameter of the hole in the center of the fixing plate was 1.4 mm, ensuring that only the optical beam that goes through the QWP and the hole can travel back and forth in the EC. We measured the beam divergence of the VCSEL output by the measurement of far-field pattern (FFP) as shown in Fig. 3.5. Fig. 3.6 shows the intensity distribution of the output beam measured at 50 mm from the VCSEL. It showed a perfect Gaussian profile with a divergence angle of only 11.82° at the FWHM. Such low divergence guarantees a low power loss of the beam caused by the limitation of the hole in the QWP fixing plates. This is an advantage of the VCSELs compared with EELs.

The photograph of the experimental setup for the EC-VCSEL is shown on the top of Fig. 3.1 (a). The VCSEL was attached to the LD mount (Thorlabs TCLDM9). The planar mirror and the intracavity thin-film QWP were mounted on a 5-axis stage allowing precise alignment of their axial positions and tilt angles. A cage system which connected the VCSEL mount and the mirror mount supplied us high mechanical stability of the EC-VCSEL.

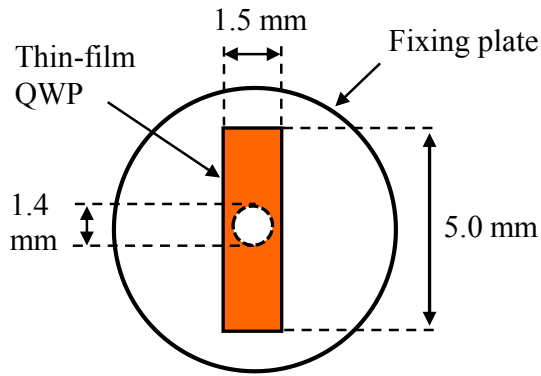


Fig. 3.4. Schematic of thin-film polyimide QWP and fixing plate.

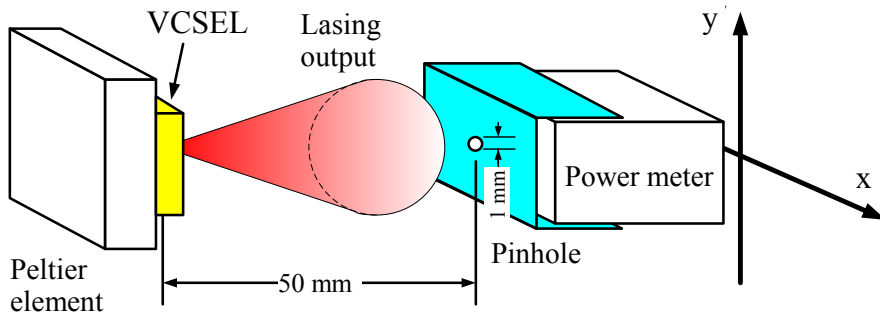


Fig. 3.5. Experimental setup of far-field pattern (FFP) measurement.

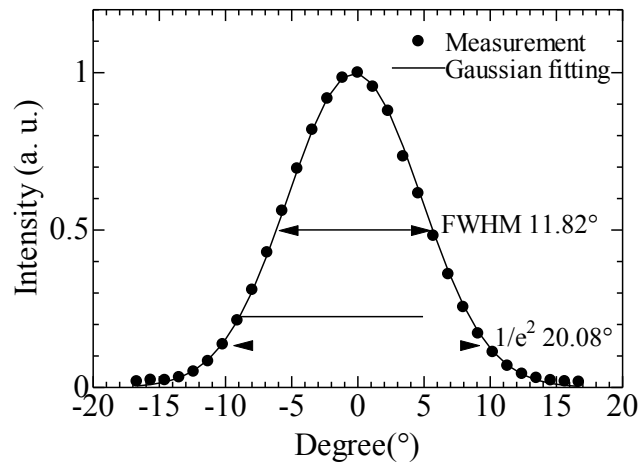


Fig. 3.6. VCSEL output beam divergence angle by FFP measurement.

In Fig. 3.1, between the EC-VCSEL and the measurement system, a polarization independent optical isolator (ISO) (OFR-FT-38X135) was inserted to prevent the reflection light from affecting the operation of the EC-VCSEL. A polarization beam splitter (PBS) (Thorlabs VBA05-1550) was used to polarization resolve the output light of the EC-VCSEL. The PBS can only polarization resolve the input light at “s” and “p” polarizations, thus a HWP was inserted on the right entrance face of the PBS to change the polarization that to be resolved by rotating the polarization of the input light. After passing through the PBS, the polarization-resolved optical output of the VCSEL was characterized using a real-time oscilloscope (Agilent DSO81304A) with a bandwidth of 13 GHz, an optical spectrum analyzer (ADVANTEST Q8384) with a wavelength resolution of 0.01 nm, and an RF spectrum analyzer (Agilent E4448A) with a bandwidth of 50 GHz. The avalanche photodiodes (APDs) (Discovery semiconductors DSO-R402) converting the optical outputs into electrical signals had a bandwidth of 10 Gb/s. In all measurements, the resolution bandwidth of the RF spectrum analyzer was set to be 300 kHz. The video bandwidth, which is the bandwidth of the low pass filter between the detector and the display of the RF spectrum analyzer, was set to be 300 kHz to reduce the noise floor of the measured spectra.

3.3 Experimental results

We measured the modulated output of EC-VCSEL with different EC length L , from 35 mm to 8 mm. L was measured with an accuracy of ± 0.5 mm. According to the results, we divided these results into three regions: longer external cavity, medium length external cavity and shorter external cavity.

3.3.1 For longer external cavity

At the beginning, L was set to be about 35 mm, which corresponds to a frequency ($f = c/4L$) of about 2 GHz. After aligning the planar mirror, the lasing threshold current of the VCSEL was reduced by about 0.6 mA due to the increase of the photon density in the VCSEL cavity caused by the feedback light. Output modulations were observed at discrete current values and the output modulation became unstable above 5 mA. Fig. 3.7 and Fig. 3.8 show the measured results at 4.83 mA. In Fig. 3.7 (a) and (b), the polarization-resolved output power at 0° and 90° show optical pulse sequences with a frequency of about 1.93 GHz. The two optical pulses sequences are complementary to each other and have similar peak intensities. Fig. 3.7 (c) shows the waveform of the total output power (non-polarization resolved), which has a frequency twice of those polarization-resolved at 0° and 90° . As shown by the vertical dotted lines, the peaks in the waveform of the total output power are corresponding to those in the polarization-resolved ones. It is clear that the polarization of the VCSEL lasing periodically switched

between 0° and 90° . The output modulation with a frequency of about 2 GHz was caused by the polarization self-modulation of the VCSEL. Fig. 3.8 shows the measured polarization-resolved RF spectrum at 0° and the optical spectrum of the total optical output at 4.83 mA. The peaks in the center of the optical spectrum are expanded and shown in linear scale in the inset. There are sidebands on both sides of the main peak. The frequency differences between the sidebands and the main peak are equal to the modulation frequency. These phenomena are identical with the results in [4].

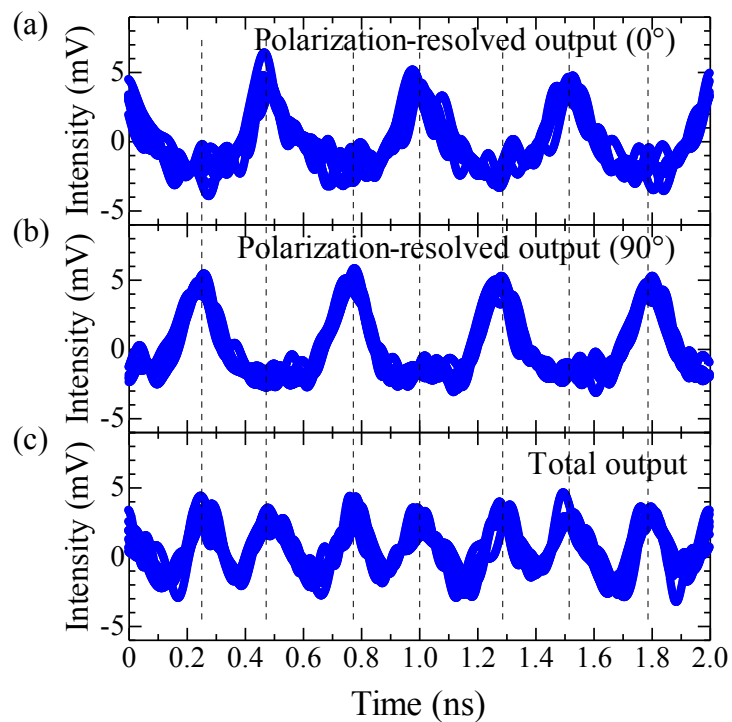


Fig. 3.7. Waveforms of polarization self-modulation outputs at 4.83 mA. (a) and (b) polarization-resolved output at 0° and 90° , (c) total output.

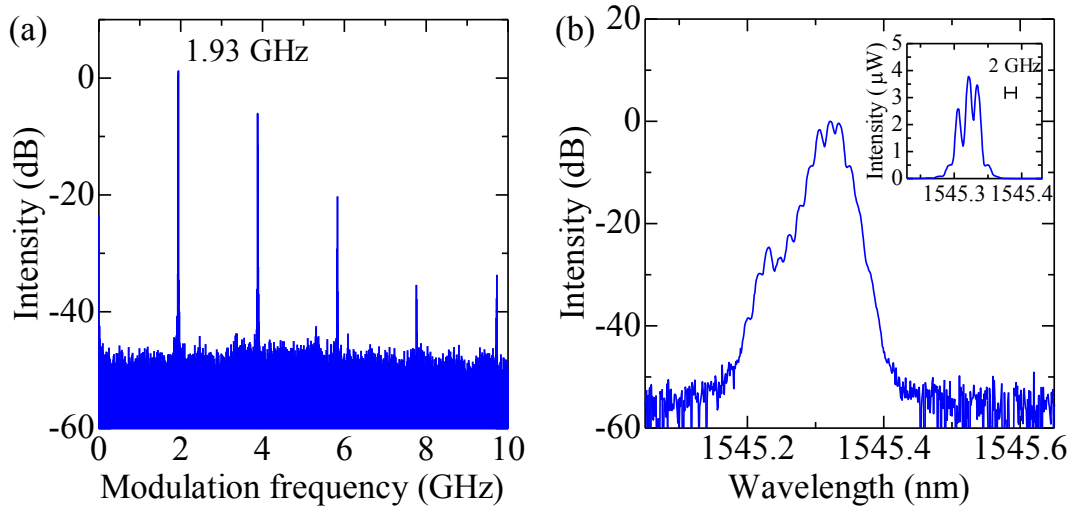


Fig. 3.8. Measured spectra at 4.83 mA. (a) RF spectrum of the polarization-resolved output at 0° , (b) optical spectrum of the total output.

Then we shortened the L to be about 16 mm, corresponding to a frequency ($f = c/4L$) of about 4.6 GHz. After aligning the planar mirror, we obtained the modulated optical output at discrete current values and the output modulation became unstable above 6 mA. The measured results at 5.64 mA are shown in Fig.3.9 and Fig. 3.10. Fig. 3.9 (a) and (b) are the waveforms of the polarization-resolved optical output at -20° and 70° directions. In the experiment, we found that the polarization-resolved waveforms at -20° and 70° had similar intensities and their peaks corresponded to the peaks in the waveform of the total output power. Thus, polarization of the VCSEL lasing alternately switched between -20° and 70° , but not 0° and 90° . The reason for this polarization shift is not clear now. The polarization dependence of the two reflection mirrors (M#1 and M#2 in Fig. 3.1), the polarization-independent isolator (ISO), and the beam splitter (BS) in the optical path were carefully checked, and we believed that they were not the

main origin for the polarization shift.

Fig. 3.10 shows the RF spectrum of the output polarization resolved at 70° and the optical spectrum of the total output. The RF spectrum has fewer harmonics than the RF spectrum at about 2 GHz shown in Fig. 3.8 (a), which means that the waveforms in Fig 3.9 are closer to a sinusoidal wave than those in Fig. 3.7. In the optical spectrum shown in Fig. 3.10 (b), the sideband on the shorter-wavelength side was much weaker than the one on the longer-wavelength side.

In conclusion, optical pulses generated by the polarization self-modulation were obtained with a frequency of about 4 GHz. Combining the results at higher frequencies that will be described later, we estimated that this operation of polarization self-modulation was not perfect and may be slightly included the beat note between two EC modes which we clearly observed for shorter L .

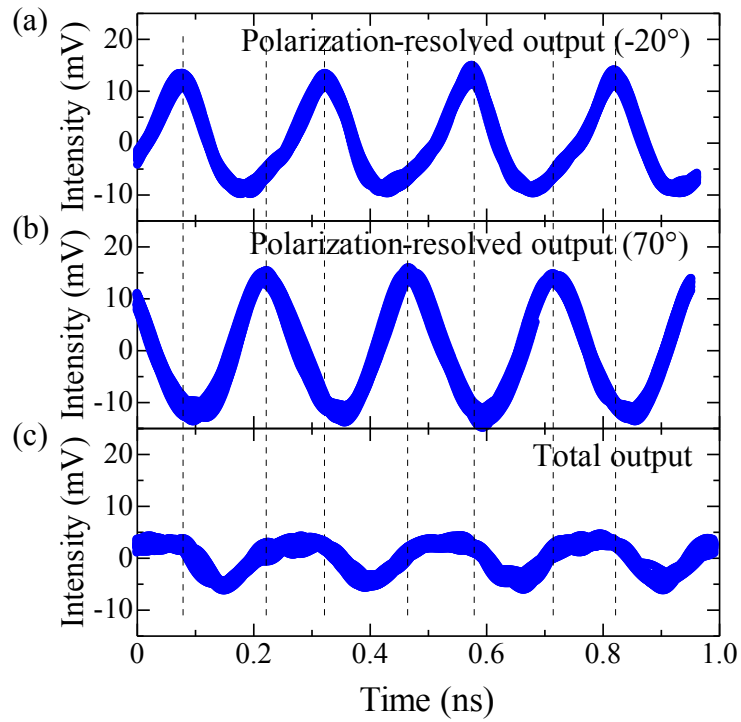


Fig. 3.9. Waveforms of polarization self-modulation outputs at 5.64 mA. (a) and (b) polarization-resolved output at -20° and 70° , (c) total output.

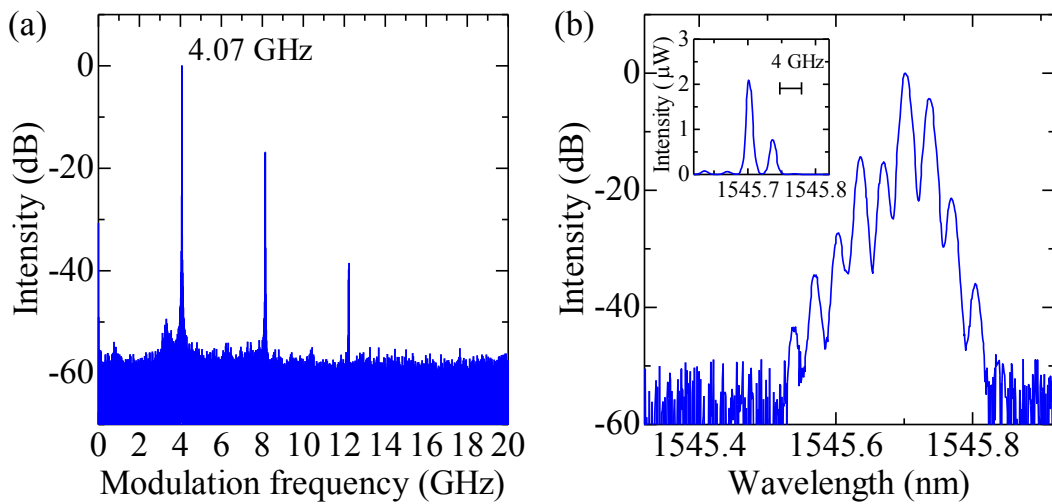


Fig. 3.10. Measured spectra at 5.64 mA. (a) RF spectrum of the polarization-resolved output at 70° , (b) optical spectrum of the total output.

3.3.2 For medium length external cavity

To investigate the modulation at higher frequency, we changed L to be about 15 mm, which corresponded to a modulation frequency of 5 GHz. After aligning of the mirror, at currents above 5 mA, we observed very unstable modulated output that seems to be caused by the polarization self-modulation of the EC-VCSEL. Fig. 3.11 shows the waveforms and RF spectrum of the modulated output at 7.29 mA. The waveforms in Fig. 3.11 (a) are unstable, though they were measured by the real-time oscilloscope during a short time of about 0.2 μ s. The waveforms on the display of the real-time oscilloscope were much more unstable in longer time scales and the modulation even stopped sometimes. Although the RF spectrum in Fig. 3.11 (b) was measured during 0.268 s, the linewidth of the peaks were broad which showed that the modulation was unstable. Furthermore, the modulation frequency was not consistent with the L .

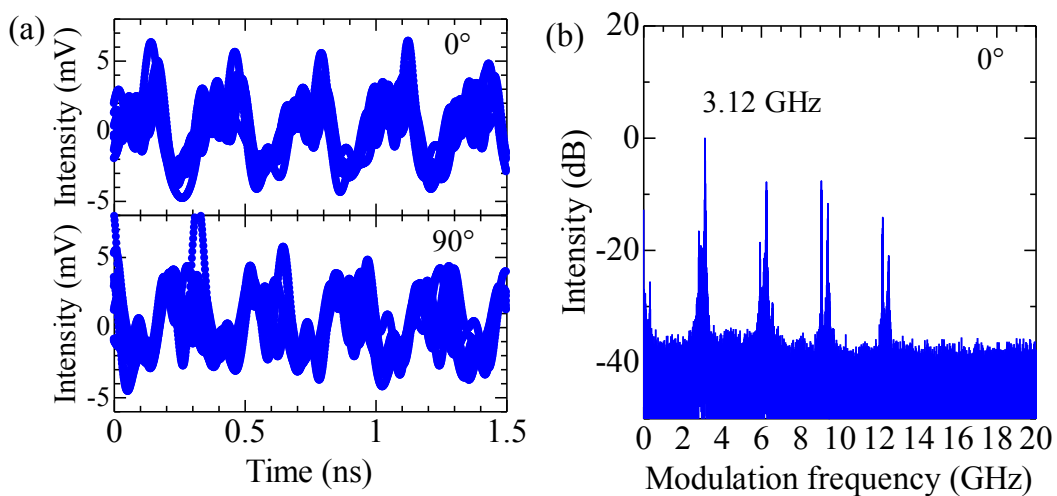


Fig. 3.11 Waveforms (a) and RF spectrum (b) of the output modulation at 7.29 mA.

At a drive current of 2.73 mA, which was slightly above the lasing threshold of the EC-VCSEL (about 2.5 mA), we observed unstable and weak optical spectrum of the total output as shown in Fig. 3.12. The peaks were labeled from 1 to 4 in Fig. 3.12 (a). The adjacent labeled peaks had the same wavelength difference. The peaks labeled 2 and 3 in the center were lasing with similar intensities. The lasing frequency difference between them was measured to be about 6.4 GHz (0.051 nm), which was identical with the measured value in the RF spectrum in Fig. 3.12 (b). The polarization difference between the two peaks was measured to be about 9.5° . Because of the weak output intensity, the main peak in the RF spectrum had a small signal to noise ratio (SNR) of only about 12 dB. We were not able to measure the waveform of the output by the oscilloscope. From the optical spectrum and the RF spectrum, we estimated that this modulation was due to the beat note between the peak 2 and peak 3 in the optical spectrum.

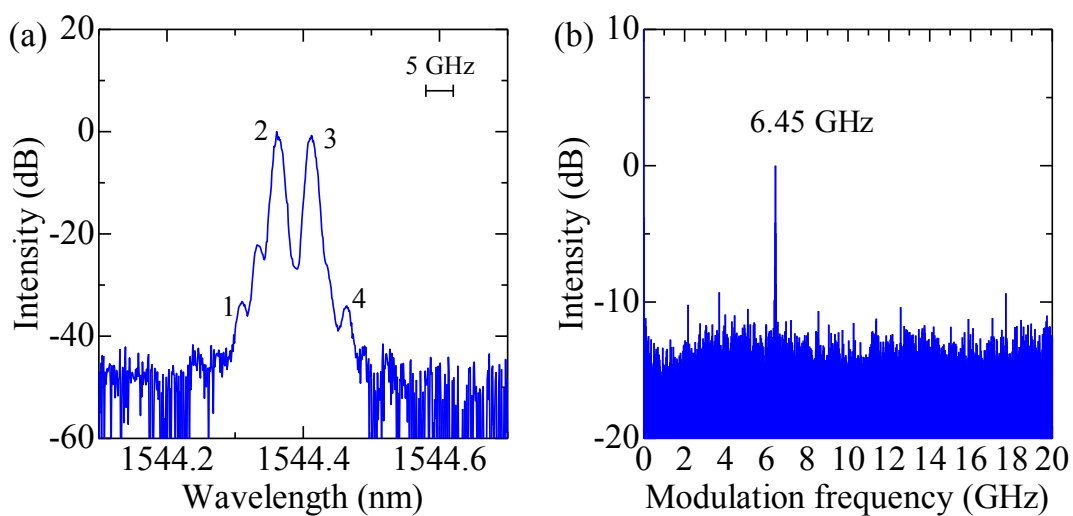


Fig. 3.12. Measured spectra of the total output at 2.73 mA. (a) Optical spectrum, (b) RF spectrum.

When L was shortened to about 11 mm, which corresponded to a frequency of about 7 GHz, we observed optical outputs similar to those at $L \approx 15$ mm. The waveform and RF spectrum of the unstable modulated output, which seems to be caused by polarization self-modulation in the EC-VCSEL at higher drive currents, are not shown in this thesis. Fig. 3.13 shows the optical spectrum and the RF spectrum observed at 2.76 mA. The peaks 2 and 3 in the center of the optical spectrum were lasing with similar intensities and the lasing frequency difference between the two peaks was about 7.1 GHz (0.056 nm), which was equal to the value measured in the RF spectrum and close to the modulation frequency determined by L . The polarization difference between the two peaks were measured to be about 7.7° . This operation was the same as that at about 5 GHz, which was considered to be the beat note between the peak 2 and peak 3 in the optical spectrum.

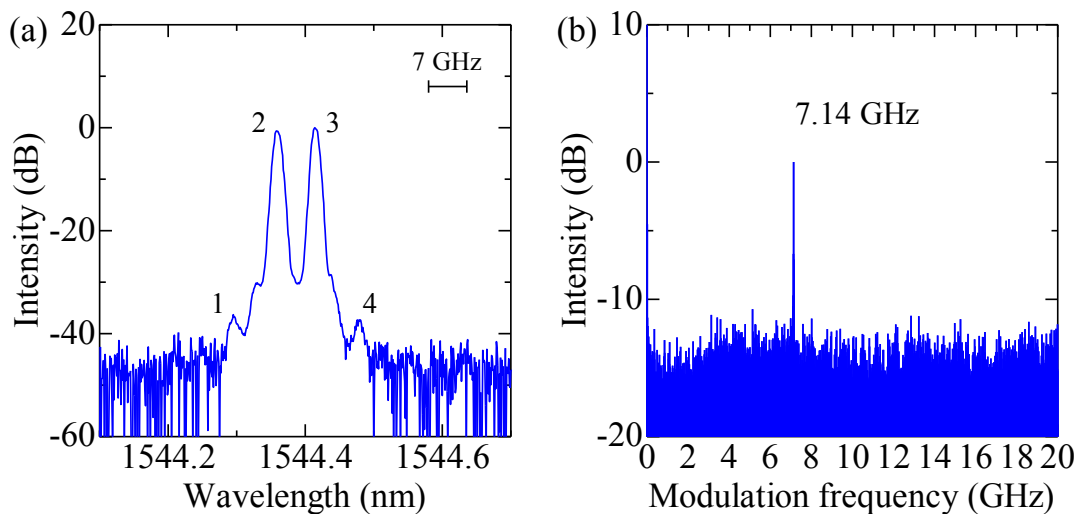


Fig. 3.13. Measured spectra of the total output at 2.76 mA. (a) Optical spectrum, (b) RF spectrum.

3.3.3 For shorter external cavity

Finally, we shortened L to be about 8 mm, which was the shortest L that could be obtained due to the limitation of the focal length and thickness of the collimating lens in the EC. Considering that we could no longer obtain optical pulses by the polarization self-modulation operation, the QWP#2 outside the EC was removed and the total output was detected by a photodiode (PD) (Discovery semiconductors DSO-R401) with a bandwidth of 20 GHz. Then, we measured the optical power, real-time waveforms, RF spectra, and optical spectra of the total output at different drive currents.

As shown in Fig. 3.14, when the drive current was increased gradually from 4.7 mA to 5.7 mA, stable optical output modulation sequences were observed at discrete current values. The optical power was polarization resolved at the strongest and the weakest polarization directions, -20° and 70° . Polarization of the optical output switched during the increase of the drive current. Similar and more stable output modulations were observed using a concave mirror with a radius of 5.08 mm (Fig. 4.7). We will explain these phenomena in detail in Sec. 4.2.2.

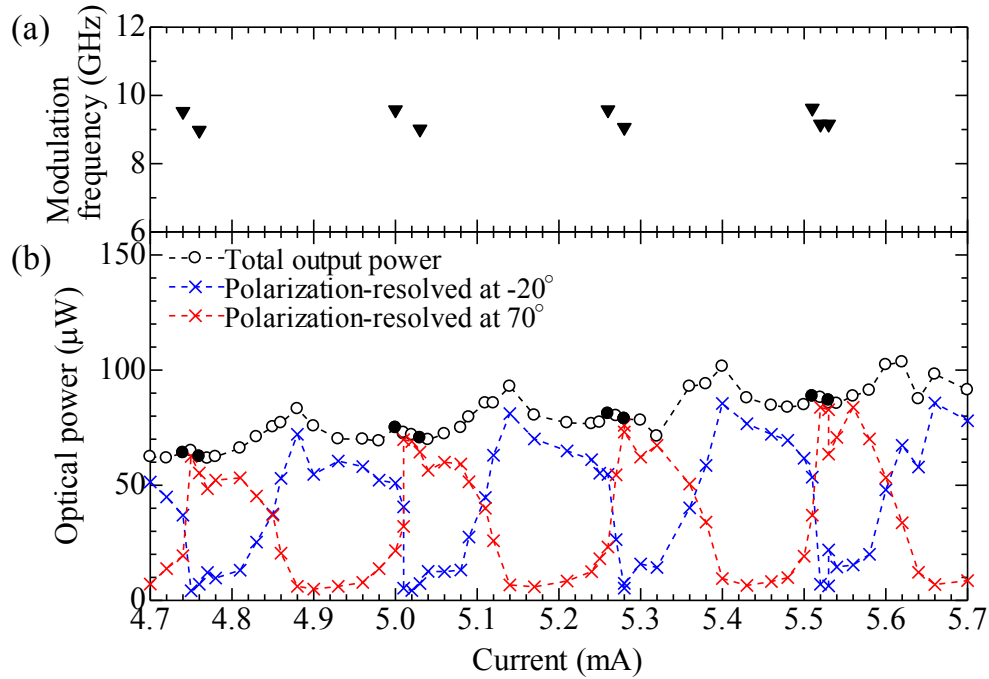


Fig. 3.14. Output modulation frequency (a) and optical power (b) as functions of drive current.

Here we show the modulation output at 5.13 mA as an example. Fig. 3.15 gives the optical spectrum and the RF spectrum of the modulated output. There were four peaks in the optical spectrum, which were considered to be the two-round-trip EC modes. The intensities of the peaks were believed to be determined by the gain spectrum. The peaks labeled 2 and 3 were lasing with similar intensities. The lasing wavelength difference between them was identical with the measured modulation frequency in the RF spectrum. Whether there are harmonic components in the RF spectrum or not is determined by the waveform of the PD input. When the waveform is sinusoidal, there is no harmonics. On the contrary, there will be some harmonics if the waveform is far from a sinusoidal wave. The waveform shown in Fig. 3.16 (a) was sinusoidal, and coincided with the RF spectrum in which there was nearly no harmonics.

This agreed with our assumption that the beat note between the peak 2 and peak 3 resulted in the output modulation. We measured the modulation depth of the output when the two peaks had different intensity ratios, as shown in Fig. 3.16 (b). The black lines shows the theoretically calculated result of a simple beating model of two optical waves with the same polarization. The measured values had the same tendency with the theoretically calculated result. With increase of the intensity ratio (I_2/I_3), the modulation depth decreased. This result strongly supports our assumption that the optical output modulation was due to the beat note of the peak 2 and peak 3 in the optical spectrum. The model of output modulation by the beat note of two lasing modes will be discussed in detail in Chapter 4.

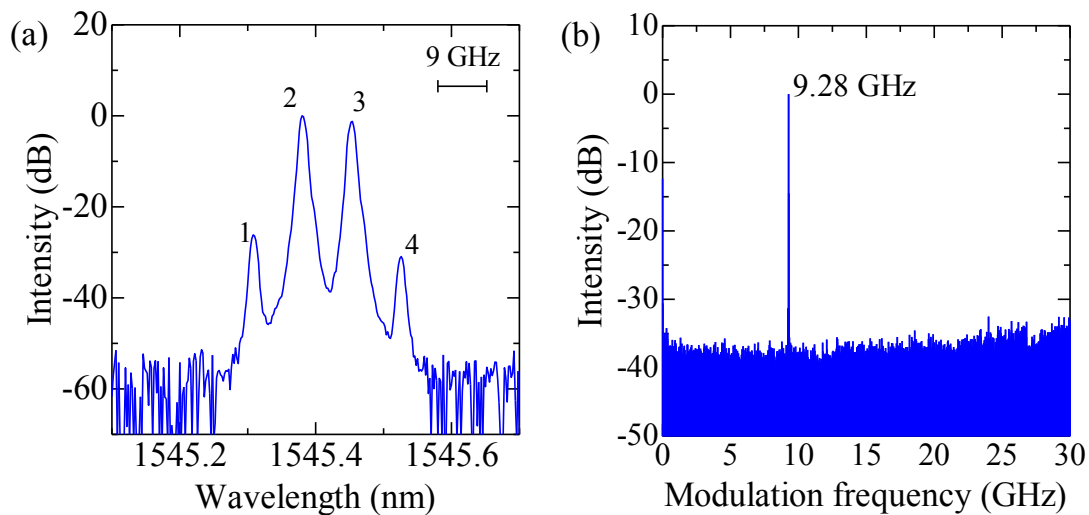


Fig. 3.15. The measured spectra of the modulation output at 5.13 mA.

(a) Optical spectrum, (b) RF spectrum.

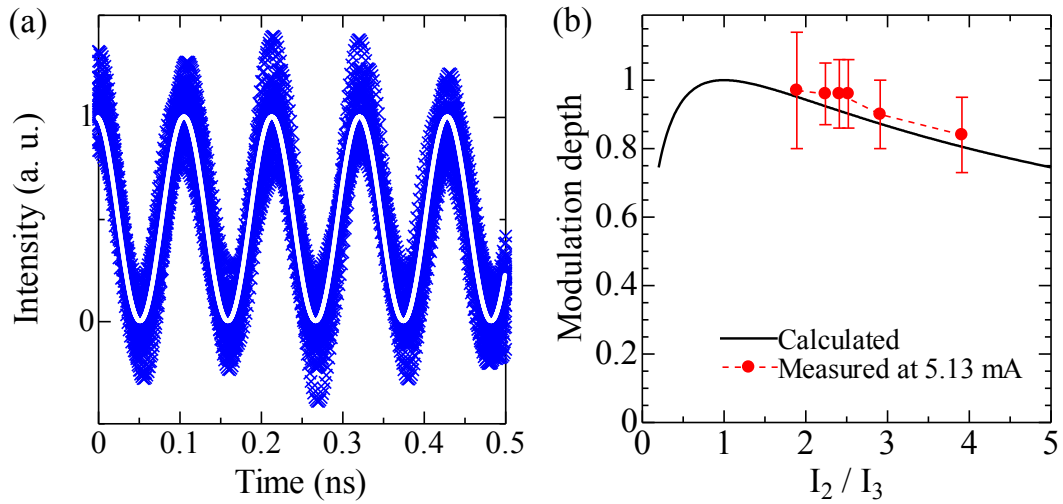


Fig. 3.16. Measured optical output at 5.13 mA. (a) Waveform. White line: 9.28-GHz sinusoidal wave. (b) Dependence of modulation depth on the intensity ratio of the peak 2 and peak 3.

3.4 Relationship between EC length and modulation mechanism

By changing the EC length L , we investigated the self-modulation at different frequencies.

From the measured output at each L , we divided the results into three regions by the difference in modulation modes, as shown in Fig. 3.17. The dots on the axis of L show the EC lengths at which we investigated the output modulation experimentally in this chapter.

For longer EC ($L \approx 35$ mm and $L \approx 16$ mm), we observed optical pulse sequences by polarization self-modulation of the EC-VCSEL at about 2 GHz and 4 GHz. For medium length EC ($L \approx 15$ mm and $L \approx 11$ mm), we observed optical output by different modulation mechanisms, i.e. unstable polarization self-modulation at higher currents and weak beat note at currents slightly above the lasing threshold of the EC-VCSEL. For shorter EC ($L \approx 8$ mm), we obtained stable modulation outputs at discrete current values, which were the beat note between

the two lasing modes. In conclusion, with the decrease of L , the modulation mechanism gradually changed from polarization self-modulation to the beat note between two lasing modes.

When an operation condition is changed, e.g. change in the pump power, lasing output power does not immediately change to the steady state but oscillates with decreasing amplitude. This output power oscillation is called relaxation oscillation and the frequency of it is called relaxation oscillation frequency (f_r). The direct intensity modulation bandwidth of semiconductor lasers is widely accepted to be limited by f_r . If we take the polarization self-modulation of the EC-VCSEL as intensity modulations of the 0° and 90° modes of the solitary VCSEL, the frequency of polarization self-modulation may be limited by f_r . The f_r of solitary VCSELs is usually in the order of several GHz, which is close to the highest frequency (~ 4 GHz) of polarization self-modulation as shown in Fig. 3.17. The detailed discussion will be described in Sec. 5.5.

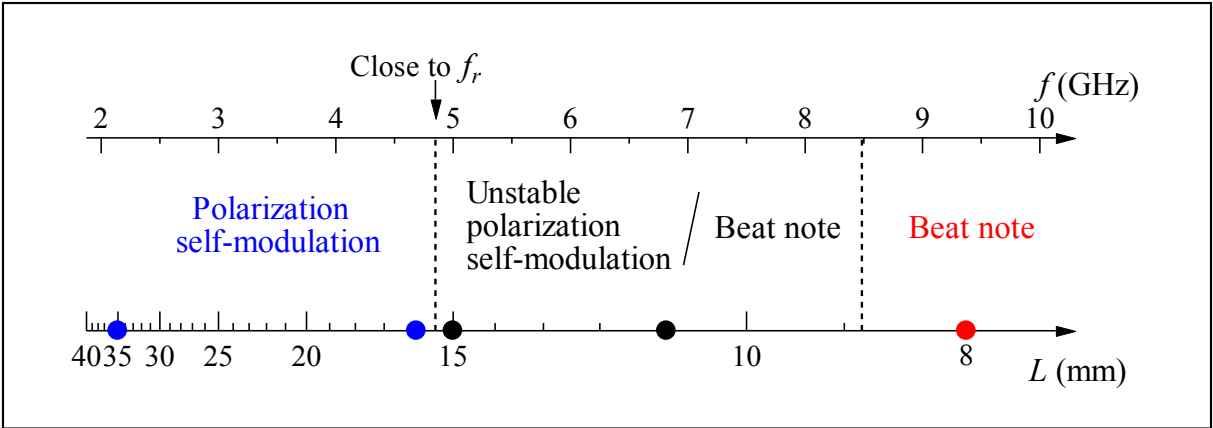


Fig. 3.17. Modulation modes depending on L . f_r : relaxation oscillation frequency of solitary VCSEL.

3.5 Conclusion

By changing the EC length L , we investigated the self-modulation in the EC-VCSEL. For longer L , we observed optical pulse sequences with frequencies of up to about 4 GHz due to polarization self-modulation, in which two orthogonally polarized modes of the VCSEL lased alternately. For medium length L , unstable polarization self-modulations were observed at higher drive currents and the optical spectra obtained at lower drive currents showed a bi-modal characteristic unstably. For shorter L , we observed stable modulation outputs of about 9 GHz due to the beat note of two lasing modes. The modulation mechanism gradually changed in the range of 15 mm–8 mm (5–9 GHz), which is believed to be limited by the relaxation oscillation of the solitary VCSEL.

3.6 References

- [1] T. Katayama, Y. Sato, T. Mori, and H. Kawaguchi, "Polarization bistable characteristics of 1.55 μm vertical-cavity surface-emitting lasers," *Jpn. J. Appl. Phys.*, vol. 46, no. 49, pp. L1231-L1233, 2007.
- [2] T. Katayama, T. Ooi, and H. Kawaguchi, "Experimental demonstration of multi-bit optical buffer memory using 1.55- μm polarization bistable vertical-cavity surface-emitting lasers," *IEEE J. Quantum Electron.*, vol. 45, no. 11, pp. 1495-1504, 2009.

- [3] T. Katayama, T. Okamoto, and H. Kawaguchi, "All-optical header recognition and packet switching using polarization bistable VCSEL," *IEEE Photon. Tech. Lett.*, vol. 25, no. 9, pp. 802-805, 2013.
- [4] H. Li, A. Hohl, A. Gavrielides, H. Hou, and K. D. Choquette, "Stable polarization self-modulation in vertical-cavity surface-emitting lasers," *Appl. Phys. Lett.*, vol. 72, no. 19, pp. 2355-2357, 1998.

Chapter 4 High-Frequency Self-Modulation in External-Cavity VCSEL with Concave Mirror and Semi-Spherical Mirror

4.1 Introduction

Generation of high-repetition-frequency optical pulses with a controllable frequency without using high-speed electronics has aroused interest. As described in the mechanism of polarization self-modulation in VCSELs in Chapter 3, the modulation frequency is determined by the EC length L . It means that to get higher modulation frequency, L should be shortened. In the experiments of pulse generation with planar partial reflection mirror described in Chapter 3, a lens is needed for collimating the diverging output from the VCSEL, which limits the shortening of L .

In this chapter, aiming at higher-repetition-frequency optical pulse generation, we report a new configuration shortening the time delay of optical feedback in an EC-VCSEL by using a thin-film QWP in the cavity and using a short-radius concave partial reflection mirror (CM) as one end of the cavity. In this case, the CM can focus the light back to the VCSEL without using the collimating lens. For further shortening of L , we used semi-spherical mirrors which were simply fabricated from small ball lens.

4.2 Experiment using concave mirror

We used two CMs with different radiuses (r), 20 mm and 5.08 mm. The 20 mm radius CM was used in the experiment to check whether the CMs were feasible to focus the output back to the VCSEL. 5.08 mm was the shortest radius that we could find in the commercially available concave mirrors.

4.2.1 20 mm radius concave mirror

The experimental setup using the 20 mm radius CM is shown in Fig. 4.1. The 1.55- μm polarization bistable VCSEL used in our experiments had a square mesa ensuring oscillation in one of the two linearly polarized modes along the edges of the mesa (0° and 90°) [1]. Fig. 4.2 (a) shows the polarization-resolved light output versus current (Light-I) curves of the solitary VCSEL in CW operation at 20°C . The polarization of the VCSEL switched twice with increasing or decreasing bias current, and each switching resulted in a hysteresis in the polarization-resolved Light-I curves. Fig. 4.2 (b) shows the lasing spectra observed at 7.7 mA when the current was decreased. The VCSEL lased with the 90° polarization and the wavelength difference between the two orthogonal polarization modes was about 0.068 nm (8.8 GHz). The CM was prepared by applying a 60% reflection coating on a commercially available plank plano-concave lens (Lattice Electro Optics BS-1525-2565-R50-B-MPC-0525-20). L was approximately equal to the r of the CM. The thin-film QWP (8 μm thick) inserted into the EC

increased L only slightly. The CM and intracavity thin-film QWP were mounted on a 5-axis stage allowing precise alignment of their axial positions and tilt angles.

The polarization-resolved optical output of the VCSEL was characterized, after passing through a PBS (Thorlabs VBA05-1550), using a real-time oscilloscope (Agilent DSO81304A) with a bandwidth of 13 GHz, an optical spectrum analyzer (ADVANTEST Q8384) with a wavelength resolution of 0.01 nm, and an RF spectrum analyzer (Agilent E4448A) with a bandwidth of 50 GHz. The APDs (Discovery semiconductors DSO-R402) converting the optical outputs into electrical signals had a bandwidth of 10 Gb/s. In all measurements both the resolution bandwidth and video bandwidth of the RF spectrum analyzer were set to be 300 kHz.

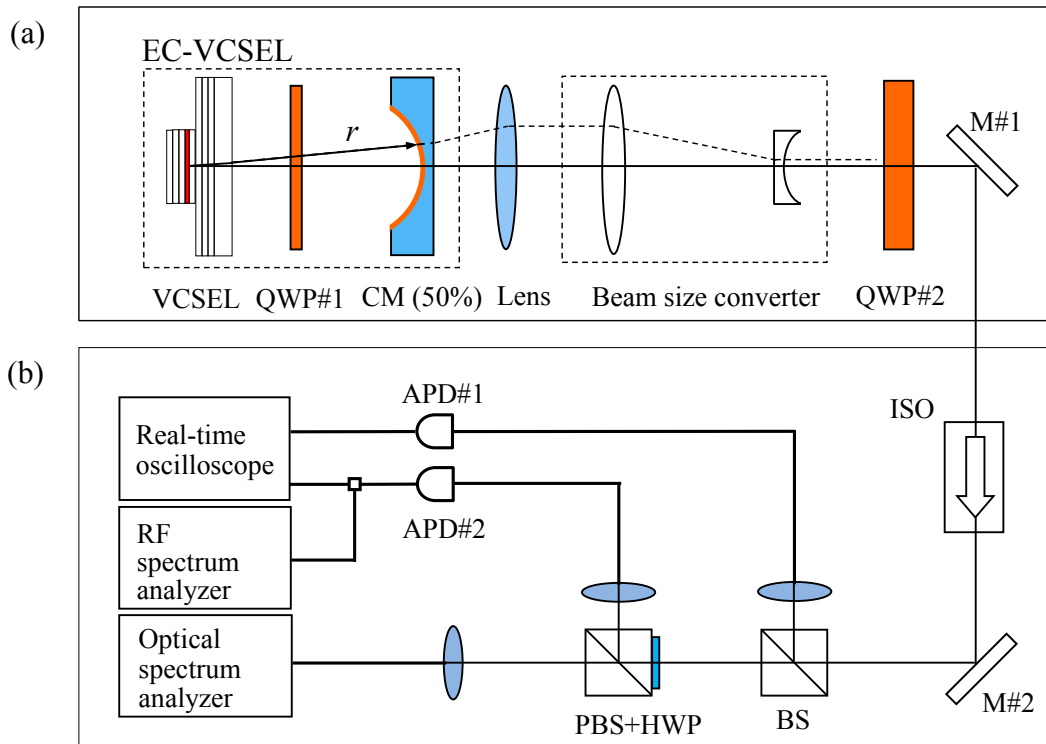


Fig. 4.1. Experimental setup for EC-VCSEL using 20 mm radius concave mirror (CM) for the EC.

(a) EC-VCSEL, (b) measurement system.

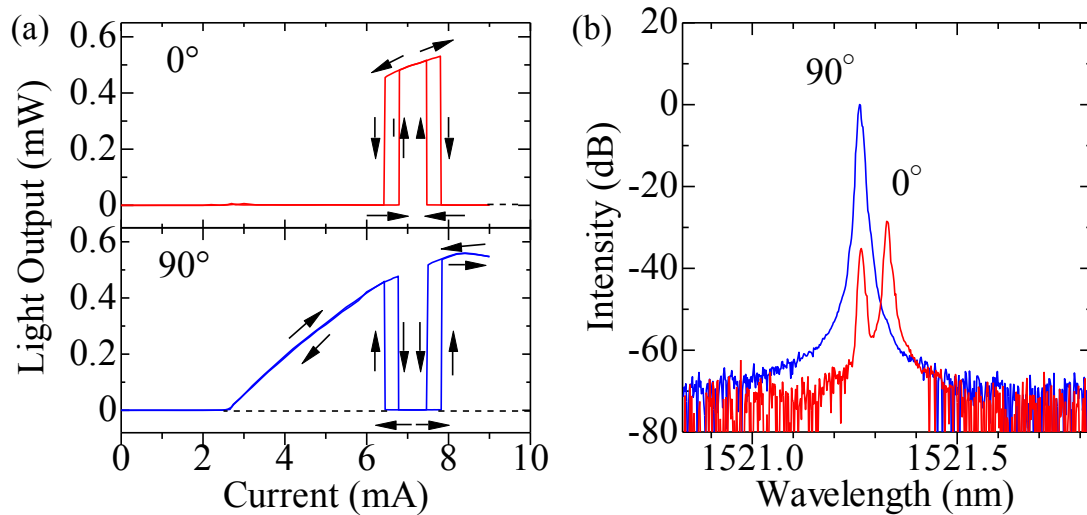


Fig. 4.2. Lasing characteristics of the polarization bistable VCSEL (Rev. 5.1 #10312309) at 20 °C used for the experiments with 20 mm radius concave mirror. (a) Polarization-resolved light output-current characteristics, (b) polarization-resolved optical spectra at 7.7 mA.

After collimating with the 20 mm radius CM, the lasing threshold current of the VCSEL was decreased by about 0.7 mA due to the increase of the photon density in the VCSEL cavity by the feedback light. This lasing threshold decrement was nearly the same as that using a 50% planar mirror for the EC. This indicated that the CM could focus the light back to the VCSEL as efficiently as the planar mirror with collimating lens. Decrement of the VCSEL lasing threshold by optical feedback was calculated using a model described in Chapter 5. Comparing the values of the lasing threshold reduction in the calculation and experiments, we estimated that the coupling efficiency of the feedback light into the laser cavity by the concave mirrors or the planar mirror were about 4~5%. This will be explained in detail in Sec. 5.5.

We obtained optical pulses by the polarization self-modulation of the VCSEL. The measurement results at 7.73 mA are shown in Fig. 4.3 and Fig. 4.4. As shown in Fig. 4.3 (a)

and (b), the polarization-resolved output at 0° and 90° showed optical pulse sequences with a frequency of about 3.46 GHz. Fig. 4.3 (c) shows the measured waveform of the total output and indicates that the 0° and 90° polarization modes oscillated alternately. Fig. 4.4 shows the measured RF spectrum and optical spectrum of the optical output at 7.73 mA. These results are similar to those of the 2 GHz and 4 GHz optical pulses generated by polarization self-modulation in Chapter 3. All of these results show that our configuration with a 20 mm radius CM and a thin-film QWP results in polarization self-modulation in the EC-VCSEL and it is feasible to focus the output back to the VCSEL by using a CM without collimating lens. Thus, it is possible to shorten L by using a shorter radius CM, as will be described in the next section.

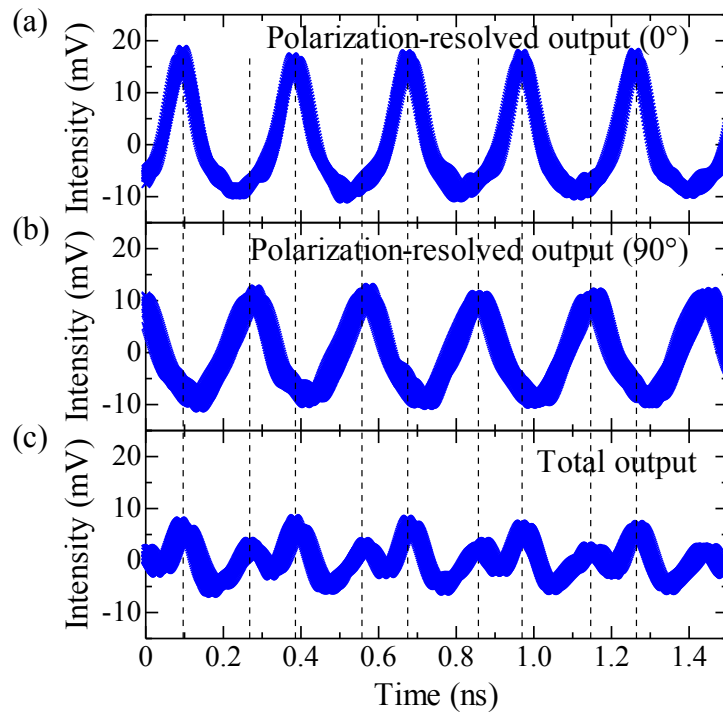


Fig. 4.3. Waveforms of polarization self-modulation outputs at 7.73 mA using the 20 mm radius CM. (a) and (b) polarization-resolved output at 0° and 90° , (c) total output.

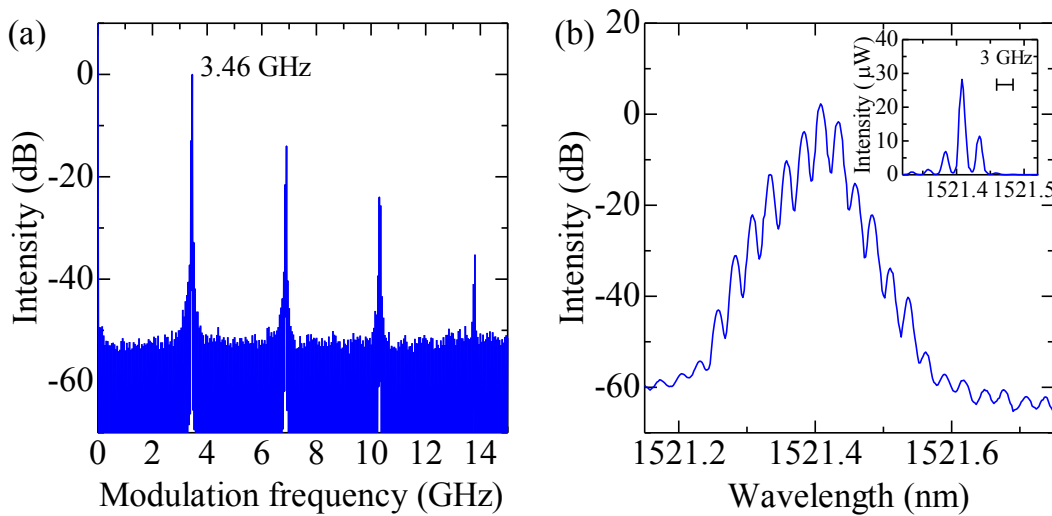


Fig. 4.4. Measured spectra at 7.73 mA. (a) RF spectrum of the polarization-resolved output at 90° , (b) optical spectrum of the total output.

4.2.2 5.08 mm radius concave mirror

The 5.08 mm radius CM was obtained by applying a 60% reflection coating on the concave surface of a plank plano-concave lens (Lattice Electro Optics BS-1525-1565-R60-UF-MPC-10mmD \times 2mmT-5.08mmR) as shown in Fig. 4.5. The edge of the lens which would prevent the CM from approaching the VCSEL mount was cut off. The cutting process was carried out by Dr. S. Hattori from Mitsubishi Diamond Industrial Co., LTD.

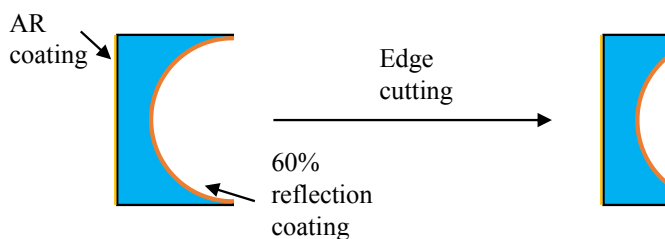


Fig. 4.5. Processing of 5.08 mm radius CM before being used for the EC.

The experimental setup is shown in Fig. 4.6. The 1.55- μm VCSEL used here is the same to that used in the experiments in Chapter 3. As shown in Fig. 4.6 (a), the EC formed by the CM had in it a thin-film QWP whose optical axis was oriented at 45° with respect to the polarization direction of the VCSEL. The polarization of the retroreflected light was rotated by 90° during each round trip in the EC. The measurement system is shown in Fig. 4.6 (b). The optical output of the EC-VCSEL was characterized using a real-time oscilloscope with a bandwidth of 13 GHz, an optical spectrum analyzer with a wavelength resolution of 0.01 nm, and an RF spectrum analyzer with a bandwidth of 50 GHz. Polarization-resolved optical power was measured after the output passed through a PBS. Each PD had a bandwidth of 20 GHz.

Due to the mechanism change of the output modulation with the shortening L , the measurement system was changed. For the measurement of the polarization self-modulated output, a QWP outside the EC is necessary to convert the modulated output from circular polarization to linear polarization [2] as shown in Fig. 4.1. When we used a CM with an r of 5.08 mm, we obtained output waveforms which were very different from those obtained using a CM with an r of 20 mm. They were sinusoidal with frequencies around 12 GHz. The measured polarization-resolved output showed that the lasing polarization of the VCSEL did not alternately switch between 0° and 90° linear polarizations. The total output of the EC-VCSEL was not constant in intensity and was linearly polarized with an extinction ratio of around 10 dB. Because the total output was linearly polarized, we measured the lasing characteristics of

the EC-VCSEL output without the QWP#2 placed the outside of the cavity (in Fig. 4.1).

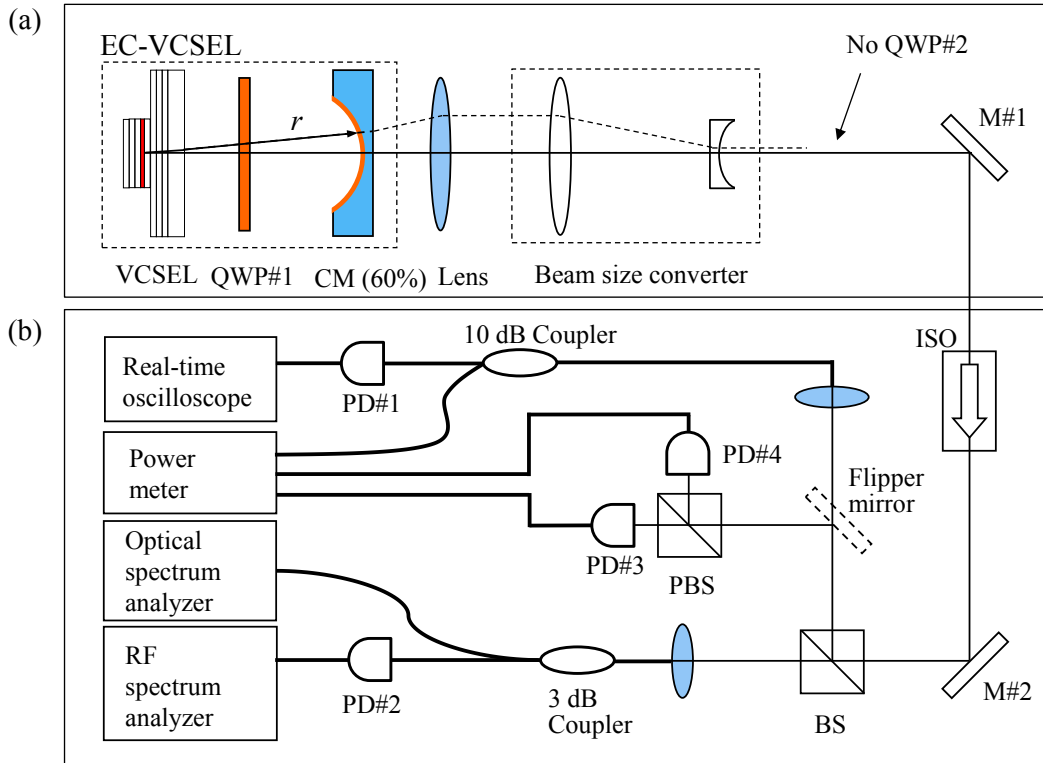


Fig. 4.6. Experimental setup for EC-VCSEL using the 5.08 mm radius CM.

(a) EC-VCSEL, (b) measurement system. (PD: photodiode).

To investigate the optical output characteristics of the EC-VCSEL using a CM with a short r of 5.08 ± 0.07 mm, we measured the optical power, polarization, RF spectra, optical spectra, and real-time waveforms of the optical output at different drive currents.

When the drive current of the VCSEL was increased gradually, stable optical output modulation sequences were produced at discrete current values. In Fig. 4.7, the stable modulation frequencies and polarization-resolved optical power are plotted against the drive

current. With increasing drive current, the modulation frequencies alternately changed between high (high f) and low (low f) values. The highest frequency, measured at a drive current of 6.95 mA, was 12.6 GHz. The corresponding L was calculated to be 5.95 mm. The DBR and substrate on the output side of the VCSEL (total thickness about 110 μm) are included in the EC. Even taking into account of the semiconductor, L should equal to r and be about 5.08 mm, which is 0.87 mm shorter than the calculated value (5.95 mm) from the modulation frequency. The reason for this length difference is not clear at the moment. As shown in Fig. 4.7 (b), when the modulations with high f were generated, the total output power increased sharply, which indicates that the composite cavity (VCSEL cavity and the EC) has high reflectivity at these wavelengths and the EC-VCSEL obtained higher net optical gain. Optical output of the EC-VCSEL was polarization resolved at the strongest and weakest polarization directions (at 20° and 110°). With increasing drive current, polarization switched between the currents at which low- f and high- f output modulations took place. As shown in Fig. 4.8, the polarizations at 6.83 mA (low f) and 6.99 mA (high f) were measured to be linear with 20.8° and 115.2° polarization directions, which were nearly orthogonal to each other. The reason why the polarizations were in these directions needs further investigation.

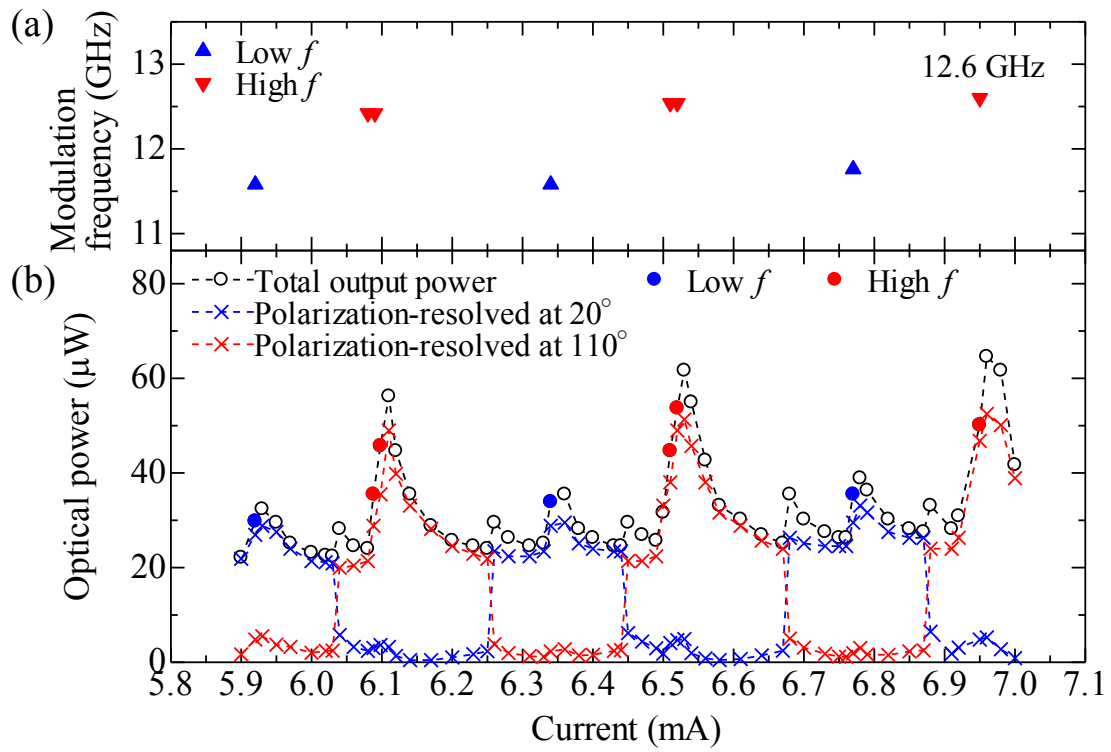


Fig. 4.7. Output modulation frequency (a) and optical power (b) as functions of drive current.

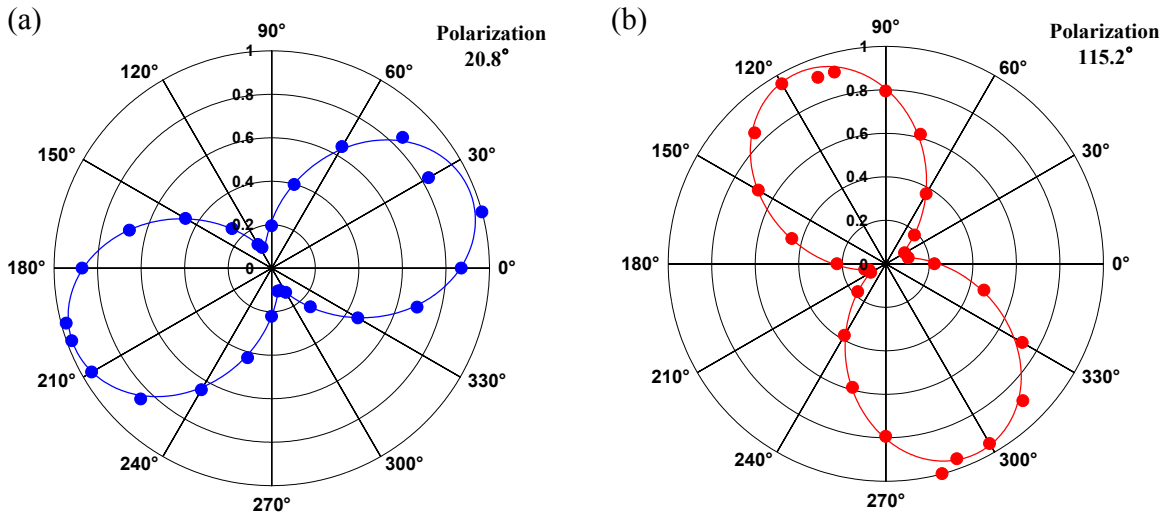


Fig. 4.8. Measured polarization of the modulated optical output.

(a) 6.83 mA (low f), (b) 6.99 mA (high f).

We measured the optical spectra of the output in detail while increasing the drive currents. Fig. 4.9 shows the change in the optical spectra from high- f modulation (6.51 mA) to low- f modulation (6.77 mA) and then to high- f modulation (6.95 mA). Spectra A, G, and M at the top and bottom of Fig. 4.9 are the measured spectra when output modulations were observed, and the four peaks in them correspond to the two-round-trip EC modes. When stable output modulation was observed, two modes (peaks 2 and 3) had nearly the same intensity and the intensities of the other two modes (peaks 1 and 4) were about 20 dB lower. The stronger two modes in the center were taken as the main modes of the EC-VCSEL lasing and the other two modes were sub-modes. This bi-modal characteristic was similar to the result reported in [3], which was explained by the assumption that the EC-VCSEL system operated in new eigenstates that were different from the free-running eigenstates of the VCSEL. The frequency differences between the two lasing modes were equal to the frequencies of the optical output modulations. When the drive current was increased from 6.51 mA (spectrum A), the shorter-wavelength peak 2 disappeared, the longer-wavelength peak 3 became dominant, and the wavelength of peak 3 increased with the drive current (spectra B-D). Then, at 6.68 mA (spectrum E) the main mode switched to the peak labeled 2 in spectrum A. There the wavelength shifted to that of the peak labeled 3 in spectrum A. This mode hopping coincided with the polarization switching shown in Fig. 4.7 (b). With further increase in the drive current (F), a new peak with the wavelength of peak 4 in spectrum A was observed, which is labeled 3 in spectra F and G. Output modulation

occurred when the two peaks had nearly the same intensity (G). Spectra G to M show the same changing procedure seen in the spectra from A to G. From these changes in the spectra, we concluded that the output modulation was due to the beat note of the two main EC modes, which was completely different from the polarization self-modulation in VCSEL with a longer EC.

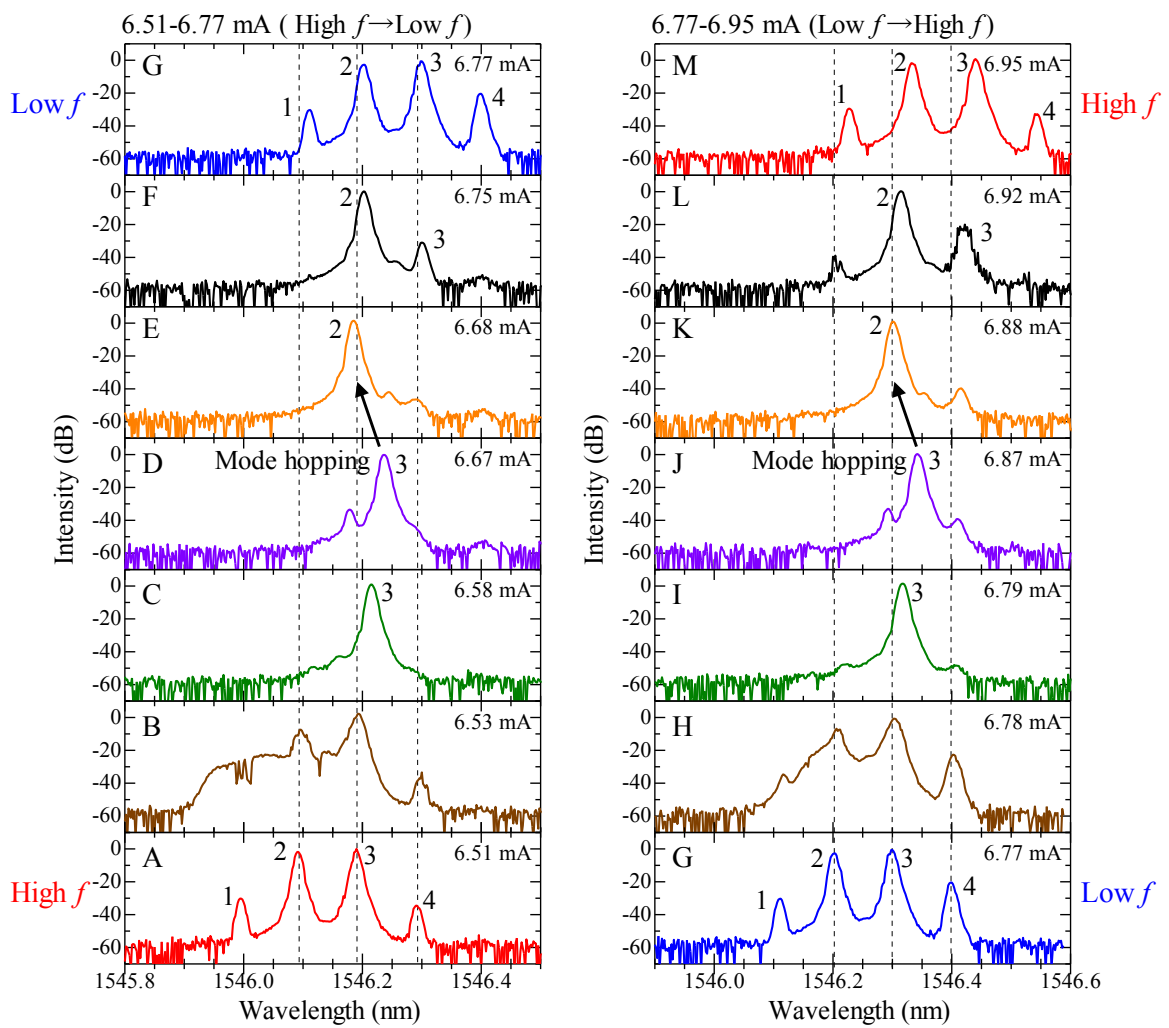


Fig. 4.9. Optical spectrum change with drive current increasing from 6.51 mA (high f) to 6.77 mA (low f) to 6.95 mA (high f).

The wavelengths of all peaks in the optical spectra shown in Fig. 4.9 are plotted against the drive current in Fig. 4.10. The black dots (●) show the wavelengths of the main modes of the EC-VCSEL. The crosses (×) show the wavelengths of the sub-modes of the EC-VCSEL. The red and blue lateral broken lines show the currents where high- f and low- f modulations occurred, respectively. Based on the wavelengths of the peaks at 5.92 mA (low f), the green lines, which show the drive current dependence of the EC modes, were drawn with an even interval of 0.092 nm. Connecting with the peaks at 6.09 mA (high f), the slope of the green lines was calculated to be 0.082 nm/mA. Due to the intra-cavity QWP, which coupled the two orthogonal polarization modes (0° and 90°) of the VCSEL between each other, the interval between the EC modes corresponded to two-round-trip in the EC. The red and blue triangles (▲ and ▲) are the measured wavelengths of the solitary VCSEL. The red and blue dotted lines are the least-square wavelength fittings of the solitary VCSEL. With increasing drive current, the temperature of the VCSEL increased, which led to an increase of the refractive index of the semiconductor and consequently an increase of the optical length of the VCSEL cavity. Thus the lasing wavelength shifted to the longer-wavelength side. The slope of the red and blue dotted lines were calculated to be about 0.541 nm/mA. The VCSEL was included in the EC. Therefore, the optical length of the EC also slightly increased with the increase of drive current. Because the EC length L was much longer than the VCSEL cavity, the wavelength change of the EC modes was much smaller than that of the solitary VCSEL. The wavelength change of the EC modes due to the increase

of temperature was calculated to be about 0.064 nm/mA, which was slightly smaller than the measured slope of the EC modes (green lines) 0.082 nm/mA in Fig. 4.10.

A high- f modulation was observed at 6.51 mA, which is indicated by the lower of the two red broken lines in Fig. 4.10. Two main EC modes lased with similar intensity at 6.51 mA. With increasing drive current, the EC-VCSEL began to lase with a single main mode and the lasing wavelength became longer because of the effect of the VCSEL cavity. The lasing wavelength gradually parted from the EC mode with which the EC-VCSEL initially lased. The lasing wavelength change was reduced by the affection of the EC, which is called mode pulling effect. Mode hopping accompanying polarization switching occurred at a certain current, as indicated by a black arrow. Then with further increase in the drive current, the sub EC mode on the longer-wavelength side became stronger. At 6.77 mA, two main EC modes began to lase with similar intensities and their beat note resulted in low- f modulation of the EC-VCSEL output. Between other drive currents where output modulations took place, the lasing wavelength showed the same changing procedure as that seen between 6.51 mA and 6.77 mA. Through the detailed measurement and analysis of the optical spectra of the EC-VCSEL, we clarified that the lasing wavelength and polarization were determined by the mode competition between the EC and the VCSEL cavity. When there were two main EC modes lasing at the same time with similar intensities, the beat note between them resulted in modulation of the EC-VCSEL output.

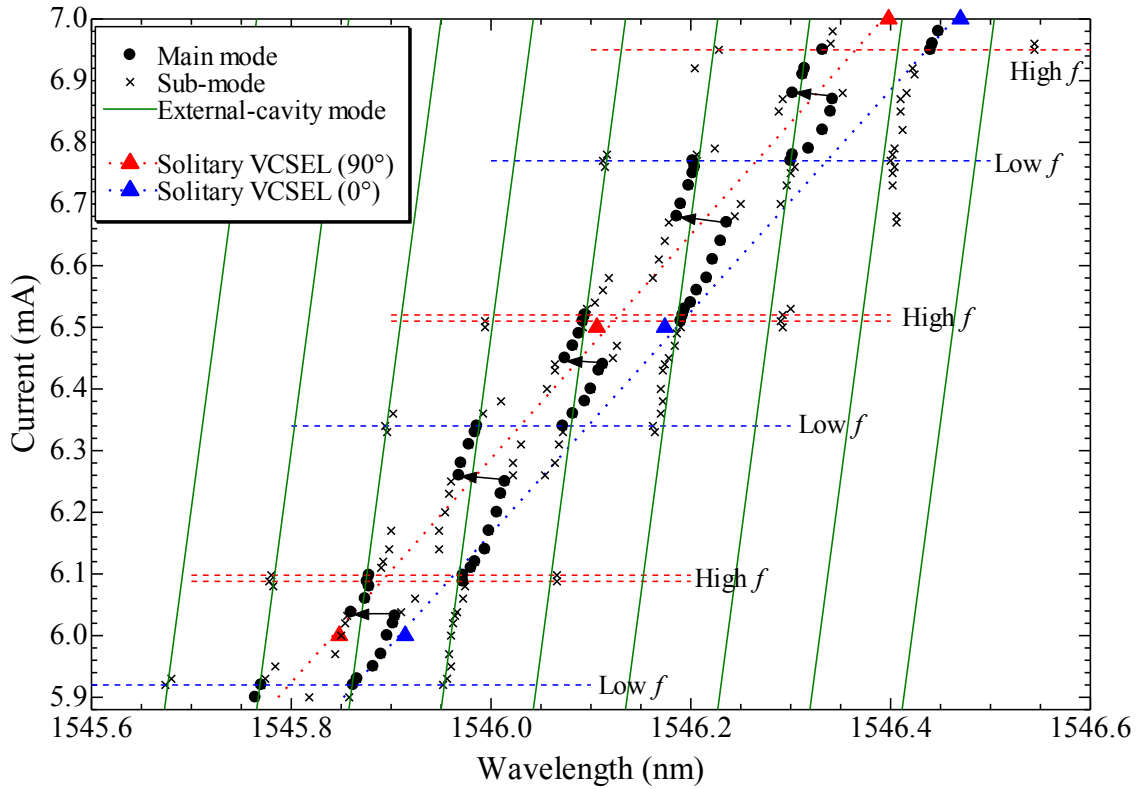


Fig. 4.10. Wavelength change of the peaks in the optical spectra with increasing drive current.

The output waveform was measured on the condition that output modulation was clearly observed. The modulation frequency of 12.52 GHz and the drive current of 6.97 mA were slightly different from the results shown in Fig. 4.7, because they were measured at a different time. Fig. 4.11 shows the waveform and the RF spectra of the total output power of the EC-VCSEL. The white line in Fig. 4.11 (a) shows a 12.52-GHz sinusoidal wave. The total output of the EC-VCSEL was sinusoidally modulated, which was consistent with its being due to beat note between two main EC modes. In the case of polarization self-modulation, for example the experimental result using the 20 mm radius CM, the two orthogonal polarization modes (0° and

90°) oscillated alternately as shown in Fig. 4.3 and the outputs were circularly polarized. The waveform of the total output shown in Fig. 4.11 (a) is sinusoidal and the polarization is linear as I mentioned, which are very different from the waveforms of the polarization self-modulation of the VCSEL.

Fig. 4.11 (b) shows the measured RF spectra. The single shot RF spectrum had a frequency of 12.45 GHz, which was in consistent with the waveform shown in Fig. 4.11 (a). The width at -20 dB was 2 MHz. As shown by the black line in Fig. 4.11 (b), the temporal stability of modulation frequency was evaluated by max hold mode of the spectrum. After been held for 30 seconds, the spectrum did not broaden anymore and had a width of about 40 MHz at -20 dB.

This is believed to be mainly caused by the mechanical instability.

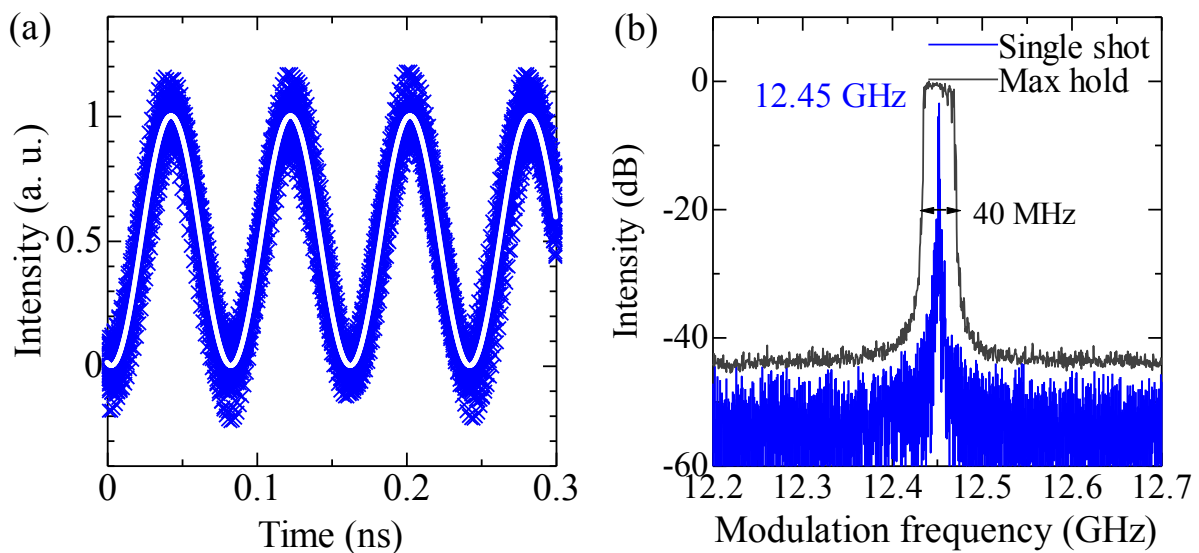


Fig. 4.11. Measured optical output of high- f modulation at 6.97 mA.
 (a) Waveform, white line: 12.52-GHz sinusoidal wave, (b) RF spectra.

From the measured optical spectra and waveforms, we confirmed that the output modulation was due to the beat note of two main EC modes that were selected by the VCSEL cavity. Theoretically, in the case of beat note between two optical waves with slightly different frequencies, modulation depth varies with the intensity ratio and polarization difference of the two optical waves. We calculated the modulation depths when the two optical waves have different intensities and the same polarization and showed the results with the black solid line in Fig. 4.12. In the experiment, when the optical output modulation was generated, the intensity ratio I_3/I_2 for peaks 2 and 3 in the optical spectra changed with small changes in the drive current. We obtained the modulation depths using the measured average optical power of PD input and the amplitudes of oscilloscope waveforms. The modulation depths measured at low- f modulation (blue dots, $I \approx 6.79$ mA) and high- f modulation (red dots, $I \approx 6.97$ mA) are plotted against I_3/I_2 in Fig. 4.12. Like the calculated results, the measured modulation depths were largest, 0.93 for the low- f modulation and 0.89 for the high- f modulation, when the two peaks had nearly the same intensity ($I_3/I_2 \approx 1$), and the modulation depth decreased with the increasing intensity difference between the two peaks. At around $I_3/I_2 \approx 2$, where the modulations had the highest stabilities, the polarization differences between peak 2 and peak 3 were measured to be about 13.7° for the low- f modulation and 20.7° for the high- f modulation. This is unlike the beat between two orthogonal modes as reported in [4]. With the consideration of these polarization differences, the calculated modulation depths decrease from 0.94 to 0.92 for low- f modulation

and 0.88 for high- f modulation. Thus the measured modulation depths at around $I_3/I_2 \approx 2$ were only about 0.05 lower than the calculated ones. This result strongly supports our assumption that the optical output modulation was due to the beat note of two main modes of the EC.

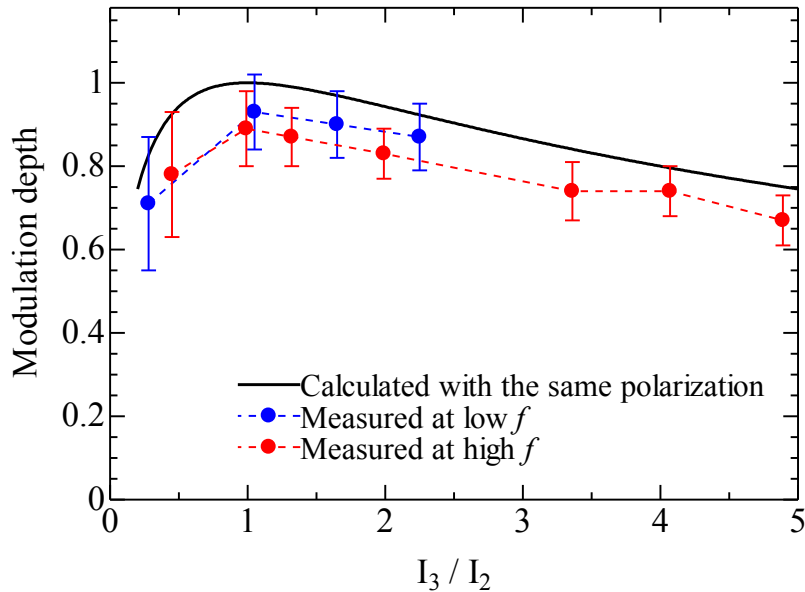


Fig. 4.12. Dependence of the measured modulation depth on the intensity ratio of peak 2 and peak 3.

In conclusion, high-frequency modulation of optical output, around 12 GHz, was observed in a new configuration of a short-EC-VCSEL using a CM and a thin-film QWP. The optical spectra showed two strong peaks, which were selected by the VCSEL cavity among the EC modes. Our detailed measurements and analysis revealed that the output modulation was the beat note between these two main EC modes having similar linear polarizations. This mechanism was different from the polarization self-modulation in VCSELs with longer ECs shown in Fig. 4.3. With increasing drive current, output modulation sequences with linear

polarizations orthogonal to each other and with frequencies alternately varied between low and high values were observed at discrete current values. The modulation depth of the lasing output was measured to be around 90%. Thus this configuration is potentially useful in high-speed applications.

4.3 Experiment using semi-spherical mirror

In the last section, we used a new configuration shortening the time delay of optical feedback in an EC-VCSEL by using a thin-film QWP and a short-radius CM as one end of the cavity. We obtained modulated optical output at around 12 GHz and found that the output modulation was due to the beat note between the two EC modes having similar polarizations, which was totally different from the polarization self-modulation in EC-VCSELs with longer EC length. To get further high-frequency output modulation, we chose a configuration using semi-spherical mirrors fabricated from small ball lens for the EC. Mirrors of this type are much more easily fabricated than short-radius CM, and supply a simple method to shorten L .

4.3.1 Fabrication of semi-spherical mirror

To get shorter L we used semi-spherical mirrors fabricated from commercially available short-radius ball lenses for the EC. The mirrors were fabricated from two ball lenses with

different r , 4 mm (Edmund #67-388) and 3 mm (Edmund #67-387). As shown in Fig. 4.13, firstly, one part of each ball lens was cut down to a certain thickness (t), 2.0 mm for the 4 mm radius ball lens and 1.0 mm for the 3 mm radius ball lens. After polishing the cutting surface, an anti-reflection (AR) coating was applied to the cutting surface. A 60% reflection coating was applied to the spherical surface. Fig. 4.14 shows the optical path between the mirror and the VCSEL. By adjusting the distance (d_2) between the semi-spherical mirror and the VCSEL, a greater part of the output light could be coupled to the VCSEL. The DBR and the substrate on the output side of the VCSEL (total thickness $d_3 \approx 110 \mu\text{m}$) introduces an optical length of longer than 0.3 mm. Thus, this thickness was also taken into consideration in the calculation of L . The thickness of the thin-film QWP was neglected here. On the basis of the thickness of semiconductor, the radius and thickness of the semi-spherical mirror, the effective L values were calculated to be about 4.6 mm for the mirror fabricated with the 4 mm radius ball lens and about 3.2 mm for that fabricated with the 3 mm radius ball lens. The optical length of the EC has slightly different values for the VCSEL output beams with different angles. The difference between the optical length of the EC when $\theta_1 = 1^\circ$ and $\theta_1 = 10^\circ$ was calculated to be 0.011 mm, for both the 4 mm radius and 3 mm radius semi-spherical mirrors. Compared to the value of the EC optical length, the EC optical length difference caused by the divergence of the VCSEL output beam was small enough that could be neglected.

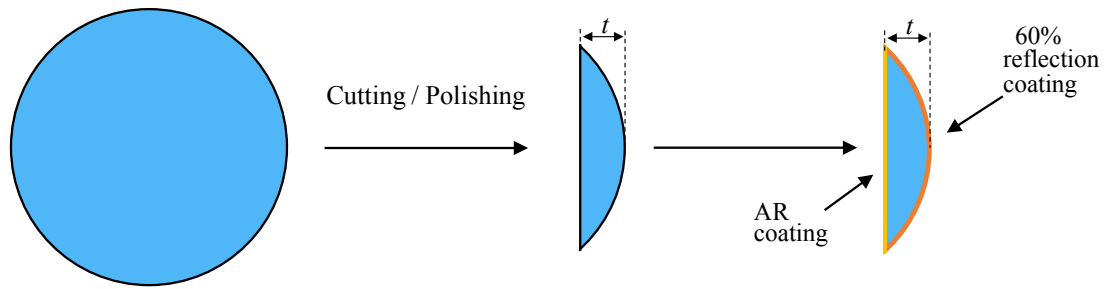


Fig. 4.13. Fabrication process of a semi-spherical mirror from ball lens.

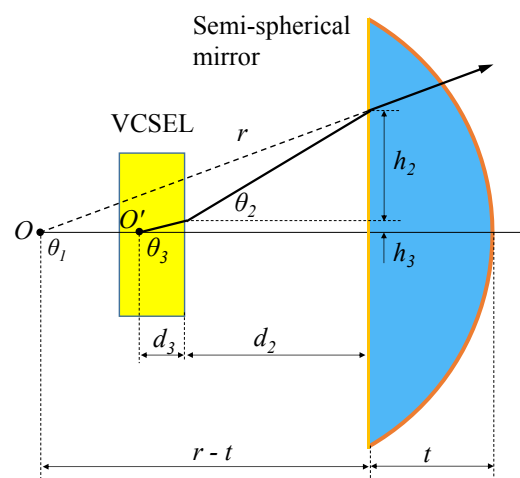


Fig. 4.14. Optical path between VCSEL and the semi-spherical mirror.

The schematic configuration of the EC-VCSEL using a semi-spherical mirror is shown in Fig. 4.15. The 1.55- μm VCSEL (Rev. 3.3 #932208) and the measurement system were the same to that used in the experiment with the 5.08 mm radius concave mirror. The optical output of the EC-VCSEL was characterized by using a 13-GHz real-time oscilloscope, an optical spectrum analyzer, and a 50-GHz RF spectrum analyzer. For conversion from optical to electrical signals we used 20-GHz PDs.

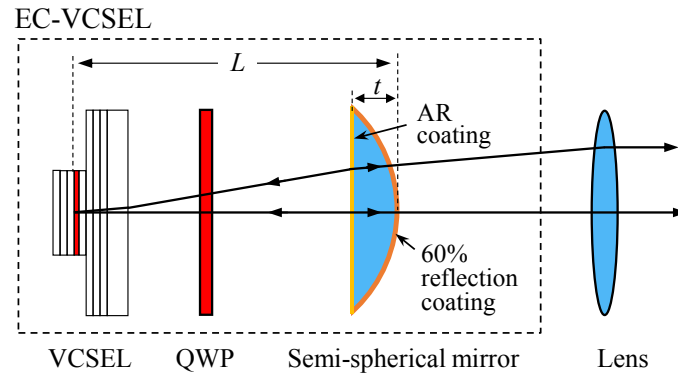


Fig. 4.15. Schematic configuration of EC-VCSEL using a semi-spherical mirror.

4.3.2 4 mm radius semi-spherical mirror

We used the semi-spherical mirror fabricated from the 4 mm radius ball lens for the EC. As shown in Fig. 4.16, we observed stable output modulations at discrete current values from 3 mA to 10 mA. When the drive current was further increased, the output modulations became unstable. The modulation frequency of the optical output alternately changed between high and low values. The highest frequency was about 13.7 GHz. The corresponding effective L was about 5.5 mm that is 0.9 mm longer than the calculated $L = 4.6$ mm. When the drive current was gradually increased from 6.0 and 7.5 mA, we measured the modulation frequency and optical power in detail as shown in Fig. 4.17. The output modulations were observed at discrete current values same as the results in Fig. 4.16. The optical output was polarization resolved at the strongest and weakest polarization angles, 20° and 110° . The polarization switched between the currents in which low- f and high- f modulations took place.

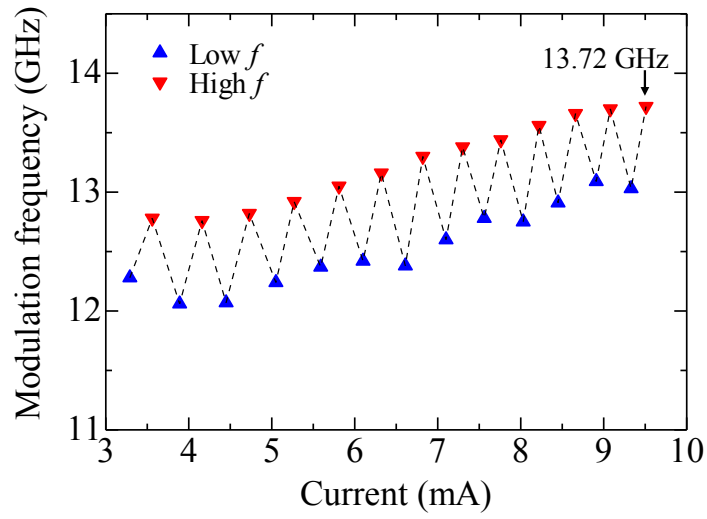


Fig. 4.16. Modulation frequencies measured from 3 mA to 10 mA.

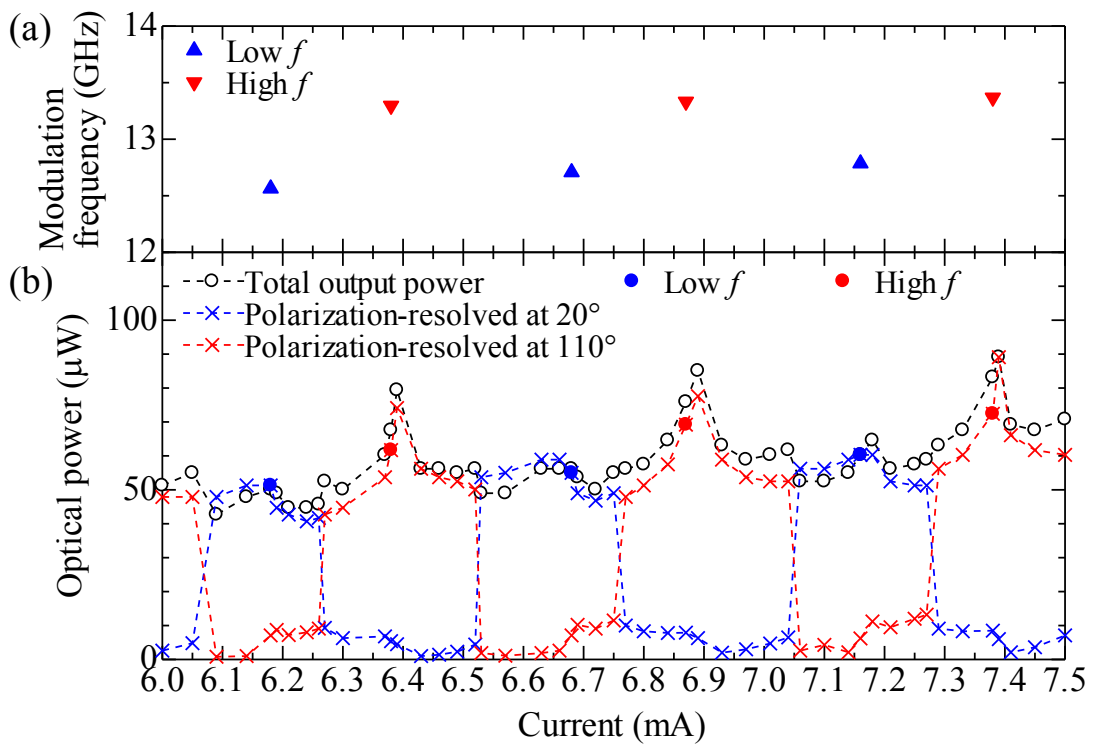


Fig. 4.17. Output modulation frequency (a) and optical power (b) as functions of drive current.

We measured the optical spectra while increasing the drive current and observed the same spectrum change to the experiment using the 5.08 mm radius CM. Fig. 4.18 shows the spectrum change from high- f modulation (6.87 mA) to low- f modulation (7.16 mA) and then to high- f modulation (7.38 mA). Output modulations occurred only when the spectra like A, G and M on top and bottom of the figure were observed. The four peaks in them corresponded to the two-round-trip EC modes. In each of them, the peaks 2 and 3 were the main modes and the others were the sub-modes. Frequency differences between the two main modes were equal to the corresponding optical output modulation frequencies. When the drive current was increased from 6.87 mA where a high- f modulation output was observed (spectrum A), the EC-VCSEL lased with a single main mode and the wavelength shifted to the longer-wavelength side. With further increase in the drive current, mode hopping occurred (spectrum D to E) which coincided with the polarization switching during the optical power measurement shown in Fig. 4.17. At spectrum G, a low- f modulation was observed. The spectrum change from low- f modulation (spectrum G, 7.16 mA) to high- f modulation (spectrum M, 7.38 mA) were the same to that from high- f modulation (spectra A, 6.87 mA) to low- f modulation (spectrum G, 7.16 mA).

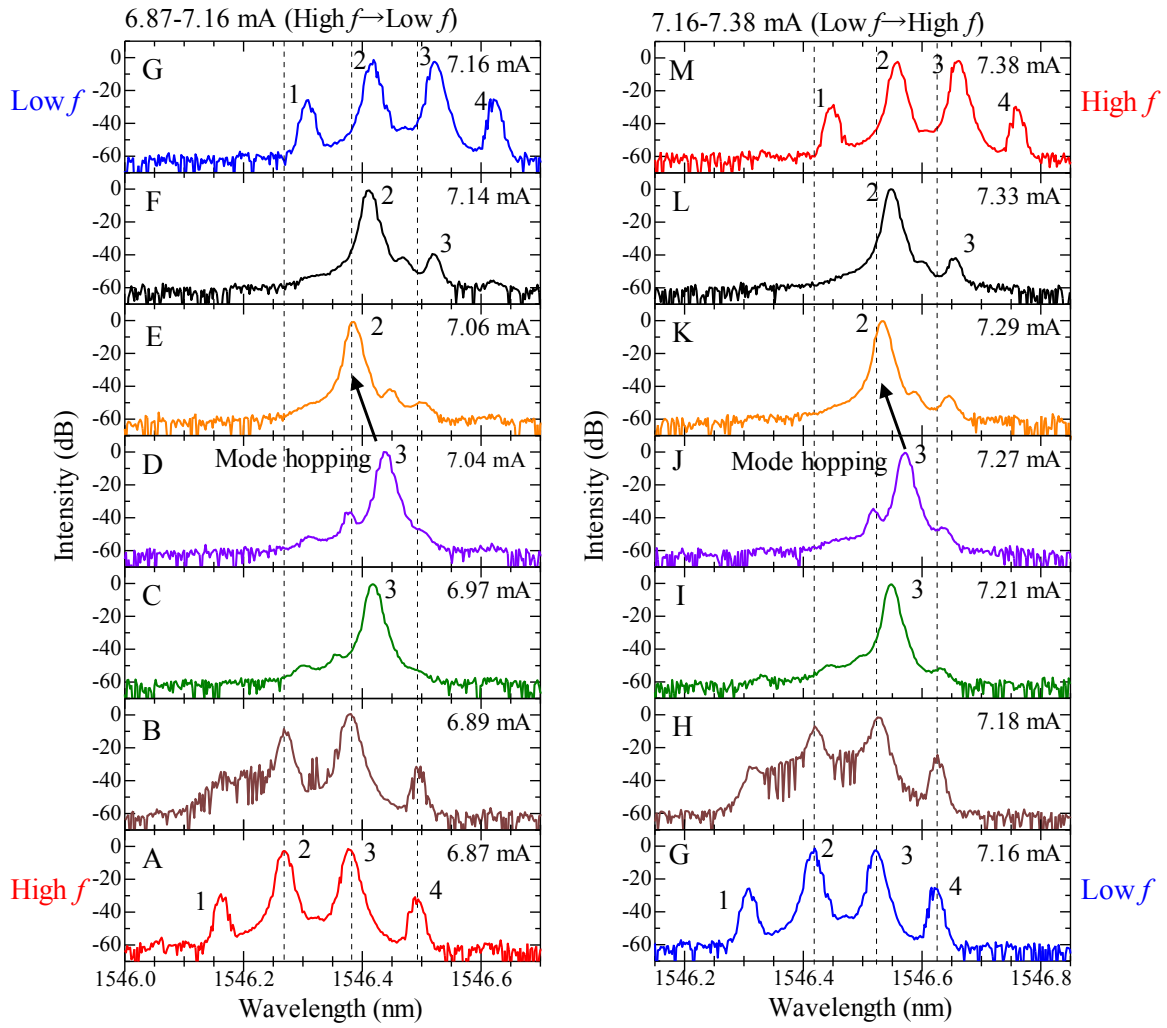


Fig. 4.18. Optical spectrum change with drive current increasing from 6.87 mA (high f) to 7.16 mA (low f) to 7.38 mA (high f) with 4 mm radius semi-spherical mirror for the EC.

The wavelengths of all peaks in the optical spectra measured from 6.0 mA to 7.5 mA are plotted against the drive current in Fig. 4.19. The black dots (\bullet) show the wavelengths of the main modes of the EC-VCSEL. The crosses (\times) show the wavelengths of the sub-modes of the EC-VCSEL. The red and blue lateral broken lines show the currents where high- f and low- f modulations occurred, respectively. The green lines show the wavelengths of the EC modes,

which depend on the drive current. The wavelength shift of the EC modes was partly due to the temperature change of the VCSEL with the increasing drive current as explained in Fig. 4.10. The red and blue triangles (▲ and ▲) show the measured wavelengths of the solitary VCSEL. The red and blue dotted lines are the least-square fitting of them.

At each lateral broken line, there are two black dots which indicates that there were two main EC modes lasing at the same time. When the drive current was increased from the values where output modulations occurred, the EC-VCSEL lased with single main mode and the wavelength gradually parted from the EC mode with which the EC-VCSEL initially lased. The lasing wavelength shift was reduced by mode pulling of the EC. As indicated by the black arrows, mode hopping accompanying polarization switching occurred at certain drive currents. With further increase of the drive current, two main EC modes lased at the same time which resulted in modulation of optical output. Through the detailed measurement and analysis of the optical spectra of the EC-VCSEL output, we clarified that the lasing wavelength and the polarization were determined by the mode competition between the EC and the VCSEL cavity. When the two main EC modes lased at the same time, the beat note between them resulted in modulation of the EC-VCSEL output.

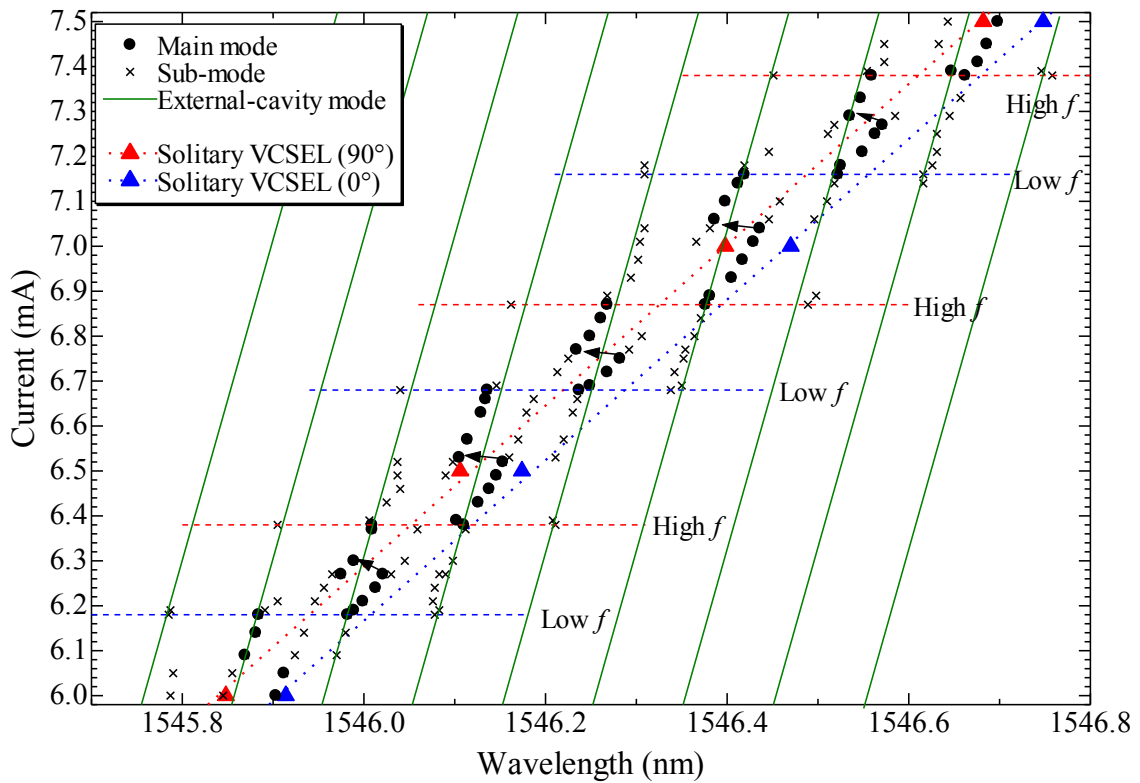


Fig. 4.19. Wavelength change of the peaks in the optical spectra with increasing current.

Fig. 4.20 (a) shows the measured waveform of high- f modulation at 7.38 mA and the white line shows a 13.4-GHz sinusoidal wave. The measured waveform fitted well with the white line, which is consistent with its being due to the beat note between two main EC modes. The linewidth of the RF spectrum shown in Fig. 4. 20 (b) was 3 MHz at -20 dB. The temporal stability of this RF spectrum was evaluated by max hold mode, which had a width of about 87 MHz at -20 dB intensity in 30 seconds and did not broaden any more. This is believed to be mainly caused by the mechanical instability.

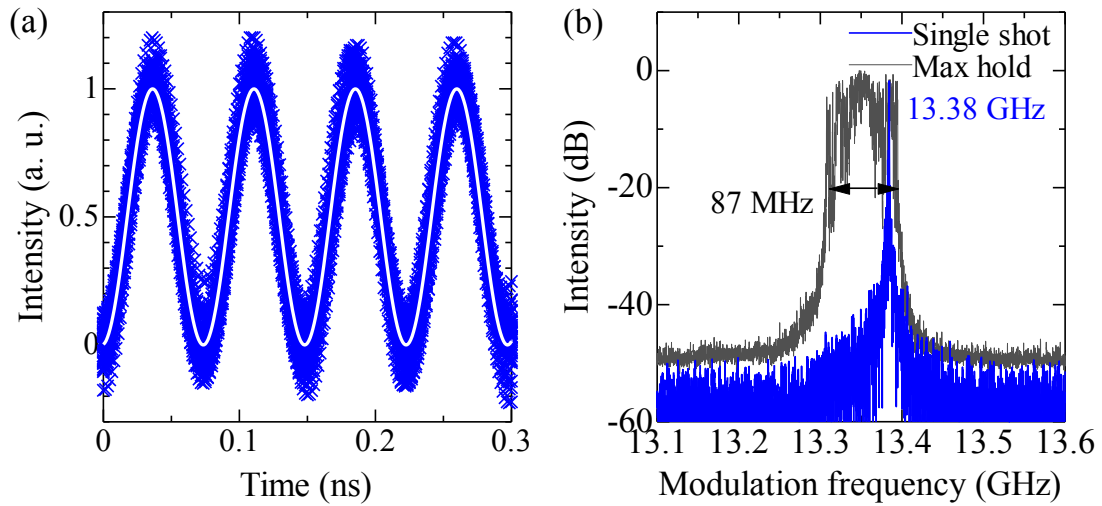


Fig. 4.20. Measured optical output modulation at 7.38 mA, using the 4 mm radius semi-spherical mirror. (a) Waveform and (b) RF spectrum of high- f modulation.

After calibrating the real-time oscilloscope and PD, we measured the modulation depths when the two main modes (peak 2 and 3 in optical spectrum) had different intensity ratios (I_3/I_2). The measured results were compared with the calculated modulation depths based on the simple beating model of two waves with the same polarization as shown in Fig. 4.21. When the two modes had nearly the same intensity, the measured modulation depths became largest, 0.86 for low f and 0.92 for high f . The modulation depths decreased as the intensity difference between the two modes increased. When the output had the highest modulation depths, the polarization differences between the two modes were measured to be about 1.0° for the low- f modulation and 11.3° for the high- f modulation. Taking these polarization differences into account, the measured modulation depths of low- f and high- f modulations were quite close to the calculated values, i.e., only 0.13 and 0.06 lower, respectively.

In conclusion, using a semi-spherical mirror which was simply fabricated from a 4 mm radius ball lens, we shortened the EC length and obtained optical output modulation of 13.7 GHz. Since the results shown in Figs. 4.17 - Fig. 4.21 had almost the same characteristics as those obtained with the 5.08 mm radius CM, we believed that this output modulation of EC-VCSEL with semi-spherical mirror was due to the beat note of the two main EC modes. The sinusoidally modulated lasing output and the results of modulation depth strongly supported our assumption.

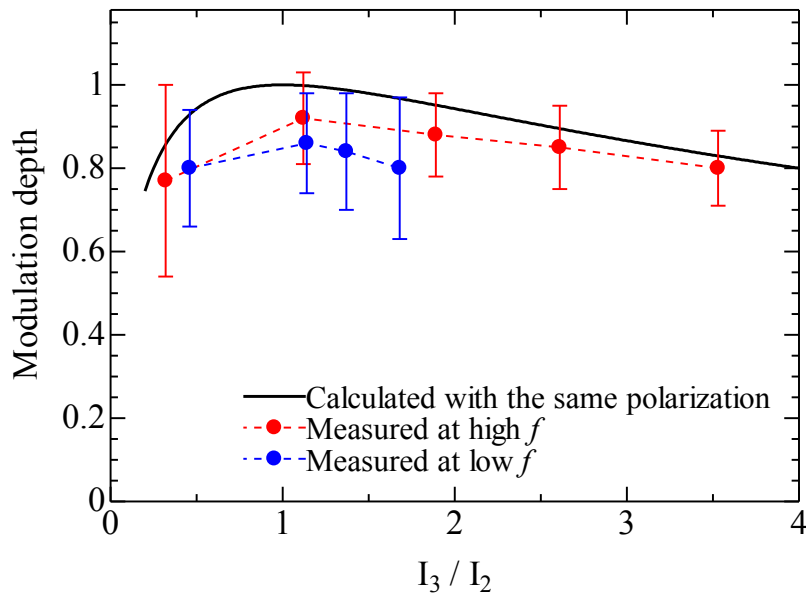


Fig. 4.21. Dependence of modulation depth on the intensity ratio of peak 2 and peak 3.

4.3.3 3 mm radius semi-spherical mirror

We also used the semi-spherical mirror fabricated from the 3 mm radius ball lens for the EC. Same measurements were carried out using this mirror as those for 4 mm radius semi-spherical

mirror. As shown in Fig. 4.22, with this semi-spherical mirror, we obtained output modulation of up to 15.3 GHz during the increasing of current from 3 mA to 10 mA. Output modulations were observed at discrete current values and the modulation frequency alternately changed between low and high values.

As shown in Fig. 4.23, in the detailed measurement of modulation frequency and optical power from 6.0 mA to 7.8 mA, optical output was polarization resolved at the strongest and weakest polarization directions, 145° and 55° . Polarizations of the low- f and high- f modulation outputs were orthogonal to each other. The polarization switched between the currents at which low- f and high- f modulations took place.

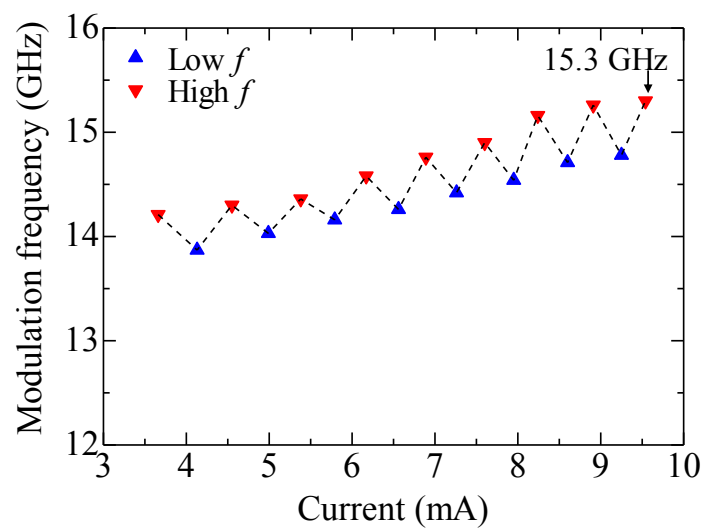


Fig. 4. 22. Modulation frequencies measured from 3 mA to 10 mA.

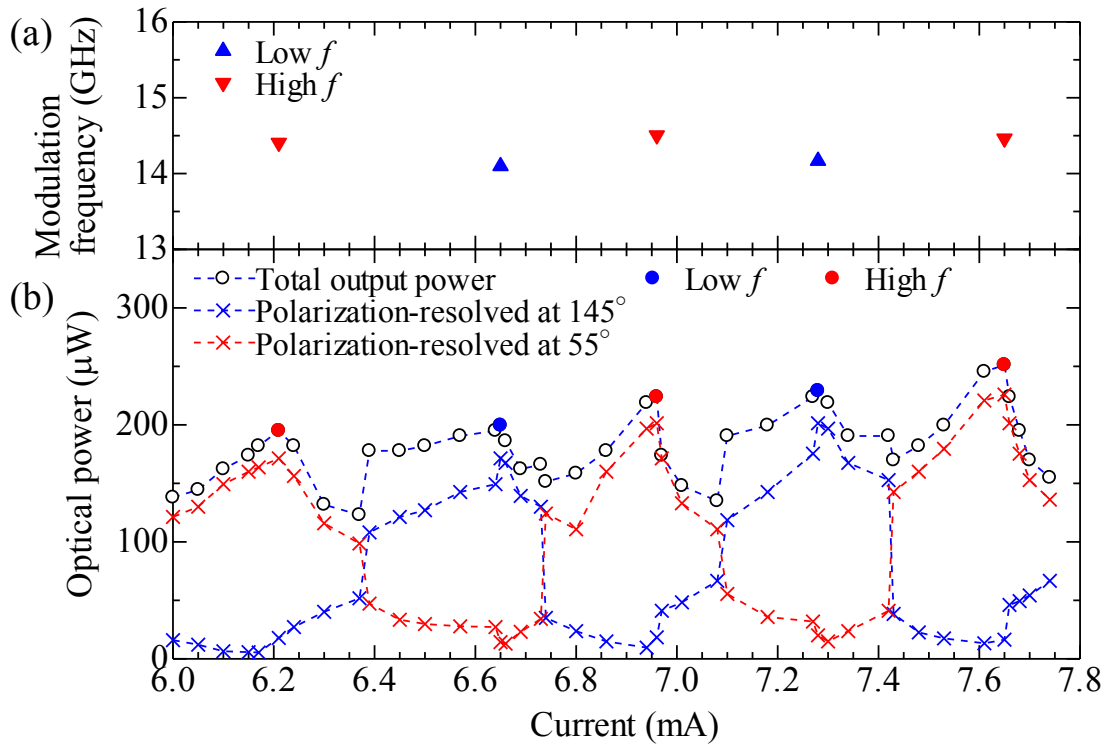


Fig. 4.23. Output modulation frequency (a) and optical power (b) as functions of drive current.

Fig. 4.24 shows the spectrum change when the current was increased from high- f modulation (6.96 mA) to low- f modulation (7.28 mA) and then high- f modulation (7.65 mA). When output modulations were observed, the spectra showed a bi-modal characteristic (spectra A, G and M). In these spectra, there were four peaks corresponding to two-round-trip EC modes. The two main modes were lasing with similar intensities and the other two sub-modes were about 35 dB lower. This intensity difference (35 dB) was larger than that in the spectra using 5.08 mm radius CM. Due to the larger frequency interval of the EC modes, the sub-modes on both sides got further from the center of the gain spectrum. When the current was increased from 6.96 mA (spectra A) where high- f modulation occurred, the EC-VCSEL lased with a single

main mode and the wavelength increased with the current. Mode hopping occurred between spectrum D and E accompanying with polarization switching. With further increase in the current, another mode on the longer-wavelength side became to lase, and low- f modulation was observed due to the beat note of the two main modes at spectrum G. Spectra G to M showed the same changing process with increasing current.

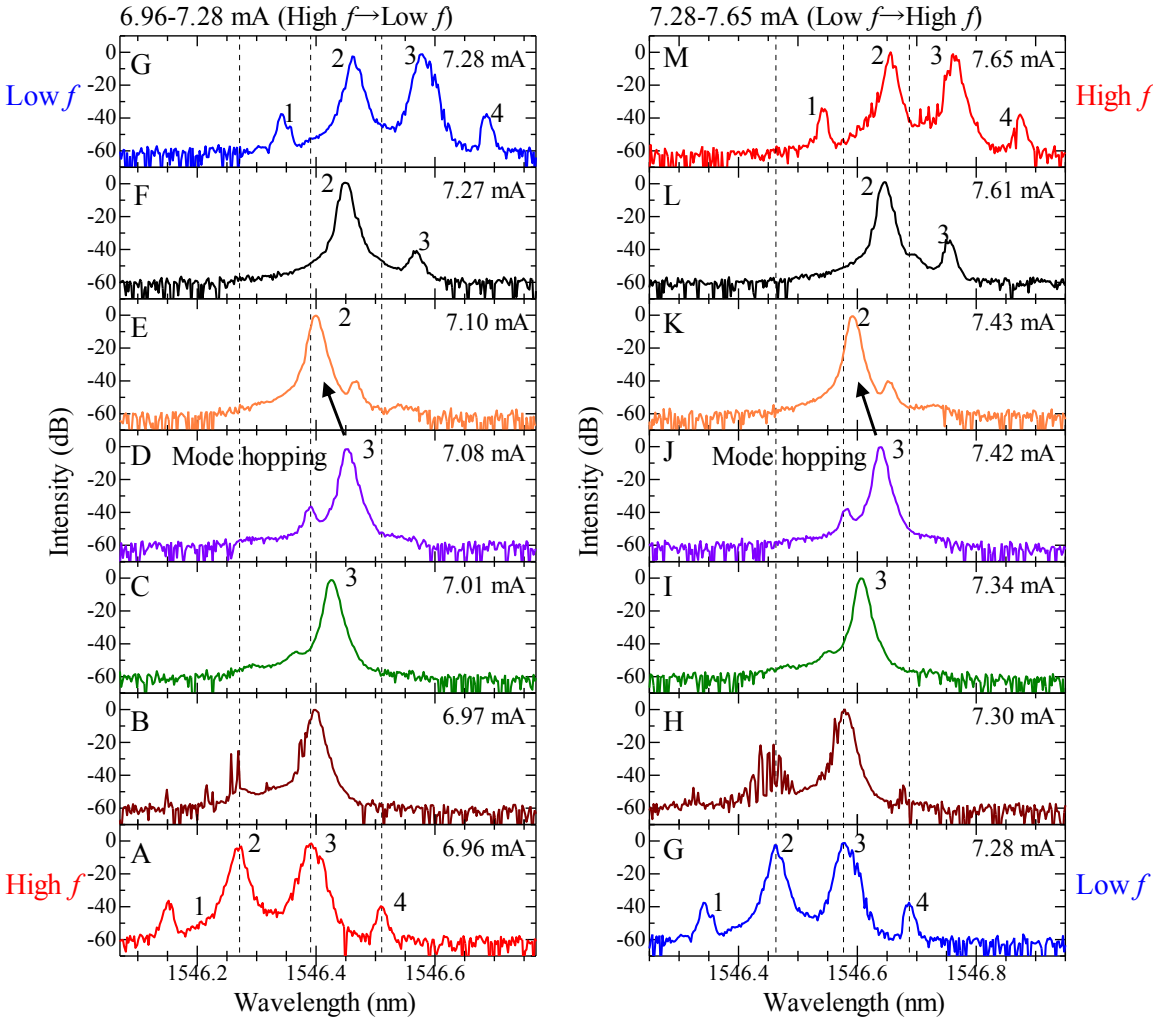


Fig. 4.24. Optical spectrum change with drive current increasing from 6.96 mA (high f) to 7.28 mA (low f) to 7.65 mA (high f) with 3 mm radius semi-spherical mirror for the EC.

The wavelengths of all peaks in the optical spectra measured from 6.0 mA to 7.8 mA are plotted against the drive current in Fig. 4.25. The black dots (●) show the wavelengths of the main modes of the EC-VCSEL. The crosses (×) show the wavelengths of the sub-modes of the EC-VCSEL. The red and blue lateral broken lines show the currents where high- f and low- f modulations occurred, respectively. The green lines show dependence of the EC modes on the drive current. The wavelength shift of the EC modes was partly due to the temperature change with the increasing drive current as explained before. The red and blue triangles (▲ and ▲) show the measured wavelengths of the solitary VCSEL. The red and blue dotted lines are the least-square fitting of them.

At each lateral broken line, there are two black dots which indicates that there were two main EC modes lasing at the same time. When the drive current was increased from the values where output modulations occurred, the EC-VCSEL lased with a single main mode and the wavelength gradually parted from the EC mode with which the EC-VCSEL initially lased. The lasing wavelength shift was reduced by mode pulling of the EC. As indicated by the black arrows, mode hopping accompanying polarization switching occurred at certain drive currents. With further increase of the drive current, two main EC modes lased at the same time which resulted in modulation of optical output. Through the detailed measurement and analysis of the optical spectra of the EC-VCSEL output, we clarified that the lasing wavelength and the polarization were determined by the mode competition between the EC and the VCSEL cavity.

When the two main EC modes lased at the same time, the beat note between them resulted in modulation of the EC-VCSEL output.

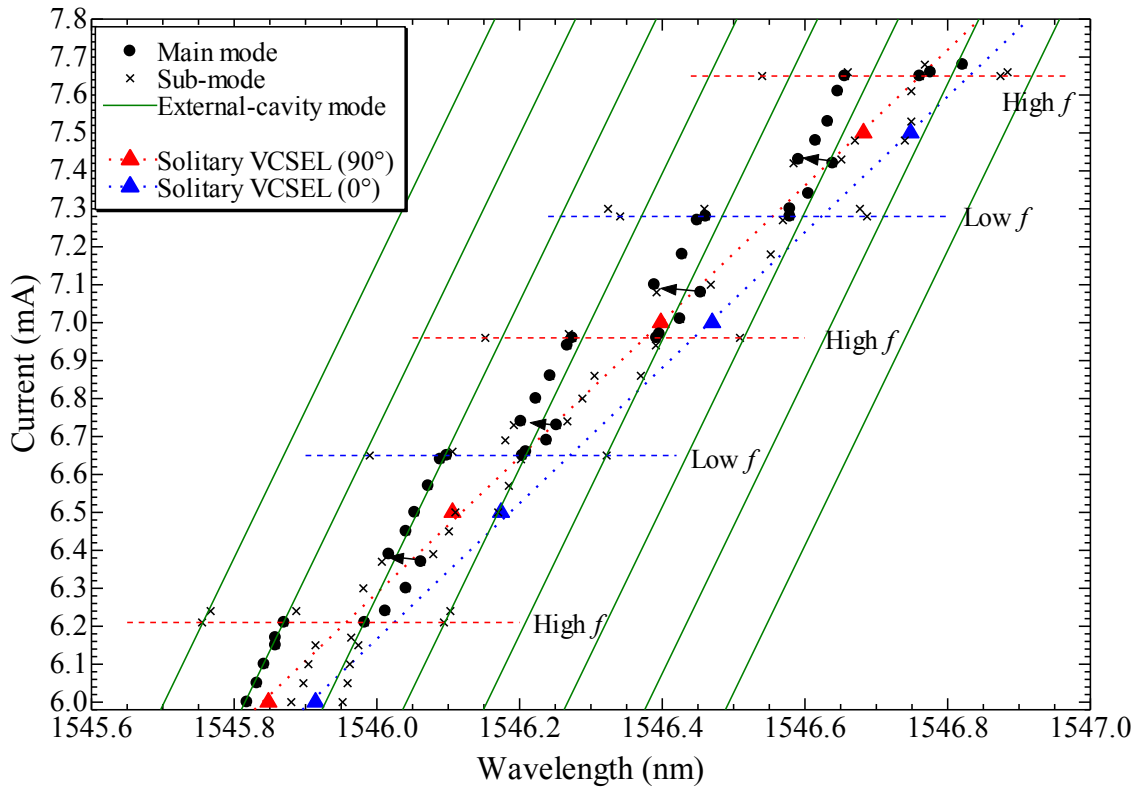


Fig. 4.25. Wavelength change of the peaks in the optical spectra with increasing current.

Fig. 4.26 shows the optical and RF spectra of the output modulation with the highest modulation frequency of 15.3 GHz. However, we could not measure the waveform and the modulation depth due to the bandwidth limitation of the real-time oscilloscope. The optical spectrum in Fig. 4.26 (a) is slightly noisy, because this spectrum was observed at the highest drive current 9.54 mA in the range that the modulations were observed as shown in Fig. 4.22.

The RF spectrum in Fig. 4.26 (b) is shown in a range of 25 GHz. There is only one peak in this wide range, from which we can know that the corresponding waveform is sinusoidal. Since the measurement results of modulation frequency, optical power, and the optical spectra had almost the same characteristics as those using 5.08 mm radius CM, we believed that these output modulations of EC-VCSEL with 3 mm radius semi-spherical mirror were due to the beat note of the two main EC modes.

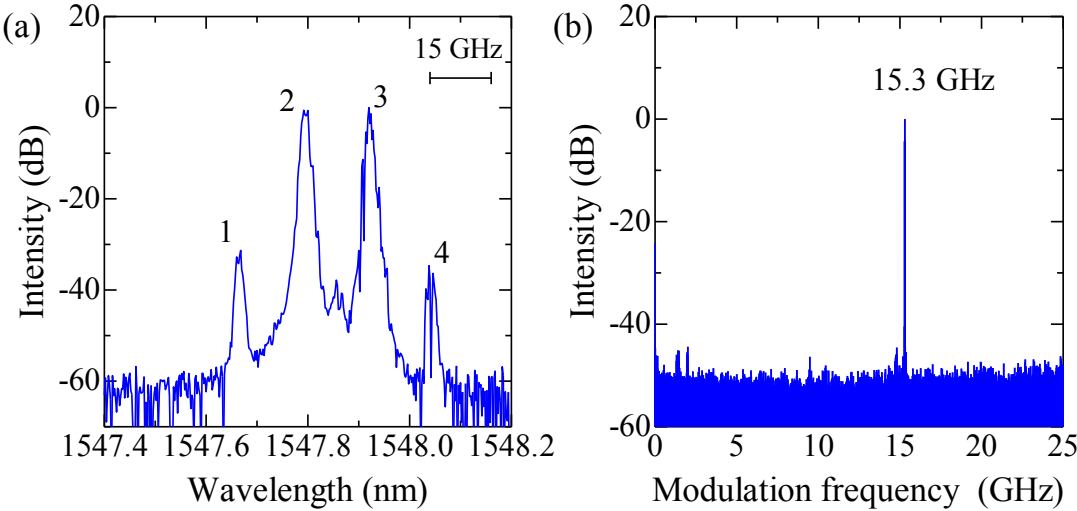


Fig. 4.26. Measured optical output modulation at 9.54 mA, using the 3 mm radius semi-spherical mirror. (a) Optical spectrum and (b) RF spectrum.

4.4 Conclusion

Aiming at higher-frequency self-modulation in EC-VCSEL, we used new configurations shortening the EC length by using short radius CMs and semi-spherical mirrors instead of the planar mirror for the EC. With the 3 mm radius semi-spherical mirror, we obtained high-frequency self-modulations of up to 15.3 GHz.

With a CM having a radius of 20 mm, a pulse sequence having a frequency of about 3.5 GHz was generated based on the well-known polarization self-modulation. This proved the feasibility of CM been used as one end of the EC. When the radius of CM was shortened to 5.08 mm, sinusoidal modulations with frequencies of about 12 GHz were generated. With changing drive current, stable modulation sequences with periodic changes in the modulation frequency and polarization direction were observed at discrete current values. We found that two main EC modes, whose frequencies were separated by nearly $c/4L$, were selected to oscillate and the beat note of them resulted in modulation of the output.

Self-modulations of up to 15.3 GHz in EC-VCSELs were obtained using semi-spherical mirrors fabricated from small ball lens. The results showed us a new and simple method for high-frequency self-modulation by further reduction of the EC length L . Therefore, we conclude that the configurations are potentially useful for generation of high-speed optical signals.

4.5 References

- [1] T. Katayama, Y. Sato, T. Mori, and H. Kawaguchi, "Polarization bistable characteristics of 1.55 μm vertical-cavity surface-emitting lasers," *Jpn. J. Appl. Phys.*, vol. 46, no. 49, pp. L1231-L1233, 2007.
- [2] S.-J. Jiang, Z.-Q. Pan, M. Dagenais, R. A. Morgan, and K. Kojima, "High-frequency polarization self-modulation in vertical-cavity surface-emitting lasers," *Appl. Phys. Lett.*, vol. 63, no. 26, pp. 3545-3547, 1993.
- [3] H. Li, A. Hohl, A. Gavrielides, H. Hou, and K. D. Choquette, "Stable polarization self-modulation in vertical-cavity surface-emitting lasers," *Appl. Phys. Lett.*, vol. 72, no. 19, pp. 2355-2357, 1998.
- [4] G. Ropars, P. Langot, M. Brunel, M. Vallet, F. Bretenaker, A. Le Floch, and K. D. Choquette, "Experimental evidence of single round-trip oscillation in polarization self-modulated vertical-cavity surface emitting lasers," *Appl. Phys. Lett.*, vol. 70, no. 20, pp. 2661-2663, 1997.

Chapter 5 Simulation of Pulse Generation using EC-VCSEL

5.1 Introduction

Through the experimental results, we knew that polarization self-modulation became impossible when the EC length L was shortened. Aiming at high-frequency pulse generation by polarization self-modulation, we simulated the polarization self-modulation in EC-VCSEL to investigate the factors that limit the operation of polarization self-modulation.

Several different models were used for simulation of the polarization self-modulation in lasers with ECs. Spin-Flip model [1], Lang-Kobayashi model [2], and Two-Mode Gain Saturation model [3] are the mostly used models. The Spin-Flip model is a four-level model which takes account of the polarization of the laser field by including the spin sublevels of the conduction and valence bands of semiconductor. This model allows the introduction of vector rate equations which account for the polarization degree of freedom of the surface-emitting laser emission [4]-[6]. Lang-Kobayashi model can describe a single longitudinal mode EEL subject to a weak to moderate external optical feedback. It is usually used in the investigation of polarization self-modulation in EELs [7]-[8]. The Two-Mode Gain Saturation model describes the operation status of two modes through gain saturation.

In our research, we investigate the polarization self-modulation in EC-VCSEL with a Two-

Mode Gain Saturation model built in the previous research of our group [9]. The parameters in this well-built model can be easily changed. This two-mode model can be seen as the expansion of the one-mode Lang-Kobayashi model. We believed that the polarization self-modulation in VCSELs is not related to the spin dynamics, thus the Spin-Flip model was not adopted. Pulse generation by polarization self-modulation in EC-VCSEL using VCSELs with different gain saturation coefficients were compared, from the viewpoints of both the highest frequency of polarization self-modulation and the waveform of the pulses. Effects of the optical feedback intensity and the carrier pump rate on the pulse generation were also discussed.

5.2 EC-VCSEL model

5.2.1 Model conception

The conception of an EC-VCSEL is shown in Fig. 5.1. Description of the light in the EC-VCSEL is given in Table 5.1. The EC-VCSEL is formed by a VCSEL and a partial mirror with a reflectivity of R_3 . The length of the EC is L . A QWP is inserted in the EC with its optical axes oriented at 45° according to the polarization of VCSEL lasing. The VCSEL can lase with either a 0° or 90° polarization mode, which is assigned to be X mode or Y mode in the calculations using two-mode rate equations. Though the VCSEL shown in Fig. 5.1 has a structure similar to the real device, it is considered to be an infinitesimal point in the calculation. The active region

of the VCSEL is shown with point A, which has a photon density of $S(t)$ and a phase of $\phi(t)$. The light goes through the output-side DBR with a power reflectivity of R_1 is shown with point B, whose photon density is weakened to be $S(t) \times (1 - R_1)$ by the reflection of DBR. On the assumption that the VCSEL is an infinitesimal point, the thickness of the DBR is neglected and no phase change occurred to the light during transmission in the DBR. After one-round trip in the EC, part of the light is reflected back to the VCSEL with its polarization rotated by 90° . The photon density at point C becomes $S(t - \tau) \times (1 - R_1) \times R_3$. The light is delayed by τ in time, which causes a phase change of $\omega\tau$. Here, ω represents the lasing angular frequency of the VCSEL. After goes through the DBR into the VCSEL cavity, the feedback light at point D will change the photon density and phase of the mode with the orthogonal polarization to A.

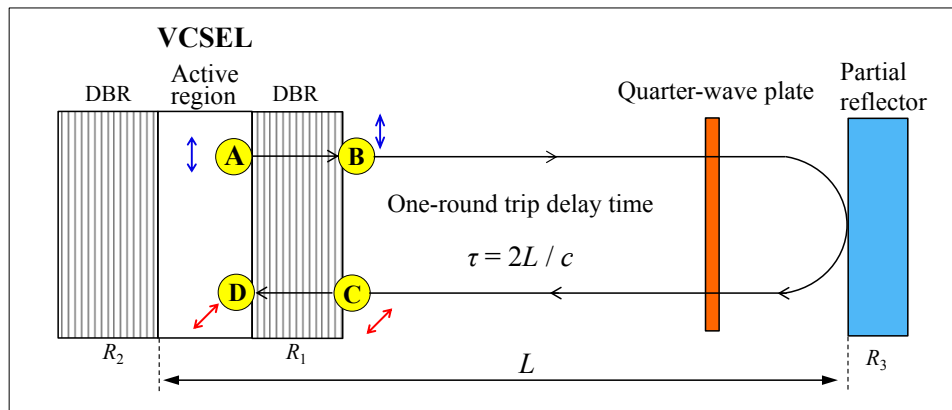


Fig. 5.1. Concept of feedback from the EC.

Table 5.1. Description of light in the EC-VCSEL in Fig. 5.1

Position	Polarization	Photon density	Phase
A	90° (0°)	$S(t)$	$\phi(t)$
B	90° (0°)	$S(t) \times (1-R_1)$	$\phi(t)$
C	0° (90°)	$S(t-\tau) \times (1-R_1) \times R_3$	$\phi(t-\tau) - \omega\tau$
D	0° (90°)	$S(t-\tau) \times (1-R_1) \times R_3 \times (1-R_1)$	$\phi(t-\tau) - \omega\tau$

5.2.2 Rate equations

In the past research of our group, the operation of high-speed optical memory based on polarization bistable VCSEL was successfully simulated using well built two-mode rate equations [9]. In the present work, we aim to analyze the pulse generation by self-modulation in EC-VCSEL using as simple a model as possible. Thus we referred the model in [9] and modified the optical injection to be the polarization-rotated feedback from the EC. The model is based on the assumption that there are two orthogonally polarized optical fields. The model can include the following two important phenomena: the polarization-rotated optical feedback to the VCSEL cavity and the cross-gain saturation between the two optical fields with orthogonal polarization.

The operation of the polarization bistable VCSEL can be expressed by the following variables: N , the carrier density in the active layer; S_x , the photon density for the 90° polarization (X mode) in the cavity; S_y , the photon density for the 0° polarization (Y mode) of

the optical field in the cavity; ϕ_X , the phase of the X mode in the cavity; and ϕ_Y , the phase of the Y mode in the cavity. The carrier angular frequencies ω_X and ω_Y are different. The EC is long enough compared to the lasing wavelength, so we assumed that standing wave could rise for both of the two modes simultaneously in the EC. The lasing wavelength difference between the two modes was neglected for the phase change of the light in the EC.

The rate equation for N is expressed as

$$\frac{dN}{dt} = P - \frac{N}{\tau_s} - v_G g_{NX} \zeta_X \times (N - N_{TR}) S_X - v_G g_{NY} \zeta_Y \times (N - N_{TR}) S_Y \quad (5-1)$$

where P , τ_s , v_G , and N_{TR} represent the carrier pump rate, carrier lifetime, group velocity of the light in the cavity, and transparency carrier density, respectively. g_{NX} and g_{NY} represent the differential gain of the two polarization modes X and Y, which have different values in our model. ζ_X and ζ_Y represent the degree of the gain suppression that will be given by (5-4) and (5-5). The first and second terms on the right-hand side of (5-1) represent the carrier injection and carrier relaxation, respectively, while the remaining terms represent the stimulated recombination by the two polarization modes.

The rate equations for the photon densities are expressed as

$$\frac{dS_X}{dt} = \Gamma v_G g_{NX} \zeta_X \times (N - N_{TR}) S_X - \frac{S_X}{\tau_p} + \frac{\sqrt{S_X \times R_3 (1 - R_1) S_Y (t - \tau)}}{\tau_c} \cos(\psi_X) + \beta \frac{N}{\tau_s} \quad (5-2)$$

$$\frac{dS_Y}{dt} = \Gamma \nu_G g_{NY} \zeta_Y \times (N - N_{TR}) S_Y - \frac{S_Y}{\tau_P} + \frac{\sqrt{S_Y \times R_3 (1 - R_1)} S_X(t - \tau)}{\tau_C} \cos(\psi_Y) + \beta \frac{N}{\tau_S} \quad (5-3)$$

where Γ , τ_P , $1/\tau_C$ and β represent the confinement factor, photon lifetime, rate of optical injection, and spontaneous emission factor, respectively. R_1 and R_3 represent the reflectivity of the output-side DBR of VCSEL and the partial reflector for the EC. $R_3(1 - R_1)S_Y(t - \tau)$ and $R_3(1 - R_1)S_X(t - \tau)$ represent the photon densities of the feedback light. After one-round trip in the EC, polarization of the Y mode will be rotated by 90° to be X mode. This polarization rotated feedback light will have an affection on the dynamics of the photon density of the X mode, and vice versa. The first, second, third, and fourth terms on the right-hand side of (5-2) and (5-3) represent the stimulated emission, loss in the cavity, optical feedback, and spontaneous emission, respectively. ν_G , Γ , τ_P , $1/\tau_C$, and β for the X mode are assumed to be equal to those for the Y mode, respectively, because the cross-sectional structure of the polarization bistable VCSEL is spatially symmetric. The degrees of the gain suppression are expressed as

$$\zeta_X = 1 - \varepsilon_{XX} S_X - \varepsilon_{XY} S_Y \quad (5-4)$$

$$\zeta_Y = 1 - \varepsilon_{YX} S_X - \varepsilon_{YY} S_Y \quad (5-5)$$

where ε_{XX} and ε_{YY} represent the self-gain saturation coefficients, ε_{XY} and ε_{YX} represent the cross-gain saturation coefficients. These coefficients express the gain suppression effects

by hole burning or the increase of the effective temperature of the electrons. The self and cross-gain saturation coefficients can be assumed to be isotropic because of the symmetric VCSEL structure. The cross-gain saturation coefficients are expected to be larger than the self-gain saturation coefficients for a wide wavelength range around the lasing wavelength [10]. The polarization bistability of the VCSEL is expected to occur when $\varepsilon_{XX}\varepsilon_{YY} < \varepsilon_{XY}\varepsilon_{YX}$ [11]. The temporal changes of ϕ_X and ϕ_Y are expressed as

$$\frac{d\phi_X}{dt} = \frac{1}{2}\alpha\Gamma\nu_G g_{NX}\zeta_X \times (N - N_{SS}) + \frac{1}{2\tau_C} \sqrt{\frac{R_3(1-R_1)S_Y(t-\tau)}{S_X}} \sin(\psi_X) + 2\pi \times \Delta f \quad (5-6)$$

$$\frac{d\phi_Y}{dt} = \frac{1}{2}\alpha\Gamma\nu_G g_{NY}\zeta_Y \times (N - N_{SS}) + \frac{1}{2\tau_C} \sqrt{\frac{R_3(1-R_1)S_X(t-\tau)}{S_Y}} \sin(\psi_Y) \quad (5-7)$$

where α and N_{SS} represent the linewidth enhancement factor and the carrier density in the steady state, respectively. The first terms on the right-hand side of (5-6) and (5-7) represent the shifts of the resonance frequencies accompanied by the change in the carrier density, while the second terms represent the phase changes induced by the optical feedback. Birefringence of the semiconductor material is considered to be the source of phase difference between the two polarization modes. This effect is expressed by the frequency difference $2\pi \times \Delta f$ between the X and Y modes, and added only in one of the two equations for the temporal changes of phase. Δf was set to be 0 GHz in the calculations for simplification.

The difference between the phase of the feedback light and the phase of the VCSEL lasing

for the two modes are expressed as

$$\psi_X = [\phi_Y(t - \tau) - \omega_Y \tau] - \phi_X(t) \quad (5-8)$$

$$\psi_Y = [\phi_X(t - \tau) - \omega_X \tau] - \phi_Y(t) \quad (5-9)$$

where τ is the one-round trip delay time in the EC. $\omega_X \tau$ and $\omega_Y \tau$ stand for the phase change after in one-round trip of the EC.

The rate of optical injection $1/\tau_C$ and the photon lifetime τ_p are related to the cavity structure parameters as in [12]:

$$\frac{1}{\tau_C} = \frac{\nu_G}{L_{eff}} \sqrt{1 - R_1} \quad (5-10)$$

$$\frac{1}{\tau_p} = \frac{2\pi c}{\lambda} \frac{1}{Q} = \nu_G \left(\alpha_{INT} + \frac{1}{L_{eff}} \ln \frac{1}{\sqrt{R_1 R_2}} \right) \quad (5-11)$$

Here, L_{eff} is the effective length of the VCSEL cavity and is related to the spatial distribution of the optical field along the cavity. R_1 and R_2 are the reflectivity of the DBRs on the output side and the opposite side, respectively. α_{INT} represents the internal loss in the cavity.

The parameter values in Table 5.2 were assumed. These values except for g_{NX} and g_{NY} were the same to those used in Ref. [9] for a 0.98- μm VCSEL. From these parameters values, the optical injection rate into the VCSEL cavity $1/\tau_C$ was calculated to be about $1.0 \times 10^{13} \text{ s}^{-1}$ and the photon lifetime τ_p was calculated to be 1.0 ps.

Table 5.2. Parameters used in the numerical analysis

Type	Symbol	Description	Value	Unit
Physical property parameters	g_{NX}	Differential gain of X	4×10^{-16}	cm^2
	g_{NY}	Differential gain of Y	Varies with P	cm^2
	N_{TR}	Transparency carrier density	10^{18}	cm^{-3}
	$\varepsilon_{XX} \ \varepsilon_{YY}$	Self-gain saturation coefficients	1×10^{-17}	cm^3
	$\varepsilon_{XY} \ \varepsilon_{YX}$	Cross-gain saturation coefficients	2×10^{-17}	cm^3
	α	Linewidth enhancement factor	3	
	τ_s	Carrier lifetime	3	ns
	β	Spontaneous emission factor	10^{-6}	
	v_G	Group velocity of light	7.9×10^9	cm s^{-1}
	α_{INT}	Internal absorption	10	cm^{-1}
VCSEL structure parameters	Γ	Confinement factor	0.05	
	A	Cross section of cavity	10×10	μm^2
	R_1	Reflectivity of output-side DBR	0.982	
	R_2	Reflectivity of opposite-side DBR	0.995	
	L_{eff}	Effective length of the VCSEL cavity	1.0	μm
	$1/\tau_C$	Optical injection rate	1.0×10^{13}	s^{-1}
Operation	P	Carrier pump rate	Variable	$\text{cm}^{-3}\text{s}^{-1}$
Other parameters	τ_p	Photon lifetime	1.0	ps
	N_{SS}	Steady state carrier density	Varies with P	cm^{-3}
	L	External cavity length	Variable	cm
	R_3	Reflectivity of external mirror	Variable	
	Δf	Frequency difference of X and Y	0	GHz

5.3 Solitary VCSEL operation

Before the simulation of the pulse generation in EC-VCSEL, the characteristics of the solitary VCSEL were investigated. By setting all the parts related to the feedback light from the EC in the rate equations (5-1) to (5-9) to be 0, the operation of the solitary VCSEL was calculated. Two different VCSELs with different gain saturation coefficients were used for the pulse generation in EC-VCSEL.

For VCSELs, the self-gain saturation coefficients and cross-gain saturation coefficients are commonly considered to have a relationship written as

$$\varepsilon_{XY} = \varepsilon_{YX} = 2\varepsilon_{XX} = 2\varepsilon_{YY} = 2 \times 10^{-17} \text{ (cm}^3\text{)}.$$

To check the effect of gain saturation coefficients, we also calculated the solitary operation of a VCSEL with a weaker cross-gain saturation effect, which is written as

$$\varepsilon_{XX} = \varepsilon_{YY} = \varepsilon_{XY} = \varepsilon_{YX} = 1 \times 10^{-17} \text{ (cm}^3\text{)}.$$

Other parameters were the same for both of these two different VCSELs. Differential gains of the two modes were set to be different,

$$g_{NX} = 4.0 \times 10^{-16} \text{ (cm}^2\text{)}$$

$$g_{NY} = 4.0 \times 10^{-16} - 0.05 \times 10^{-44} (P - 0.8 \times 10^{28}) \text{ (cm}^2\text{)}$$

where g_{NX} kept constant with the change of the carrier pump rate P , g_{NY} decreased with the increase of P by a rate of $0.05 \times 10^{-44} \text{ cm}^5\text{s}$, and crossed with g_{NX} at $P = 0.80 \times 10^{28} \text{ cm}^{-3}\text{s}^{-1}$.

The operation of the solitary VCSELs with different gain saturation coefficients were

calculated and are shown in Fig. 5.2 and Fig. 5.3. Important parameters i.e., (a) differential gain, (b) gain, (c) magnification of gain shown in (b), and (d) photon density are shown with the change of P . P was increased from 0 to $1.80 \times 10^{28} \text{ cm}^{-3}\text{s}^{-1}$ and then decreased to 0. In Fig. 5.2, a hysteresis is observed in the pump-photon density curve of the VCSEL with gain saturation coefficients $\varepsilon_{XX,YY} : \varepsilon_{XY,YX} = 1:2$, ranged from $P = 0.70 \times 10^{28} \text{ cm}^{-3}\text{s}^{-1}$ to $P = 1.00 \times 10^{28} \text{ cm}^{-3}\text{s}^{-1}$. The center of the hysteresis region is at $P = 0.85 \times 10^{28} \text{ cm}^{-3}\text{s}^{-1}$, slightly higher than the cross pump value $P = 0.80 \times 10^{28} \text{ cm}^{-3}\text{s}^{-1}$. Due to the larger cross-gain saturation coefficient, the lasing mode switched at different values during the increasing and decreasing of P . In the hysteresis region, the VCSEL can lase with X or Y mode. In Fig. 5.3, the VCSEL with gain saturation coefficients $\varepsilon_{XX,YY} : \varepsilon_{XY,YX} = 1:1$ lased with Y mode which had higher gain at $P < 0.80 \times 10^{28} \text{ cm}^{-3}\text{s}^{-1}$. Then the lasing mode switched to X at $P = 0.80 \times 10^{28} \text{ cm}^{-3}\text{s}^{-1}$, where the gains of the two modes crossed with each other. There was no large change of the total output power due to the small gain difference of the two linearly polarized modes.

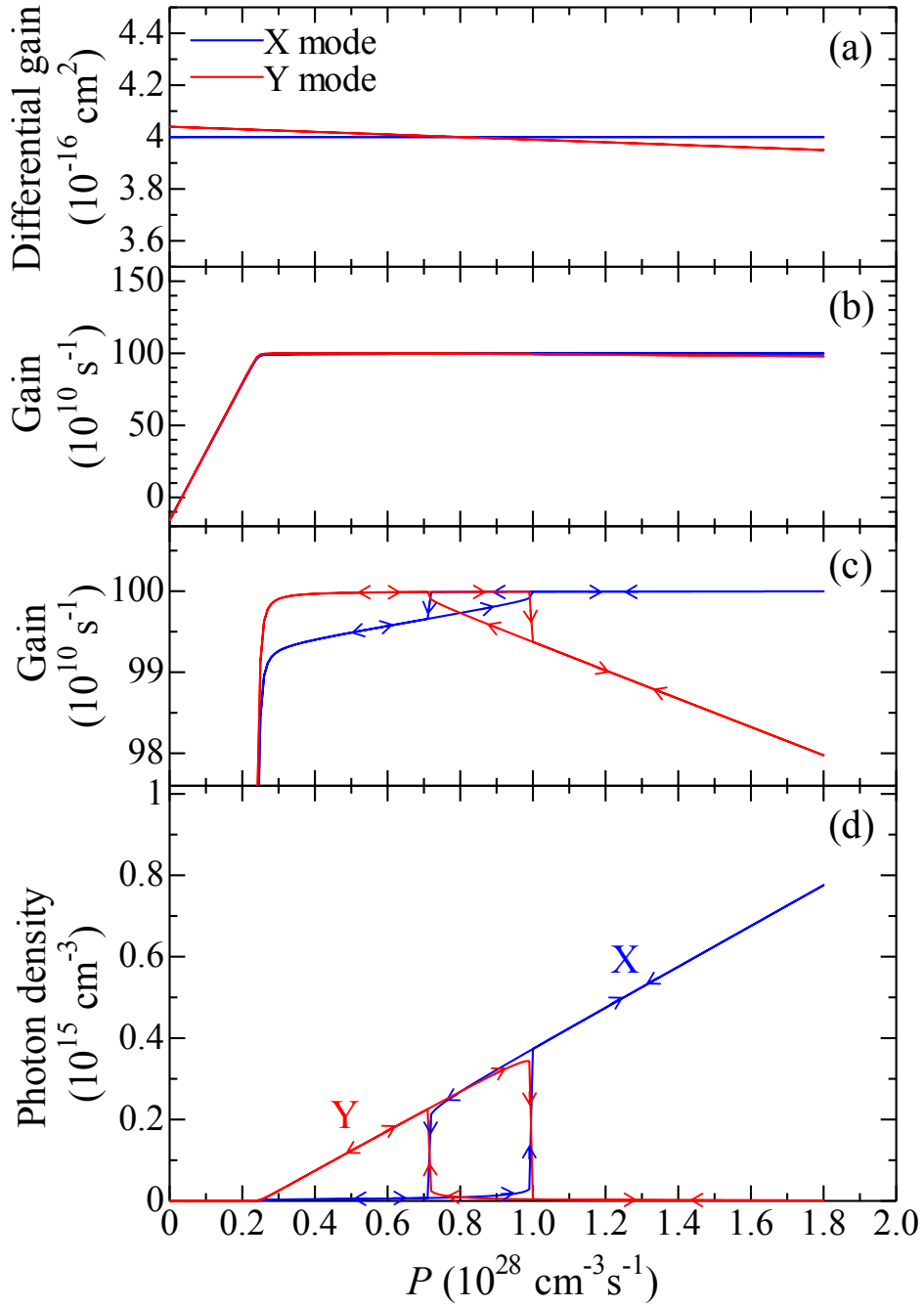


Fig. 5.2. Operation of solitary VCSEL with gain saturation coefficients $\epsilon_{XX,YY} : \epsilon_{XY,YX} = 1:2$.

- (a) differential gain, (b) gain, (c) magnification of gain in (b),
- (d) photon density change with the increase and then decrease of P .

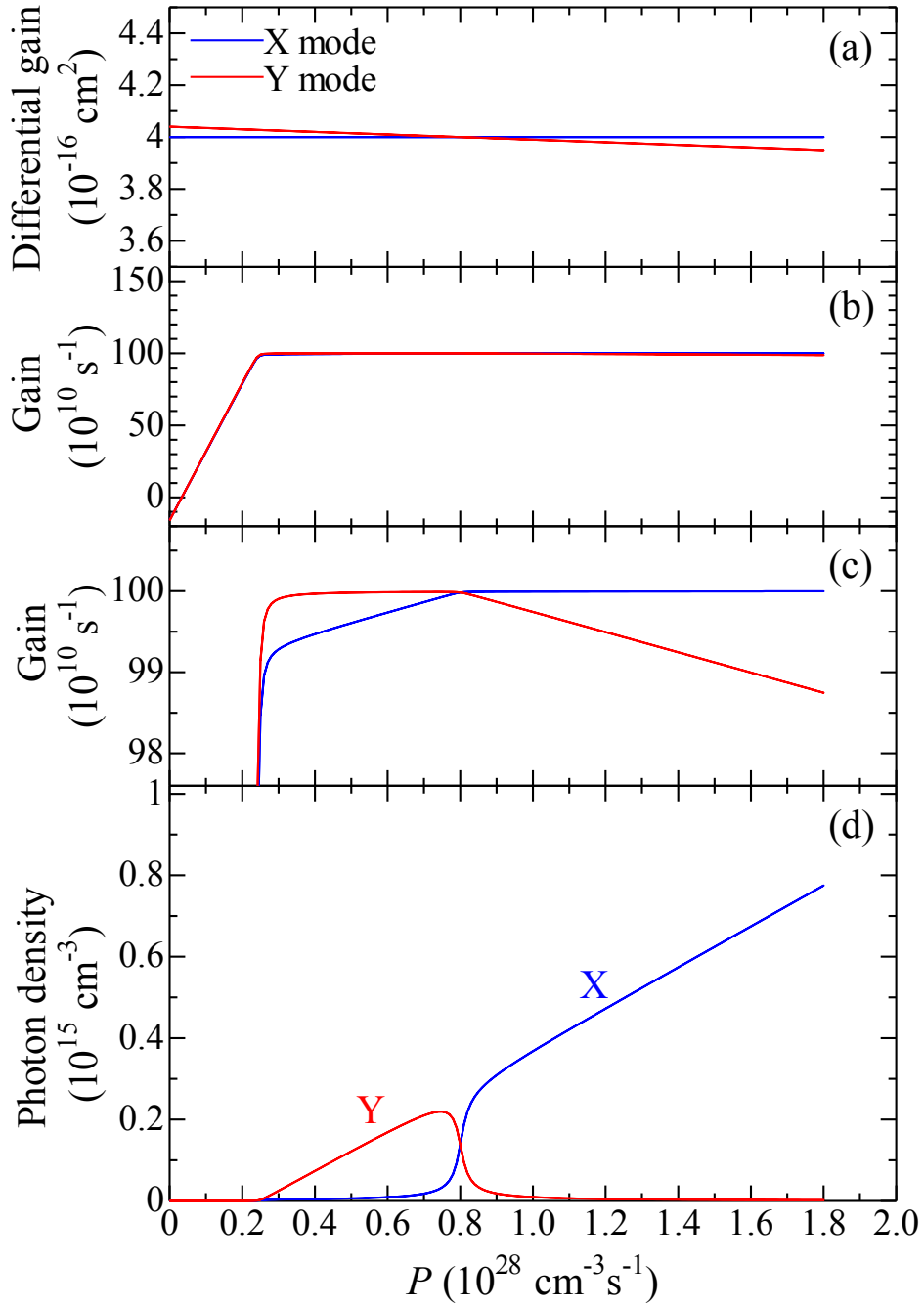


Fig. 5.3. Operation of solitary VCSEL with gain saturation coefficients $\varepsilon_{XX,YY} : \varepsilon_{XY,YX} = 1:1$.

- (a) differential gain, (b) gain, (c) magnification of gain in (b),
- (d) photon density change with the increase and then decrease of P .

5.4 EC-VCSEL operation

After the investigation of solitary VCSEL operation, we calculated the operation of VCSEL under polarization-rotated feedback from the EC. The effects of gain saturation coefficients, feedback intensity, and carrier pump rate on the polarization self-modulation were investigated. In the investigation of the effects of these three factors on the pulse generation, the EC length L varied from 2.5 to 75 mm. As shown in Table 5.3, the corresponding frequencies are from 30 GHz to 1 GHz, under the relationship: $f = c/4L$.

Table 5.3. Different L and their corresponding modulation frequencies $f = c/4L$

L (mm)	f (GHz)
2.5	30.0
3	25.0
5	15.0
7.5	10.0
10	7.5
15	5.0
20	3.75
50	1.5
75	1.0

5.4.1 Effect of gain saturation coefficient of the VCSEL

VCSEL with stronger cross-gain saturation effect ($\varepsilon_{xx,yy} : \varepsilon_{xy,yx} = 1 : 2$) shows a hysteresis in the pump-photon density curve at solitary operation as shown in Fig. 5.2. The lasing light strongly suppresses the other mode with the orthogonal polarization. Thus, this VCSEL is

considered to have an advantage for the polarization switching between the two modes. To investigate the effect of gain saturation coefficients, we compare the pulse generation results by adding polarization-rotated optical feedback from EC to the two different VCSELs as shown in Fig. 5.4 and Fig. 5.5. The VCSELs operated in solitary state, and P was increased from 0 to $1.10 \times 10^{28} \text{ cm}^{-3}\text{s}^{-1}$. After the solitary operation at $P = 1.10 \times 10^{28} \text{ cm}^{-3}\text{s}^{-1}$ for 1000 ns, the EC and QWP were added. There was no feedback light into the VCSEL during the first one round trip delay $\tau = 2L/c$. Reflectivity of the EC R_3 was set to be 0.08.

Fig. 5.4 shows the output waveforms in the last 1 ns (999–1000 ns) of the 1000 ns operation after EC was added. A VCSEL with gain saturation coefficients $\varepsilon_{XX,YY} : \varepsilon_{XY,YX} = 1:2$ was used here. At $L = 75 \text{ mm}$, the two modes of the VCSEL lased unstably. From $L = 50 \text{ mm}$ to $L = 10 \text{ mm}$, the output of the EC-VCSEL alternately changed between the X and Y modes with frequencies of about $f = c/4L$. With the shortening of L , the waveforms of the optical pulses gradually changed from square wave to sinusoidallike. When L was further shortened to shorter than 7.5 mm, no polarization self-modulation occurred and the two modes lased with CW at the same time.

Fig. 5.5 shows the output waveforms in the last 1 ns (999–1000 ns) of the 1000 ns operation after EC was added. Gain saturation coefficients of the VCSEL were $\varepsilon_{XX,YY} : \varepsilon_{XY,YX} = 1:1$. At $L = 75 \text{ mm}$, the two modes of the VCSEL lased unstably. At $L = 50 \text{ mm}$, the output of the EC-VCSEL alternately changed between X and Y modes with a frequency of about 1.5 GHz, which

was consistent with $f = c/4L$. The waveforms of the optical pulses were sinusoidal. At $L = 15$ mm and $L = 10$ mm, the X and Y modes lased at the same time with narrow pulses. The mode with higher intensity alternately changed between the X and Y modes. At $L = 20$ mm, $L = 7.5$ mm, and $L = 5$ mm, no pulses were generated. The two modes lased with CW simultaneously with the same intensity.

Comparing the results in Fig. 5.4 and Fig. 5.5, we found that the EC-VCSEL using VCSEL with gain saturation coefficients $\epsilon_{XX,YY} : \epsilon_{XY,YX} = 1:2$ could generate optical pulses by polarization self-modulation in a wider frequency range than that using the VCSEL with gain saturation coefficients $\epsilon_{XX,YY} : \epsilon_{XY,YX} = 1:1$. This result indicates that the VCSEL with stronger cross-gain saturation effect is more suitable for polarization switching between the two linearly polarized modes. About the waveforms of the optical pulse, we compared the optical output at $L = 50$ mm for the two VCSELs. Compared with the sinusoidallike optical waves generated using the VCSEL with $\epsilon_{XX,YY} : \epsilon_{XY,YX} = 1:1$, the waveform of the optical output pulses using VCSEL with $\epsilon_{XX,YY} : \epsilon_{XY,YX} = 1:2$ was much closer to a square wave, which is more preferable to be used as optical clock signal in the optical communication systems. The reason is that during polarization switching, the lasing mode strongly suppresses the other mode with the orthogonal polarization when the cross-gain saturation effect is strong, which can be seen from the polarization switching of the solitary VCSEL shown in Fig. 5.2 and Fig. 5.3.

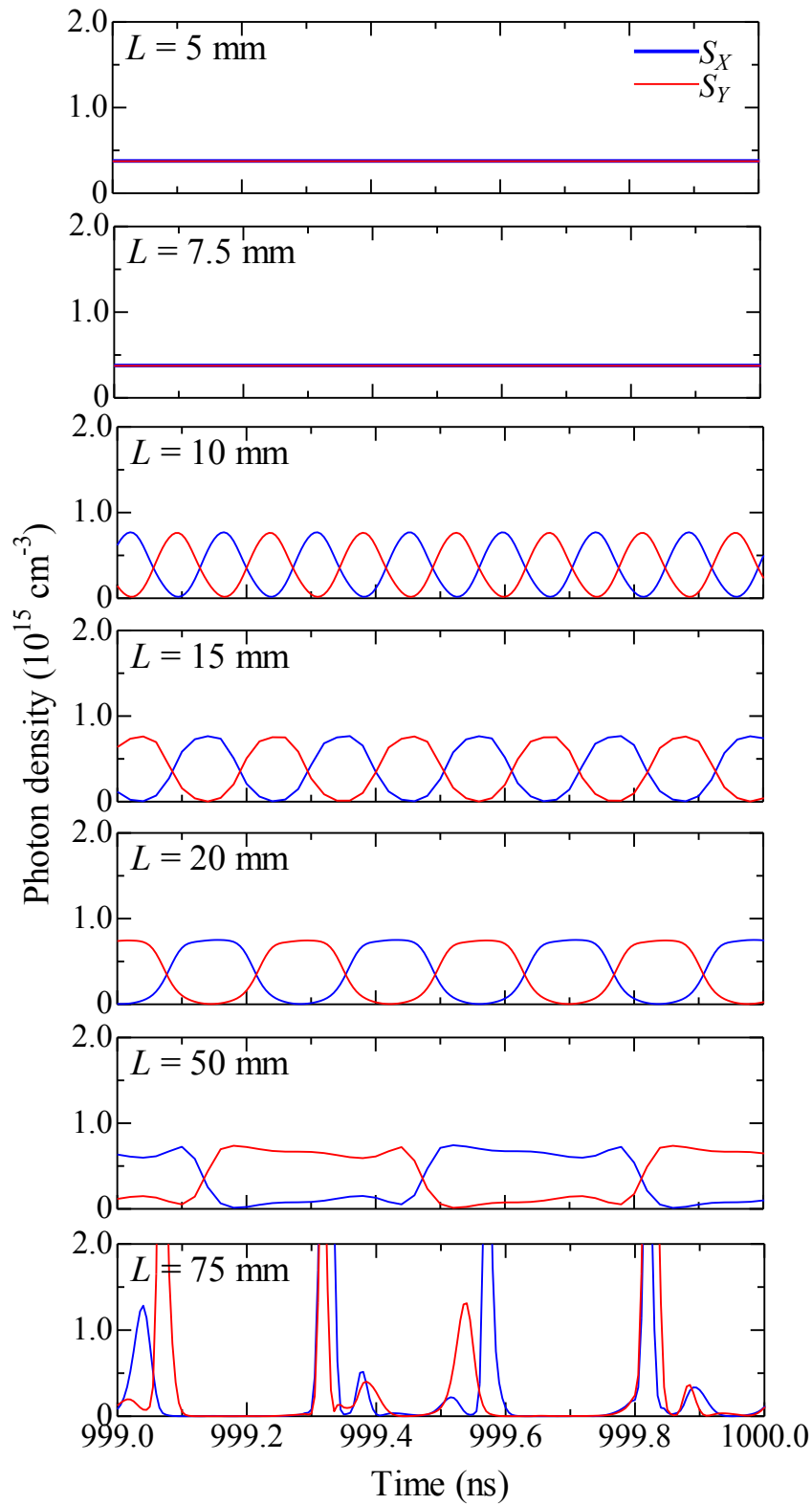


Fig. 5.4. Optical output using VCSEL with gain saturation coefficients $\epsilon_{XX,YY} : \epsilon_{XY,XY} = 1:2$ for the EC-VCSEL with $P = 1.10 \times 10^{28} \text{ cm}^{-3} \text{ s}^{-1}$ and $R_3 = 0.08$.

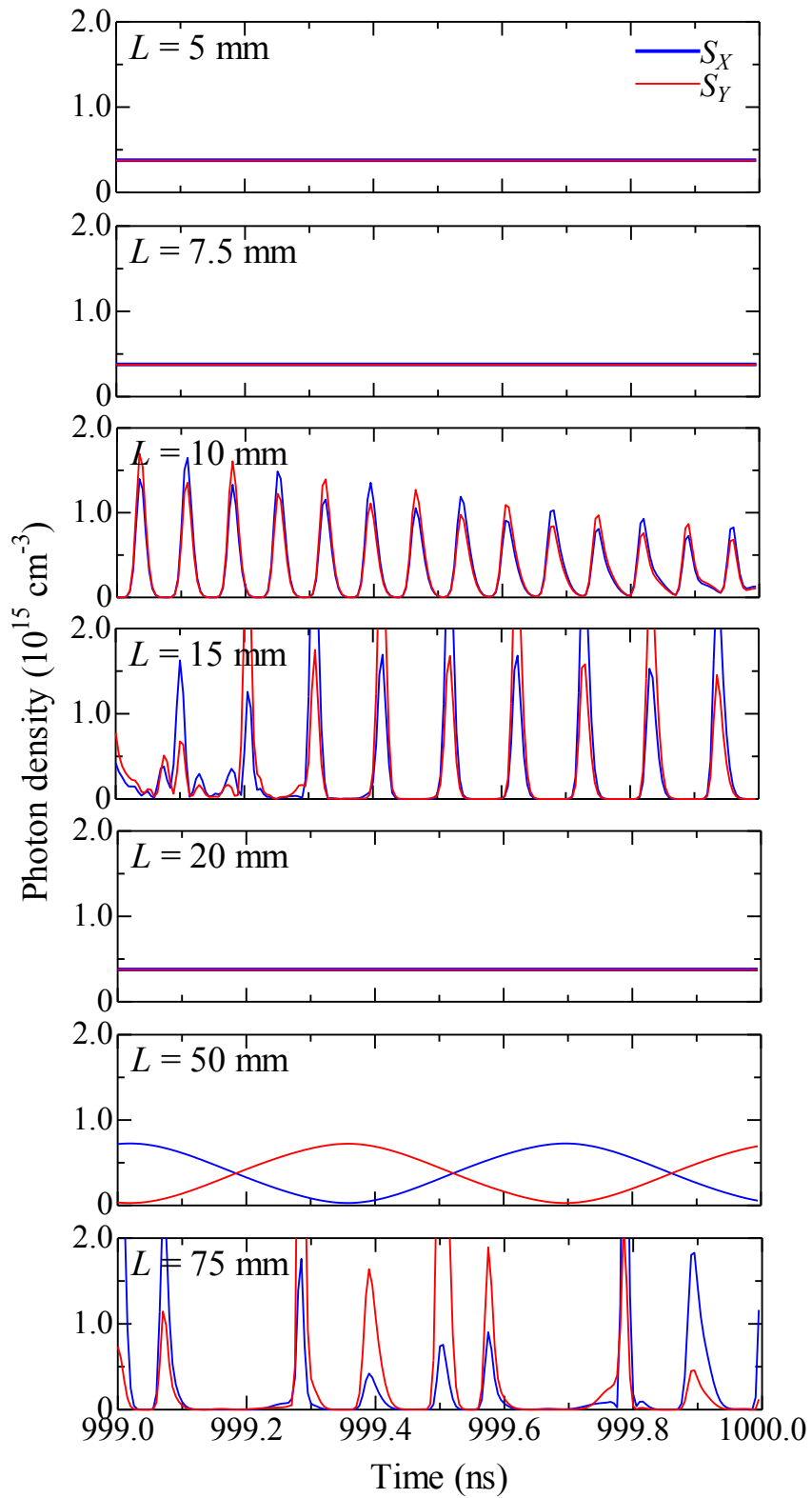


Fig. 5.5. Optical output using VCSEL gain saturation coefficients $\epsilon_{XX,YY} : \epsilon_{XY,YX} = 1:1$ for the EC-VCSEL with $P = 1.10 \times 10^{28} \text{ cm}^{-3} \text{ s}^{-1}$ and $R_3 = 0.08$.

In conclusion, the VCSEL with gain saturation coefficients $\varepsilon_{XX,YY} : \varepsilon_{XY,YX} = 1:2$ is more suitable for pulse generation by polarization self-modulation in EC-VCSEL. Optical pulses can be generated in a wider frequency range and the waveforms of the pulses can be much closer to square waves.

5.4.2 Effect of optical feedback intensity

The power of the optical feedback is another important factor for the pulse generation. When the EC length L is shortened, higher power of optical feedback is needed for higher-frequency polarization self-modulation [3] [9]. This will be discussed in detail in this section.

To investigate the effect of optical feedback intensity on the polarization self-modulation, calculations for the EC-VCSEL with different EC reflectivity R_3 were carried out. A VCSEL with gain saturation coefficients $\varepsilon_{XX,YY} : \varepsilon_{XY,YX} = 1:2$ which is considered to be more suitable for pulse generation was used for the EC-VCSEL. The parameters of the VCSEL itself were the same as those used in the calculation of solitary VCSEL operation in Fig. 5.2. The VCSEL operated in a solitary state, and P was increased from 0 to $1.10 \times 10^{28} \text{ cm}^{-3}\text{s}^{-1}$. After solitary operation at $P = 1.10 \times 10^{28} \text{ cm}^{-3}\text{s}^{-1}$ for 1000 ns, the EC and QWP were added. Fig. 5.6 and Fig. 5.7 show the output waveforms in the last 1 ns (1499–1500 ns) of the 1500 ns operation after EC was added, for $R_3 = 0.03$ and $R_3 = 0.20$, respectively. The output waveforms for $R_3 = 0.08$ are already given in Fig. 5.4.

In Fig. 5.6, when $R_3 = 0.03$, the optical output of the two linearly polarized modes were modulated periodically only at $L = 20$ mm. The two modes were lasing at the same time with low modulation depth of the optical output. At $L = 75$ mm and $L = 50$ mm, though periodical optical pulses were not generated, the dominant mode alternately changed. At $L = 15$ mm or shorter, after the EC was added to the VCSEL, output power variations were observed for a short time, and then the EC-VCSEL operated at CW state.

In Fig. 5.7, when $R_3 = 0.20$, optical pulses were generated by polarization self-modulation in the EC-VCSEL from $L = 20$ mm to $L = 5$ mm. Like the results shown in Fig. 5.4, the waveform of the optical pulses changed from square wave to sinusoidallike with the increase of modulation frequency. At $L = 75$ mm and $L = 50$ mm, the lasing mode of the VCSEL alternately changed between the two modes. However, extra polarization switching occurred during each period. For example, at $L = 75$ mm, after the polarization switching at about 1499.3 ns, the Y mode should lase continuously for about 0.5 ns if the switching frequency is determined by $c/4L$. However, unexpected polarization switching occurred between 1499.50~1499.62 ns. The intensity of the optical feedback is much stronger than the power needed for the polarization switching. After the polarization switching at 1499.3 ns, the fluctuation of the optical output power resulted in the extra polarization switching.

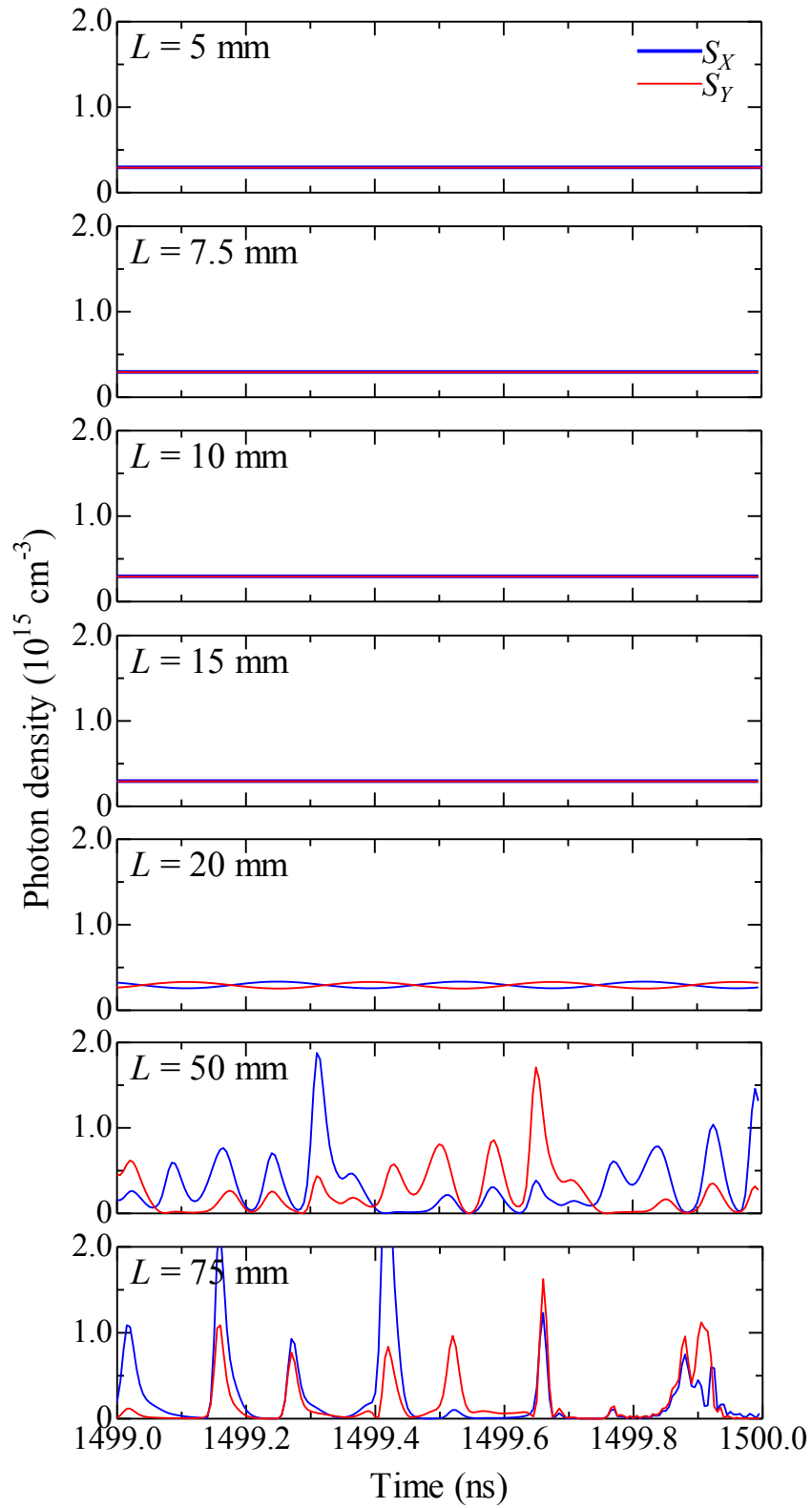


Fig. 5.6. Optical output using VCSEL with gain saturation coefficients $\epsilon_{XX,YY} : \epsilon_{XY,YX} = 1:2$ for the EC-VCSEL with $R_3 = 0.03$, at $P = 1.10 \times 10^{28} \text{ cm}^{-3}\text{s}^{-1}$.

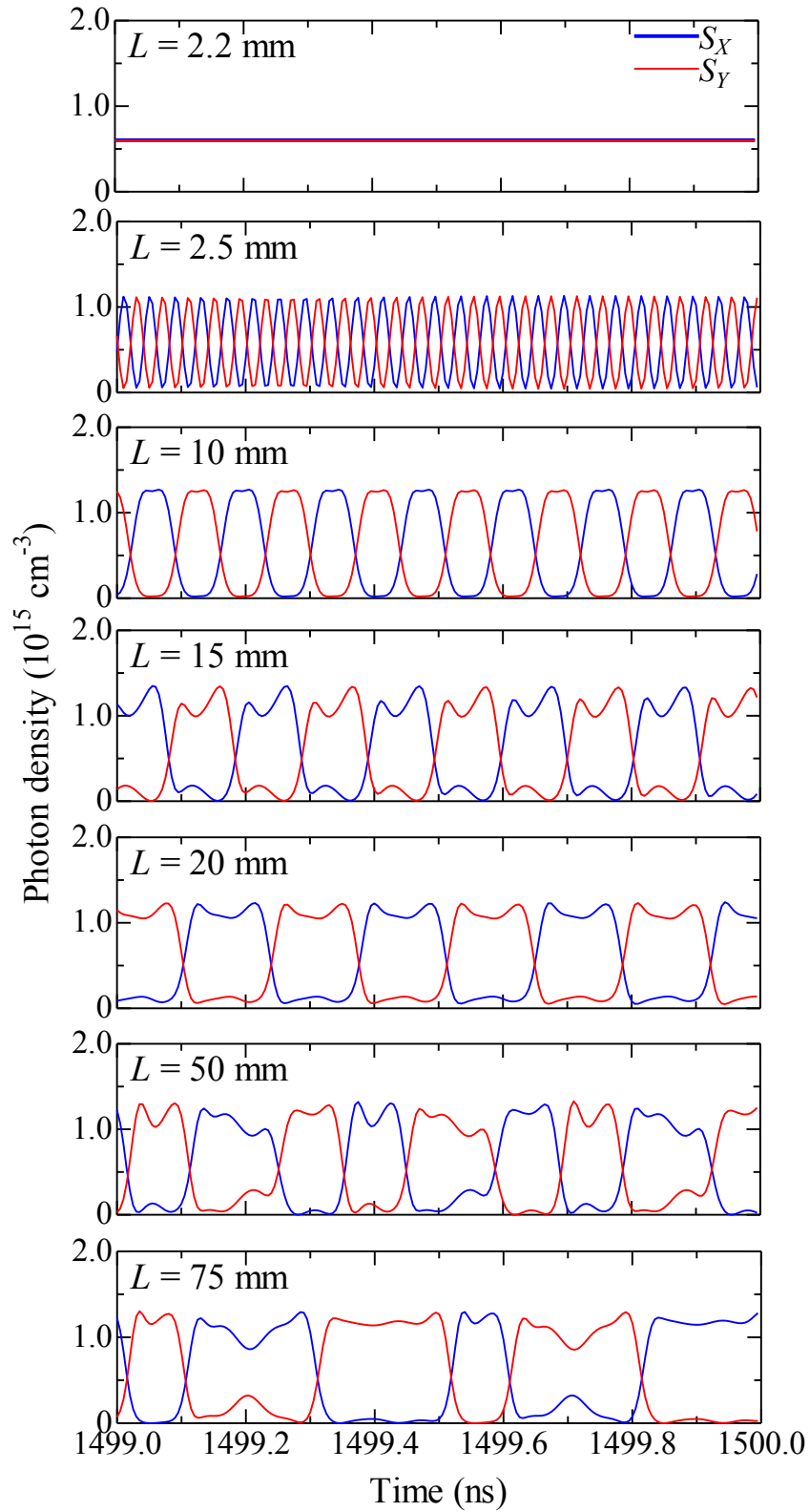


Fig. 5.7. Optical output using VCSEL with gain saturation coefficients $\epsilon_{XX,YY} : \epsilon_{XY,YX} = 1:2$ for the EC-VCSEL with $R_3 = 0.20$, at $P = 1.10 \times 10^{28} \text{ cm}^{-3}\text{s}^{-1}$.

Comparing the results of pulse generation in EC-VCSEL with different optical feedback intensities shown in Fig. 5.4, 5.6 and 5.7, we found that the highest frequency of the pulses that can be generated greatly depended on R_3 . As shown in Fig. 5.8, with the increase of R_3 , from 0.03 to 0.20, the highest frequency of the pulses increased from 3.75 to about 25 GHz.

To summarize, the intensity of optical feedback greatly affected the pulse generation by polarization self-modulation in EC-VCSEL. When the intensity of optical feedback was increased by using ECs with higher reflectivity R_3 , the highest frequency of the optical pulses that could be generated was increased. When L was shortened, the duration of each pulse is reduced which leads to higher input peak power requirement to cause periodical polarization switching of the VCSEL [9].

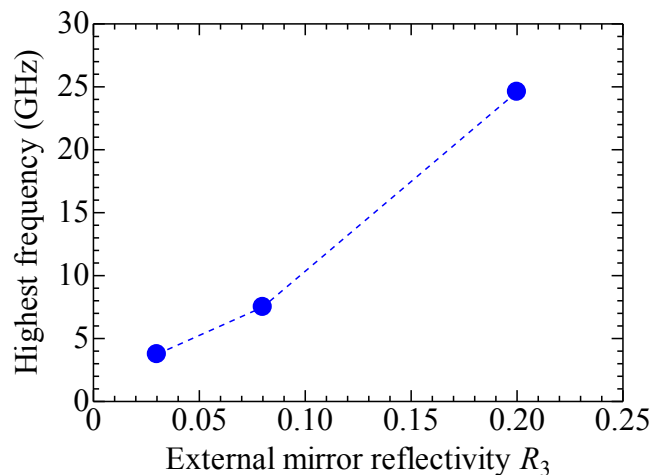


Fig. 5.8. Highest frequency of optical pulses that can be generated for different R_3 .

5.4.3 Effect of carrier pump rate

In the investigation of the effect of optical feedback intensity on the polarization self-modulation in EC-VCSEL, it was found that the highest frequency of the optical pulse that could be generated can be improved by increasing the EC reflectivity R_3 . Increasing the output power of the VCSEL itself can be another method to increase the intensity of optical feedback into to the VCSEL for a given R_3 . In addition, change of the carrier density in VCSEL becomes faster at higher carrier pump rates, which leads to higher relaxation oscillation frequency f_r of the solitary VCSEL. We simulated the pulse generation in EC-VCSEL when the VCSEL was driven at different carrier pump rates P between $0.40 \times 10^{28} \text{ cm}^{-3}\text{s}^{-1}$ and $1.80 \times 10^{28} \text{ cm}^{-3}\text{s}^{-1}$. Like the results discussed in the former sections, the VCSEL with gain saturation coefficients $\varepsilon_{XX,YY} : \varepsilon_{XY,YX} = 1:2$ which is preferable for pulse generation was used for the EC-VCSEL. The VCSEL was set to operate in its solitary state. P was increased from 0 to the selected value. Then, after the 1000 ns stable CW operation of the solitary VCSEL, the EC and QWP were added which resulted in the polarization-rotated optical feedback into the VCSEL. For all the calculations, R_3 was set to be 0.08. The output waveforms in the last 1 ns (1499–1500 ns) of the 1500 ns operation at each P after EC and QWP was added are shown in Fig. 5.9 to Fig. 5.13. The results for $P = 1.10 \times 10^{28} \text{ cm}^{-3}\text{s}^{-1}$ were the same to those shown in Fig. 5.4 and will not be shown here again.

At $P = 0.40 \times 10^{28} \text{ cm}^{-3}\text{s}^{-1}$ (Fig. 5.9), the polarization of VCSEL lasing switched between X

and Y when $L = 50$ mm. With further shortening of L , the CW operations of the EC-VCSEL were observed where the two modes had the same intensity. At $P = 0.60 \times 10^{28} \text{ cm}^{-3}\text{s}^{-1}$ (Fig. 5.10), the operation of polarization self-modulation was not obtained when $L \leq 20$ mm. At $P = 0.85 \times 10^{28} \text{ cm}^{-3}\text{s}^{-1}$ (Fig. 5.11), successful polarization self-modulation operations were obtained when $L \geq 20$ mm. At $L = 15$ mm, the duty ratio of the pulses was much smaller than 50%. As shown in the inset on the right, intensity of the peaks changed with time in a wide time range. This may be caused by the influence of the relaxation oscillation of the VCSEL. As described in Fig. 5.4, at $P = 1.10 \times 10^{28} \text{ cm}^{-3}\text{s}^{-1}$, from $L = 50$ mm to $L = 10$ mm, the output of the EC-VCSEL alternately changes between the X and Y modes with frequencies close to $f = c/4L$. When P was further increased to $1.40 \times 10^{28} \text{ cm}^{-3}\text{s}^{-1}$ (Fig. 5.12) and $1.80 \times 10^{28} \text{ cm}^{-3}\text{s}^{-1}$ (Fig. 5.13), polarization self-modulations were observed even when L was shortened to 5 mm. We checked the operation of EC-VCSEL with shorter L until no polarization self-modulation occurred.

It is clearly seen in Fig. 5.13 ($P = 1.80 \times 10^{28} \text{ cm}^{-3}\text{s}^{-1}$) that with the shortening of L , the waveforms of the optical pulses gradually changed from square wave to sinusoidallike. At $P = 1.40 \times 10^{28} \text{ cm}^{-3}\text{s}^{-1}$ and $L = 5$ mm in Fig. 5.12, the modulation depth of the optical pules decreased. To increase the modulation depth, stronger optical feedback is needed. An example for this, in Fig. 5.6 when $R_3 = 0.03$ and $L = 20$ mm, the output pulses have a very small modulation depth, however, the modulation depth is greatly increased when R_3 was increased to be 0.20 in Fig. 5.7.

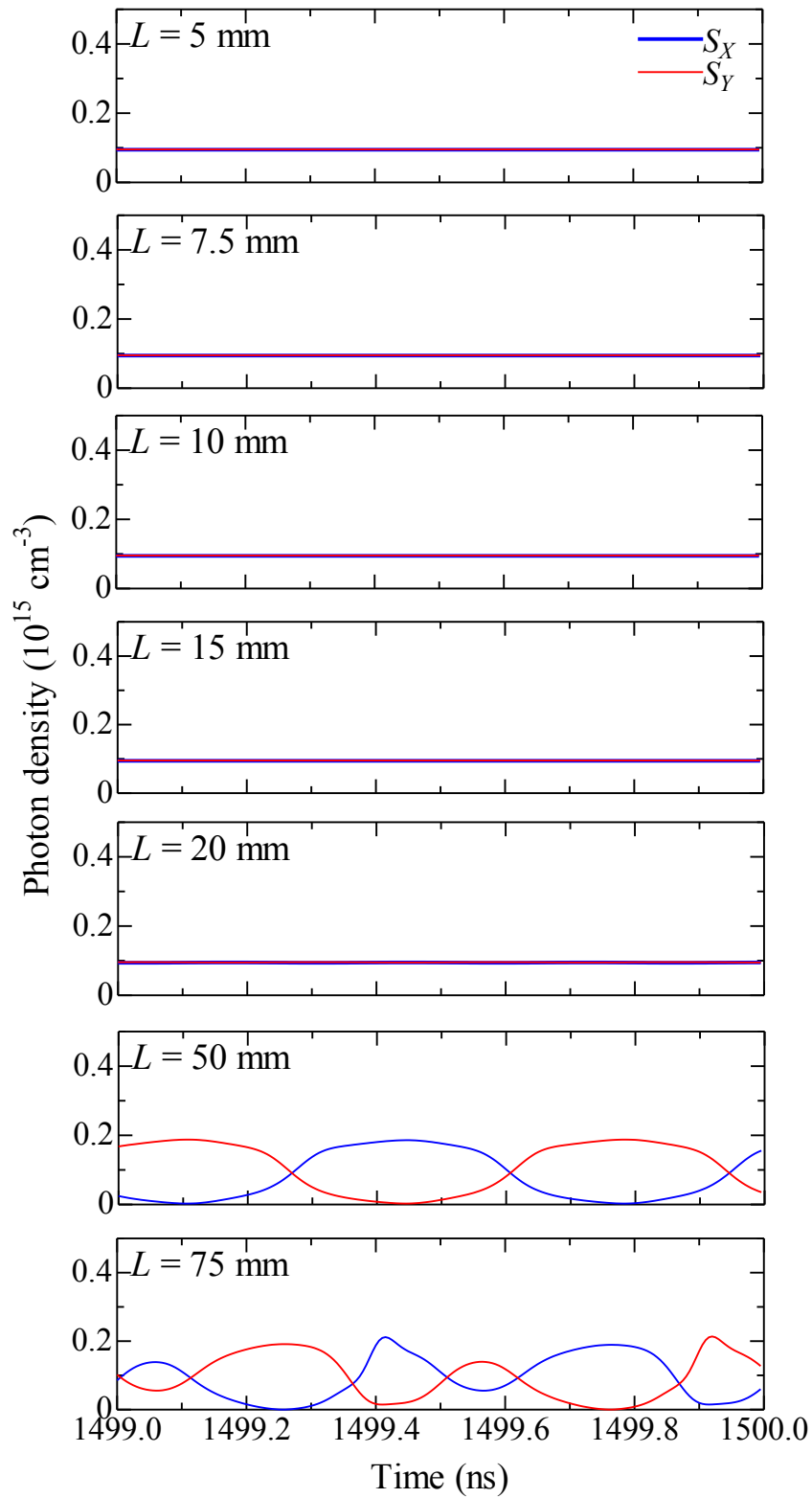


Fig. 5.9. Optical output using VCSEL with gain saturation coefficients $\epsilon_{XX,YY} : \epsilon_{XY,YX} = 1:2$ for the EC-VCSEL at $P = 0.40 \times 10^{28} \text{ cm}^{-3} \text{ s}^{-1}$. $R_3 = 0.08$ and $L = 5\text{--}75 \text{ mm}$.

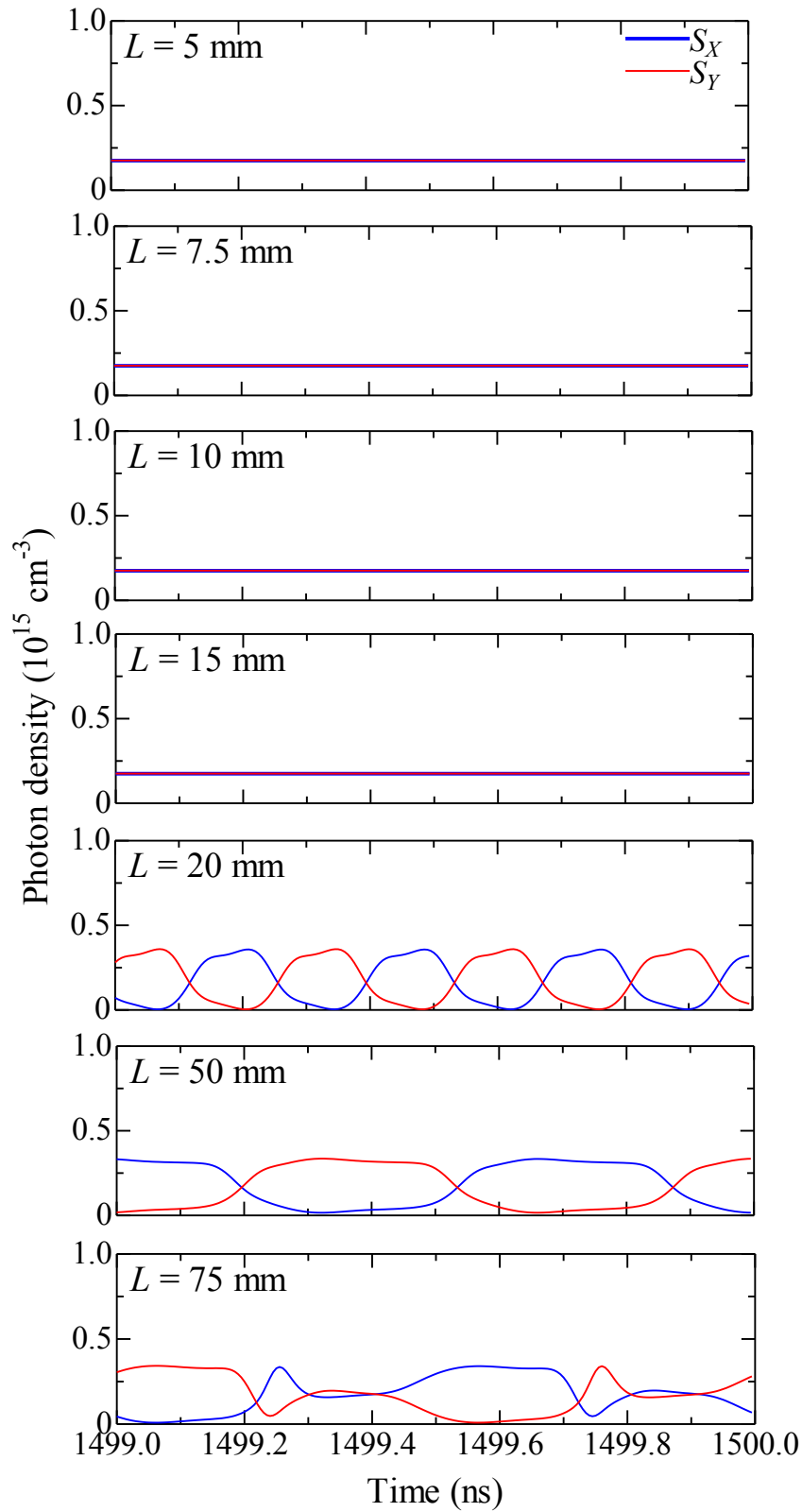


Fig. 5.10. Optical output using VCSEL with gain saturation coefficients $\epsilon_{XX,YY} : \epsilon_{YY,XX} = 1:2$ for the EC-VCSEL at $P = 0.60 \times 10^{28} \text{ cm}^{-3}\text{s}^{-1}$. $R_3 = 0.08$ and $L = 5\text{--}75 \text{ mm}$.

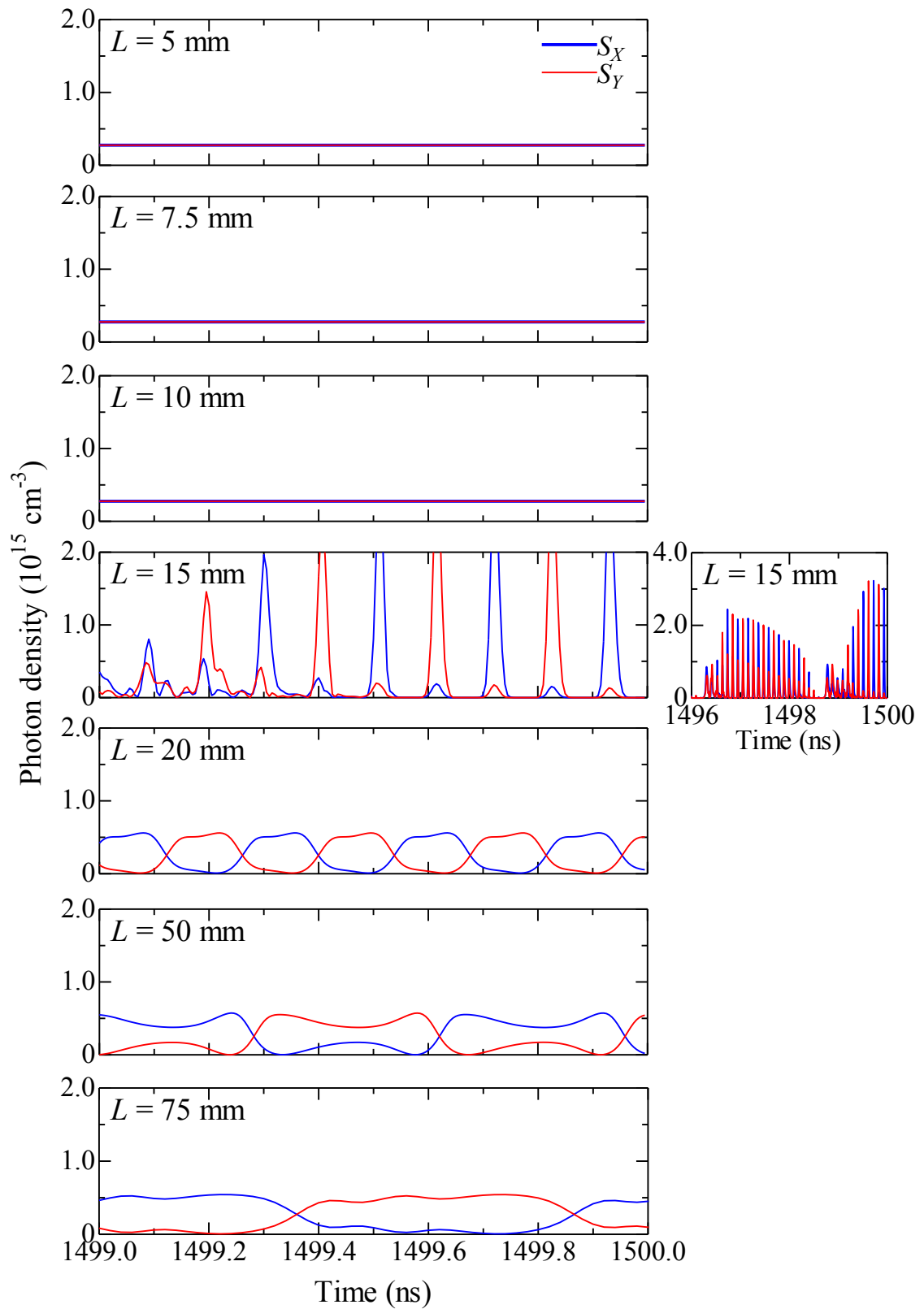


Fig. 5.11. Optical output using VCSEL with gain saturation coefficients $\varepsilon_{XX,YY} : \varepsilon_{YY,XX} = 1:2$ for the EC-VCSEL at $P = 0.85 \times 10^{28} \text{ cm}^{-3} \text{ s}^{-1}$, $R_3 = 0.08$ and $L = 5\text{--}75 \text{ mm}$.

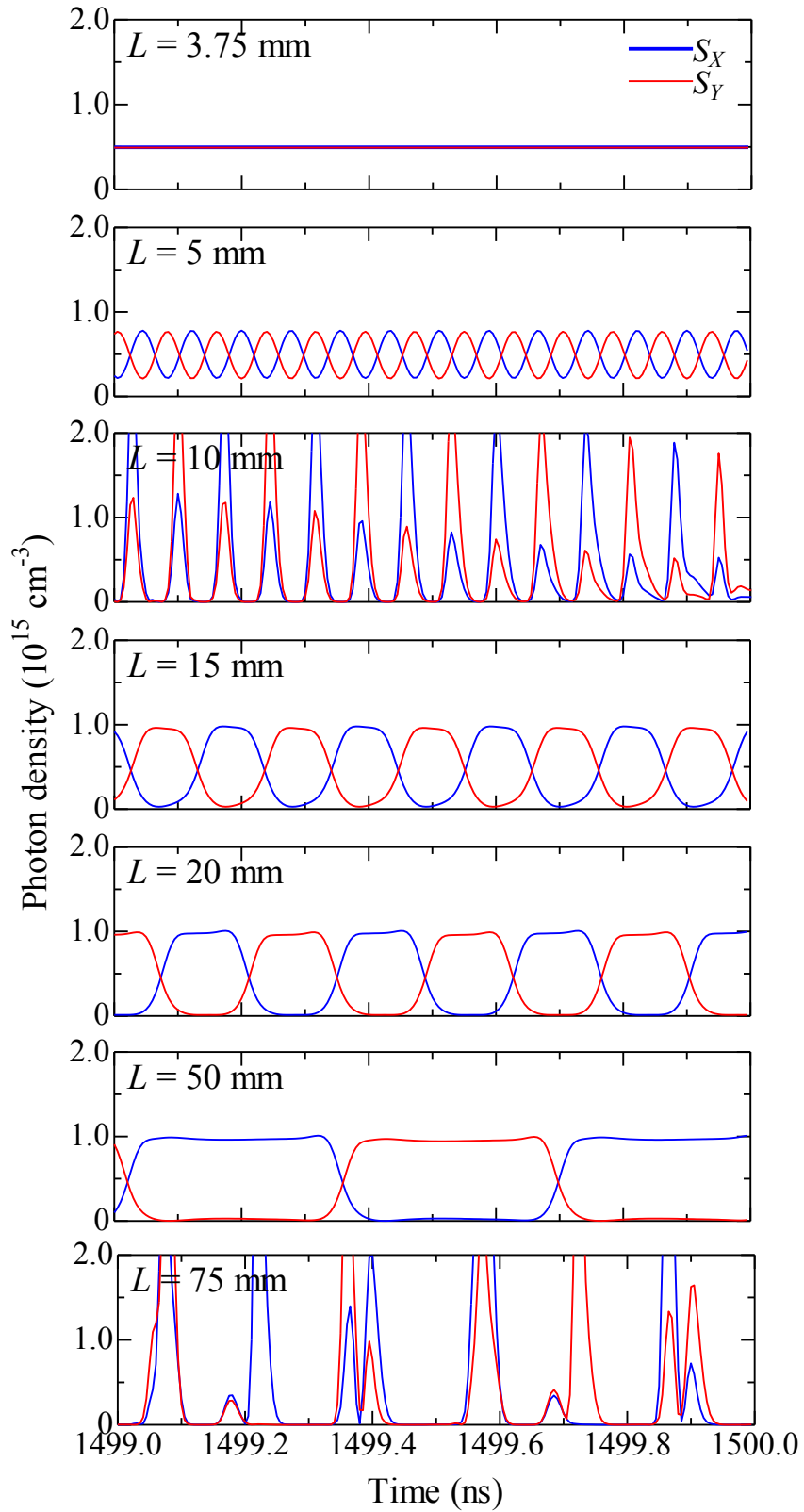


Fig. 5.12. Optical output using VCSEL with gain saturation coefficients $\varepsilon_{XX,YY} : \varepsilon_{YY,XX} = 1:2$ for the EC-VCSEL at $P = 1.40 \times 10^{28} \text{ cm}^{-3}\text{s}^{-1}$. $R_3 = 0.08$ and $L = 3.75\text{--}75 \text{ mm}$.

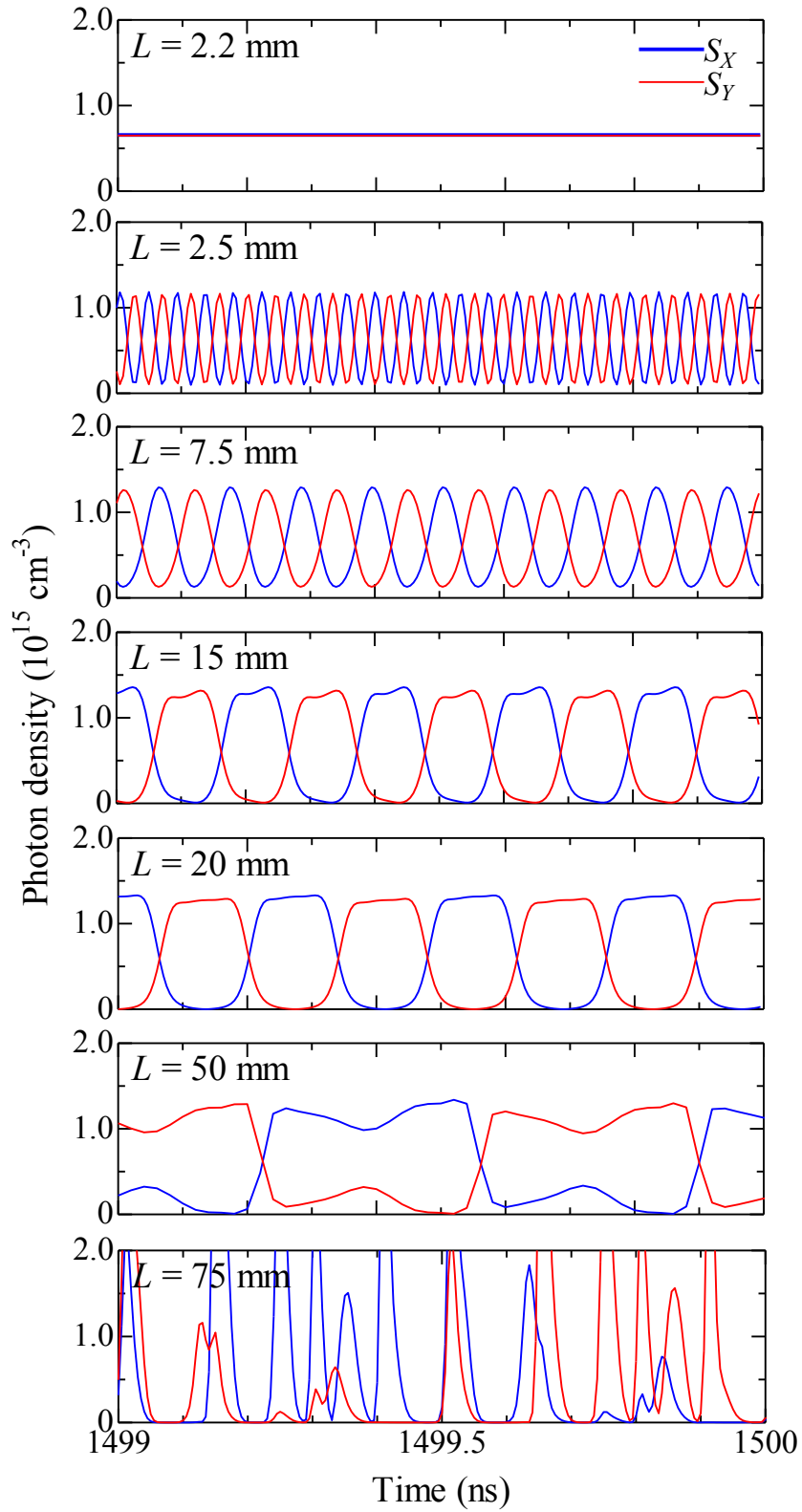


Fig. 5.13. Optical output using VCSEL with gain saturation coefficients $\varepsilon_{XX,YY} : \varepsilon_{XY,YX} = 1:2$ for the EC-VCSEL at $P = 1.80 \times 10^{28} \text{ cm}^{-3}\text{s}^{-1}$. $R_3 = 0.08$ and $L = 2.2\text{--}75 \text{ mm}$.

To discuss the effect of P on the pulse generation, the highest repetition frequencies of the pulses generated by polarization self-modulation in EC-VCSEL are plotted in Fig. 5.14 against P . With the increase of P , higher frequency polarization self-modulation in the EC-VCSEL became possible without increasing R_3 . This result suggests that increasing the drive current to the value where the VCSEL output power starts to saturate in experiments may be an effective method to improve the performance of polarization self-modulation in EC-VCSELs.

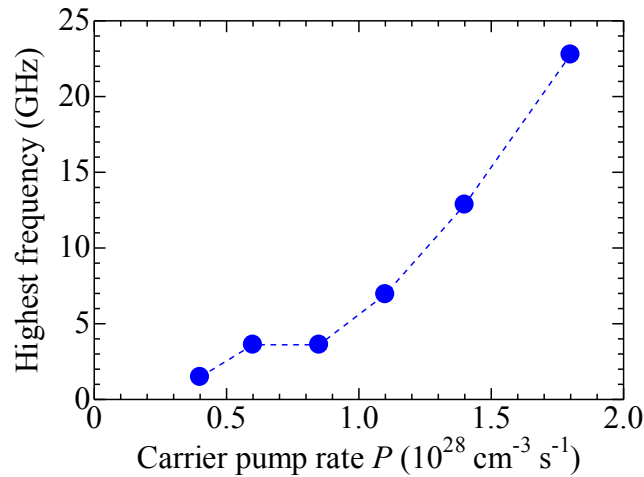


Fig. 5.14. The highest frequency of optical pulses that can be generated with increasing P . $R_3 = 0.08$.

5.5 Comparison with experimental results

We investigated the effects of gain saturation coefficients, optical feedback intensity, and carrier pump rate P on the pulse generation by polarization self-modulation in EC-VCSELs. Here we compare the results of simulation and the results in the experiments described in

Chapter 3. As shown in Fig. 5.15, in the simulation results for $P = 1.40 \times 10^{28} \text{ cm}^{-3}\text{s}^{-1}$ and $R_3 = 0.08$, we obtained four different lasing patterns in the EC-VCSEL.

Lasing pattern A: unstable lasing of X and Y modes.

Lasing pattern B: pulse generation by polarization self-modulation.

Lasing pattern C: narrow pulse lasing of X and Y modes at the same time.

Lasing pattern D: CW lasing of the X and Y modes with the same intensity.

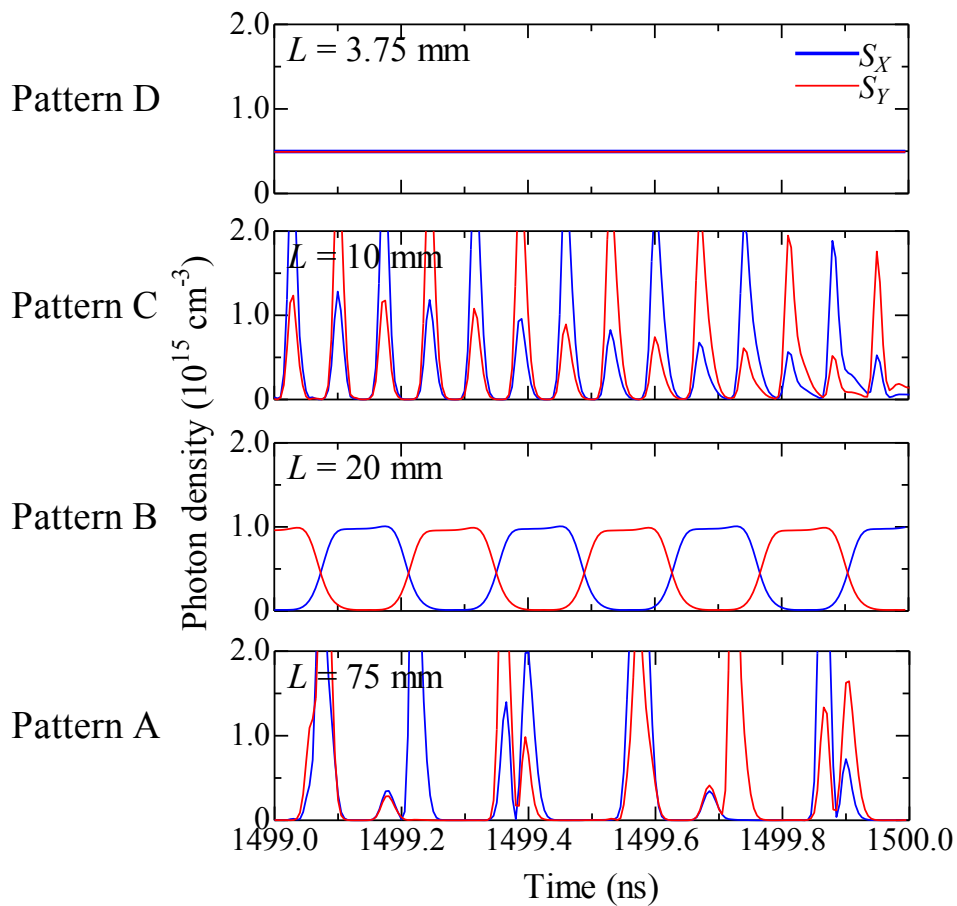


Fig. 5.15. Four different lasing patterns at $P = 1.40 \times 10^{28} \text{ cm}^{-3}\text{s}^{-1}$ and $R_3 = 0.08$.

We plotted all of the simulation results that belong to different lasing patterns in Fig. 5.16 together with the experimental results by polarization self-modulation in Chapter 3. The horizontal axis of Fig. 5.16 is normalized by the lasing threshold $P_{th} \approx 0.25 \times 10^{28} \text{ cm}^{-3}\text{s}^{-1}$ in the simulation or the lasing threshold drive current $I_{th} \approx 3.0 \text{ mA}$ of the solitary VCSEL in experiments. Fig. 5.16 is divided into four regions with different colors by the lasing patterns. Pink, yellow, green and gray for the lasing pattern A–D, respectively. The brown squares connected with dotted line shows f_r of the EC-VCSEL. These values were calculated from the photon density changes when R_3 was increased to 0.08 abruptly during the operation that stable polarization self-modulation occurred in the EC-VCSEL with $R_3 = 0.06$ at each carrier pump rate P . The green line shows f_r of the solitary VCSEL. The parameters used in the simulation are for 0.98- μm VCSELs. If we use the parameters for 1.55- μm VCSELs, f_r of the solitary VCSEL will become lower. The two red double circles \odot show the pulse generation results by polarization self-modulation in the experiments using a 1.55- μm VCSEL and a planar mirror in Chapter 3. Note that, the two red double circles were obtained at different L and different drive currents. When L was set to be about 35 mm, we obtained optical pulses by polarization self-modulation with a frequency of about 2 GHz at 4.83 mA. When L was set to be about 16 mm, we obtained optical pulses by polarization self-modulation with a frequency of about 4 GHz at 5.64 mA. No stable optical pulse sequence generated by polarization self-modulation was obtained when L was further shortened.

For the simulation results, in the region of $P/P_{th} < 4$, we obtained optical pulses by polarization self-modulation (lasing pattern B) with frequencies lower than f_r of the solitary VCSEL (green line). At modulation frequencies higher than the f_r , no pulse was obtained and the X and Y modes lased with the same and constant intensity (lasing pattern D). This phenomenon is in good agreement with our experimental results. However, at higher P , polarization self-modulations with frequencies higher than f_r of the solitary VCSEL were obtained. In this case, the feedback is strong due to the high intensity output of the solitary VCSEL. Thus, polarization self-modulation of the EC-VCSEL becomes fast. In our experiments, the VCSEL lasing output power began to saturate at currents 3 to 4 times of the lasing threshold I_{th} . We were not able to do the experiment of pulse generation at drive currents much higher than I_{th} . This result of the calculation suggests us that using VCSELs with lower I_{th} may be a feasible way to generate higher frequency optical pulses by polarization self-modulation.

The pink triangles \blacktriangle around the green line in Fig. 5.16 show the lasing pattern C, where X and Y modes lase with narrow pulses at the same time. In these cases, the frequency of polarization self-modulations are close to f_r of the solitary VCSEL, and the polarization self-modulation and the relaxation oscillation are generated simultaneously.

Unstable lasing (lasing pattern A) of the EC-VCSEL was observed at high carrier pump rates when $L = 75$ mm. This phenomenon was similar to the results in our experiments with

planar mirror that at $L \approx 35$ mm and $L \approx 16$ mm as explained in Sec. 3.3.1, optical pulse generation became unstable when the drive current was set to be relatively high values.

To generate higher-frequency optical pulse by polarization self-modulation in the EC-VCSEL, one direct way is to increase f_r of the solitary VCSEL. f_r can be expressed as

$$f_r = \frac{1}{2\pi} \sqrt{\frac{1}{\tau_S \tau_P}} \sqrt{\frac{P_0}{P_{th}} - 1} \sqrt{\frac{\nu_G g_N \Gamma N_{TR}}{\tau_S}} \quad (5-12)$$

where P_0 and P_{th} are the steady state carrier pump rate and lasing threshold carrier pump rate, respectively [13]. Other parameters are the same as those introduced in the Table 5.2. The equation (5-12) suggests three ways to increase the relaxation oscillation frequency f_r : increasing the differential gain g_N or steady state carrier pump rate P_0 , or decreasing the photon lifetime τ_P . The differential gain g_N can be increased by cooling the laser. The photon lifetime τ_P can be reduced by decreasing the length of the laser cavity. Polarization self-modulation with higher frequencies may become possible by increasing the f_r using these methods.

Different to the CW lasing (pattern D) in the simulation, we got optical pulses by beat note of two EC modes when L was shortened in our experiments. With the increase of the wavelength interval of the EC modes, the bandwidth of the VCSEL gain spectrum should be expanded in order to obtain enough gain for the EC modes. Decreasing the Q factor of the VCSEL may be

an effective method to realize this.

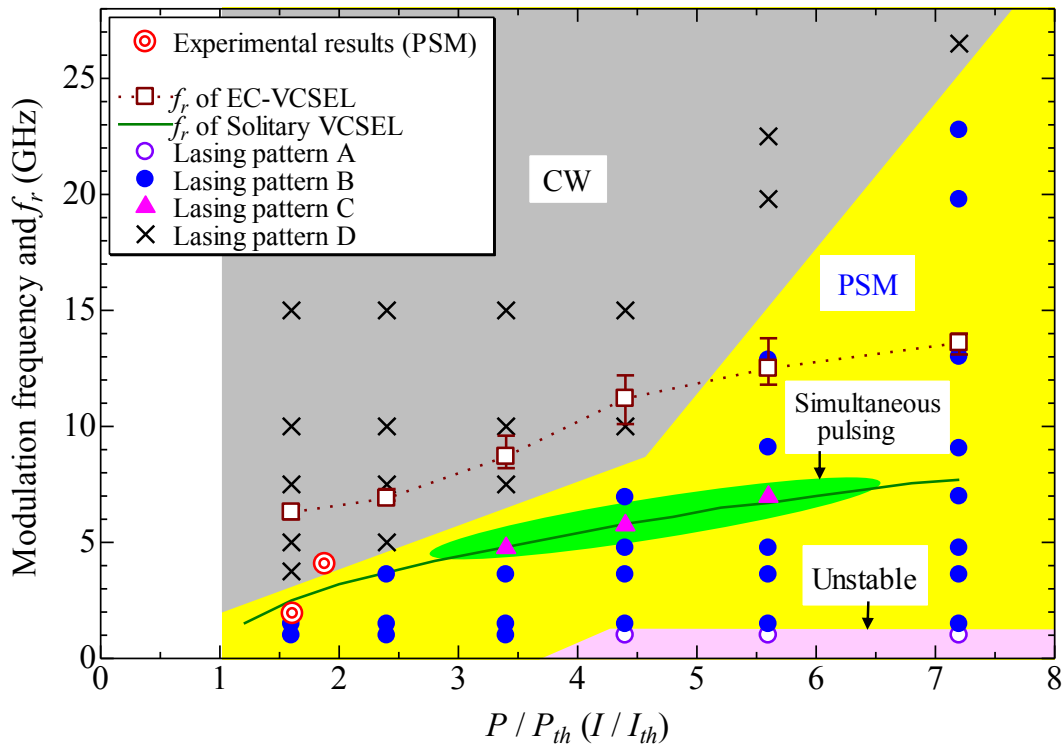


Fig. 5.16. Comparison between the simulation results ($R_3 = 0.08$) and the experimental results shown in Chapter 3. PSM: polarization self-modulation, f_r : relaxation oscillation frequency.

We summarize all the modulation frequencies, which we observed both in the experiments and the simulation, in Fig. 5.17. The experimental results shown in Fig. 5.17 (a) are divided into three regions depending on the modulation mechanism. The yellow region is for polarization self-modulation (longer L), the blue region is for unstable transition range (medium length L), and the green region is for the beat note between two EC modes (shorter L). The positions of the concave mirrors and semi-spherical mirrors were adjusted by micrometers while checking the lasing threshold reduction of the VCSEL in the experiments. Based on the alignment tolerance of these mirrors, the error bar of the EC length were set to be ± 0.3 mm. Fig.

5.17 (b) shows the frequencies of polarization self-modulation obtained in the simulation. The two black lines show the modulation frequencies calculated from $f = c/4L$.

The modulation frequency in Fig. 5.17 changes with L , which indicates that the modulation frequency is mainly determined by L . In the region of polarization self-modulation (yellow) in the experiments, the modulation frequencies are nearly the same to the calculated f , which coincides with the results with long L in the simulation. However, with the shortening of L , modulation frequencies in both the experimental and simulation results lower become lower than the calculated frequencies $f = c/4L$, especially when $L < 5$ mm. In this region, the experimental results show the same tendency with the simulation results, even though the output modulation were caused by the beat note of two EC modes. Choquette et al. also observed the same phenomenon that the modulation frequency becomes lower than that of $f = c/4L$, when L is short both in the experiment and simulation [3]. The reason is not clear now.

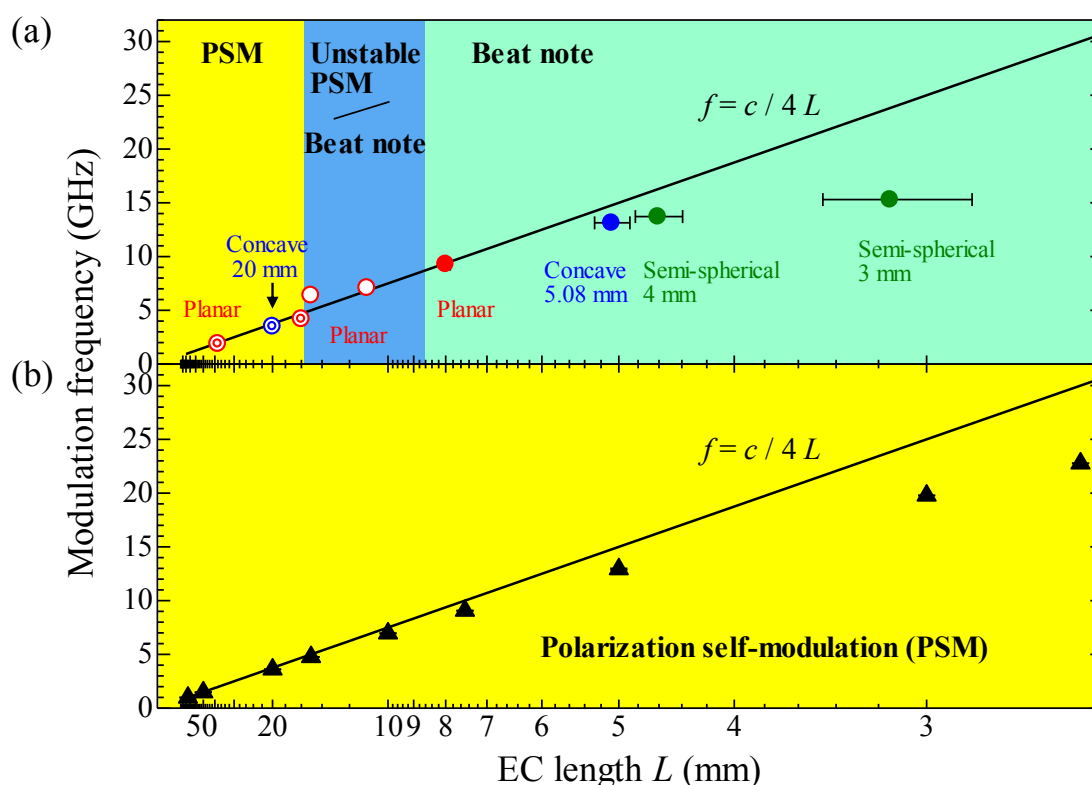


Fig. 5.17. The modulation frequencies of optical output obtained in (a) experiments and (b) simulation.

When there is an EC, the lasing threshold current I_{th} decreases, compared with the solitary VCSEL. In the experiments, we used five different mirrors for the EC with reflectivity of 50% or 60%, which were higher than those used in the simulation 3~20%. The reflectivity difference in the experiment and simulation is caused by the coupling efficiency of the feedback by external mirror to the VCSEL, because the coupling efficiency of the feedback light to the VCSEL cavity was set to be 100% in the simulation. To check the coupling efficiency of optical feedback to the VCSEL in the experiments, we evaluated the reduction of the lasing threshold current (ΔI_{th}) as shown in Table 5.4. The lasing threshold currents were decreased by ~20%

using different mirrors for the EC.

Table 5.4. Decrement of VCSEL lasing threshold ΔI_{th} using different mirrors in the experiments

Mirror for EC	Reflectivity	VCSEL	Solitary I_{th}	ΔI_{th} (mA)	ΔI_{th} (%)
Planar	50%	#932208	3.0 mA	0.5~0.6 mA	17~20%
Concave $r = 20$ mm	50%	#10312309	2.6 mA	0.7 mA	27%
Concave $r = 5.08$ mm	60%	#932208	3.0 mA	0.7 mA	23%
Semi-spherical $r = 4$ mm	60%	#932208	3.0 mA	0.6 mA	20%
Semi-spherical $r = 3$ mm	60%	#932208	3.0 mA	0.5 mA	17%

We investigated the reduction of lasing threshold carrier pump rate (ΔP_{th}) by changing the reflectivity of external mirror R_3 in our EC-VCSEL simulation model. The calculated results are shown in Fig. 5.18. ΔP_{th} was 16% and 24% when $R_3 = 0.01$ and 0.03 , respectively. Comparing the results in Table 5.4 and Fig. 5.18, it is found that the ΔI_{th} in the experiments corresponds to the ΔP_{th} for $R_3 = 0.02\sim 0.03$ in the simulation, which are only 4~5% of the reflectivity of the mirrors used in the experiments (50% or 60%). That is to say, 4~5% of the reflected light from the external mirrors were coupled back into the VCSEL cavity in the experiments. This coupling efficiency is similar to that in Ref. [14]. If we improve the coupling efficiency of the feedback from the external mirrors, pulse generation will be possible using mirrors with lower reflectivity and we can get higher output power from the EC-VCSEL.

Polarization self-modulations with higher frequencies can also be generated at the same currents that we used in the experiments.

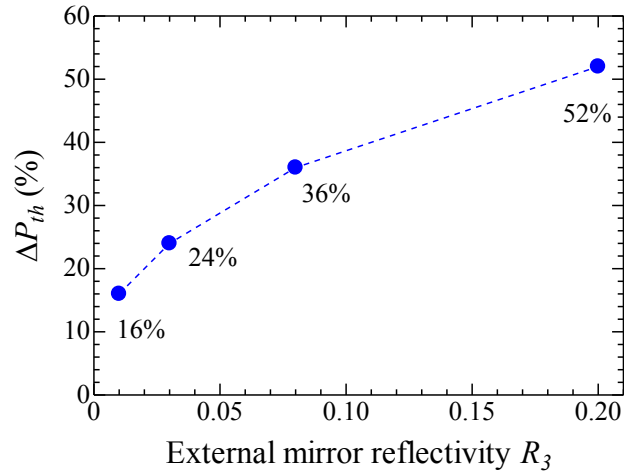


Fig. 5.18. Reduction of VCSEL lasing threshold carrier pump ΔP_{th} in the simulation.

5.6 Conclusion

In this chapter, numerical calculations and analysis using two-mode rate equations were carried out to systematically investigate the polarization self-modulation in the EC-VCSEL.

In the investigation of the effect of gain saturation coefficients of the VCSEL, we found that VCSELs with $\varepsilon_{XX,YY} : \varepsilon_{XY,YX} = 1:2$ is suitable for generation of high repetition frequency pulses by polarization self-modulation than those with $\varepsilon_{XX,YY} : \varepsilon_{XY,YX} = 1:1$. For both cases, when L is long, the waveforms of the pulses are close to square waves and the waveforms

change from square to sinusoidallike with the shortening of L . However, the waveforms of the pulses were closer to square waves even for short L in the case of VCSELs with $\varepsilon_{XX,YY} : \varepsilon_{XY,YX} = 1:2$. In the discussion on the effect of optical feedback intensity R_3 , it was clarified that the polarization self-modulation with higher frequency became possible with stronger feedback. The results of pulse generation at different P showed that higher frequency polarization self-modulation in EC-VCSELs is possible by increasing the carrier pump rate P .

In the comparison between the results of simulation and experiments, we clarified that at low carrier pump rate P (or current), the highest frequency of polarization self-modulation operation is limited by f_r of the solitary VCSEL. At around f_r , the polarization self-modulation and the relaxation oscillation were simultaneously generated.

We concluded from both the experiments and the simulation that the frequency of polarization self-modulation is determined by L ($f = c/4L$), when L is long.

5.7 References

- [1] M. San Miguel, Q. Feng, and J. V. Moloney, "Light-polarization dynamics in surface-emitting semiconductor lasers," *Phys. Rev. A*, vol. 52, no. 2, pp. 1728-1739, 1995.
- [2] R. Lang, and K. Kobayashi, "External optical feedback effects on semiconductor injection laser properties," *IEEE J. Quantum Electron.*, vol. QE-16, no. 3, pp. 347-355, 1980.

- [3] H. Li, A. Hohl, A. Gavrielides, H. Hou, and K. D. Choquette, "Stable polarization self-modulation in vertical-cavity surface-emitting lasers," *Appl. Phys. Lett.*, vol. 72, no. 19, pp. 2355-2357, 1998.
- [4] F. Robert, P. Besnard, M. L. Chares, and G. M. Stephan, "Polarization modulation dynamics of vertical-cavity surface-emitting lasers with an extended cavity," *IEEE J. Quantum Electron.*, vol. 33, no. 12, pp. 2231-2239, 1997.
- [5] C. Masoller, and N. B. Abraham, "Polarization dynamics in vertical-cavity surface-emitting lasers with optical feedback through a quarter-wave plate," *Appl. Phys. Lett.*, vol. 74, no. 8, pp. 1078-1080, 1999.
- [6] D. W. Sukow, T. Gilfillan, B. Pope, M. S. Torre, A. Gavrielides, and C. Masoller, "Square-wave switching in vertical-cavity surface-emitting lasers with polarization-rotated optical feedback: experiments and simulations," *Phys. Rev. A*, vol. 86, no. 3, 033818, 2012.
- [7] T. Erneus, A. Gavrielides, and M. Sciamanna, "Stable microwave oscillations due to external-cavity-mode beating in laser diodes subject to optical feedback," *Phys. Rev. A*, vol. 66, no. 3, 033809, 2002.
- [8] Y.-H Hong, R. Ju, P. S. Spencer, and K. A. Shore, "Investigation of polarization bistability in vertical-cavity surface-emitting lasers subjected to optical feedback," *IEEE J. Quantum Electron.*, vol. 41, no. 5, pp. 619-624, 2005.
- [9] J. Sakaguchi, T. Katayama, and H. Kawaguchi, "High switching-speed operation of optical

- memory based on polarization bistable vertical-cavity surface-emitting laser,” *IEEE J. Quantum Electron.*, vol. 46, no. 11, pp. 1526-1534, 2010.
- [10] Y. Takahashi, and H. Kawaguchi, “Polarization-dependent gain saturations in quantum-well lasers,” *IEEE J. Quantum Electron.*, vol. 37, no. 7, pp. 864-871, 2000.
- [11] C. L. Tang, A. Schremer, and T. Fujita, “Bistability in two-mode semiconductor lasers via gain saturation,” *Appl. Phys. Lett.*, vol. 51, no. 18, pp. 1392-1394, 1987.
- [12] S. Wieczorek, B. Krauskopf, T.B. Simpson, and D. Lenstra, “The dynamical complexity of optically injected semiconductor lasers,” *Phys. Rep.*, vol. 416, no. 1-2, pp. 1-128, 2005.
- [13] A. Yariv, and P. Yen, *Photonics: optical electronics in modern communications*, 6th edition, Oxford University Press, New York, 2007.
- [14] C. J. Smith, W.-D. Li, G. Wysocki, and S. Y. Chou, “Electric current tuning the self-oscillation frequency of EC-VCSELs,” *IEEE Photon. Technol. Lett.*, vol. 25, no. 17, pp. 1707-1710, 2013.

Chapter 6 Summary and Outlook

6.1 Summary

This research aims at high-repetition-frequency optical pulse generation by self-modulation in EC-VCSEL. This all-optical pulse generation method has the advantages of low power consumption, low cost, and high speed. We investigated the pulse generation both experimentally and numerically and obtained the results as follows:

In the experiments using different mirrors for the EC:

1. Using a planar mirror, we investigated the self-modulation in EC-VCSEL with different L . With shortening of L , the mechanism of output modulation changed from polarization self-modulation to the beat note between two modes.
2. We obtained optical pulses by polarization self-modulation with frequencies of up to 4 GHz.
3. Using a concave mirror with a radius of 5.08 mm and a thin-film QWP, we observed sinusoidal output modulations with frequencies of about 12 GHz. Through detailed measurements of the optical output, we clarified that the output modulations in this case were due to the beat note between two EC modes with similar polarizations.
4. For the output modulations due to beat note of two EC modes, the wavelength and

polarization of the EC-VCSEL output were determined by the mode competition between the EC and the VCSEL cavity.

5. For further shortening of the EC, we used semi-spherical mirrors. High-frequency modulations up to 15.3 GHz were obtained by the beat note of two EC modes.

In the numerical investigation of polarization self-modulation using two-mode rate equations:

6. Through the comparison of pulse generation using VCSELs with different gain saturation coefficients $\varepsilon_{XX,YY} : \varepsilon_{XY,YX} = 1:2$ and $\varepsilon_{XX,YY} : \varepsilon_{XY,YX} = 1:1$, we found that VCSELs with stronger cross-gain saturation effects are suitable for the high-repetition-frequency optical pulse generation by polarization self-modulation.
7. Higher-repetition-frequency optical pulse generation may be possible with stronger optical feedback or higher carrier pump rate.
8. Through the comparison with our experimental results, we found that in the low carrier pump rate region where $P/P_{th} < 4$, the highest frequency of polarization self-modulation in the EC-VCSEL is limited by the relaxation oscillation frequency of the solitary VCSEL.

In conclusion, we experimentally investigated the pulse generation by self-modulation in EC-VCSEL using different types of mirrors and a thin-film QWP. We clarified that the output modulation mechanism changed from polarization self-modulation to the beat note between

two EC modes with similar polarizations when EC was shortened, and the mechanism change was not depend on the types of mirrors. Through the comparison with the simulation results, we found that in the low carrier pump region the highest frequency of polarization self-modulation is limited by the relaxation oscillation frequency of the solitary VCSEL. The results also showed us that generation of higher frequency optical pulses by polarization self-modulation is possible by using VCSELs with lower threshold currents.

6.2 Outlook

As described in Sec. 5.5, to get higher-repetition-frequency optical pulses by polarization self-modulation, f_r of the solitary VCSEL should be increased. Using a low Q factor VCSEL with low reflectivity DBR on the output side, a shorter photon lifetime [1] and a higher injection rate of the feedback light can be realized at the same time. Lau et al. [2] reported that the resonance frequency of VCSELs can be greatly enhanced by injection locking. Fig. 6.1 shows the proposed experimental setup for the external injection light to increase f_r of the solitary VCSEL. To improve the stability of the optical pulse, the LD mount and the mirror mount are mounted on one motorized stage. For precise alignment of the tilt angle and the position of the mirror and the thin-film QWP, the mirror mount is electrically controlled. A collimating lens with short focal length is used to decrease its limitation to the shortening of EC length. Using

the experimental setup in Fig. 6.1, higher-frequency stable polarization self-modulation will be possible and the waveform of the generated pulses can be closer to square wave which is preferable in optical signal processing.

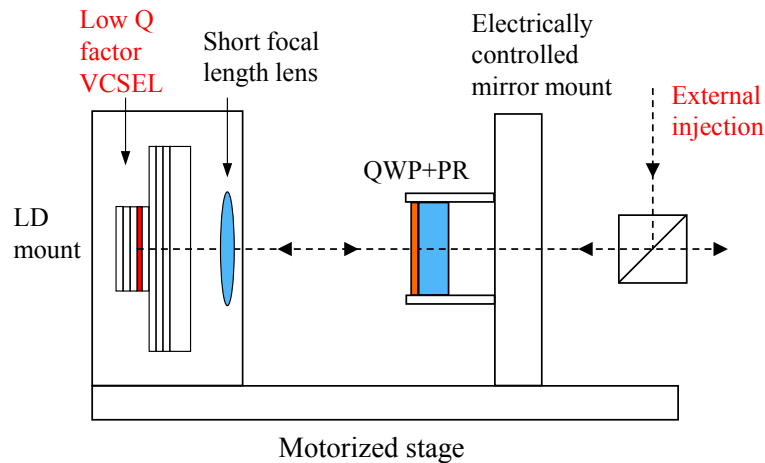


Fig. 6.1. Experimental setup for higher-frequency and stable polarization self-modulation.

For further shortening of the EC length, we proposed several different methods as follows:

- (a) Use semi-spherical mirrors that fabricated from much smaller radius ball lenses for the EC.
 - (b) Apply reflection coating on the input surface of the optical fiber and couple the VCSEL output directly into the fiber.
 - (c) Integrate a VCSEL and a QWP with pairs of DBR, which can work as the external reflection mirror.
- Fig. 6.2 shows the schematic of an integrated EC-VCSEL. DBRs with several pairs are used as the EC partial reflector (EC-PR). The intracavity QWP is fixed below the EC-PR. The EC length is precisely changed by adjusting the height of the cantilever using the voltage source for repetition frequency control. There will be many other different methods to shorten the EC. Note that at frequencies above f_r of solitary VCSEL, the

output modulation output will be caused by the beat note of EC modes. In that case, a wider bandwidth of the gain spectrum of the VCSEL becomes essential because the EC modes must have enough gain.

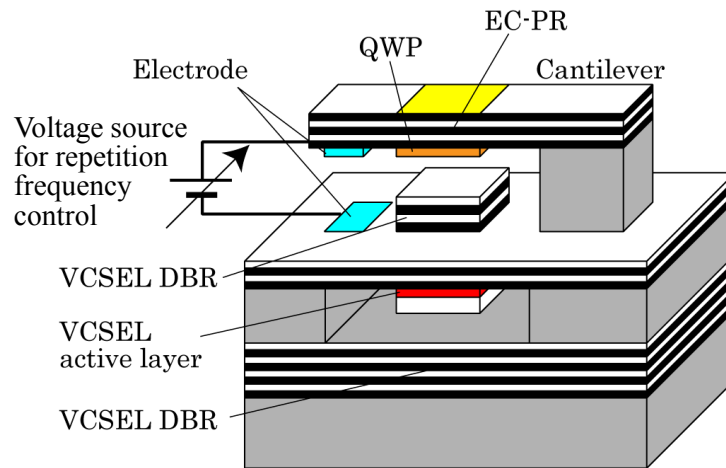


Fig. 6.2. Schematic of integrated EC-VCSEL.

In the future, the high-frequency optical pulse signals generated using this all-optical and frequency-variable method are expected to be used in many fields, such as optical communication, time-keeping, metrology, and sensing. Here we briefly discuss the application of optical pulses in 3R signal regeneration as an example. As described in the background in Sec. 1.1, the rapid growth of internet traffic has called for the development of all-optical communication networks. We propose an all-optical 3R signal regeneration system using two polarization-bistable VCSELs as the key device. Pulse generation by polarization self-modulation has an advantage that two complementary optical pulse sequences polarized at 0° and 90° can be generated simultaneously. As shown in Fig. 6.3, the proposed system is

composed of two parts, an all-optical pulse generator and an all-optical retiming circuit.

Polarization self-modulation of the EC-VCSEL#1 generates optical pulse signals, in both 0° and 90° polarizations. The optical pulse signals will be used as set and reset signal in the retiming circuit. VCSEL#2 works as an AND gate here. As shown in the timing chart in Fig. 6.4, by adjusting of the timing and intensities of the optical clock signals and the degraded external signal, the lasing polarization of VCSEL#2 is switched, only when the total power exceeds the switching threshold. After going through the polarizer, the output signal of VCSEL#2 will have the same information as the original signal, and 3R signal regeneration can be realized at the same time. The high-repetition-frequency optical pulses generated by the beat note of the EC modes can also be used in this system after the processing of beam splitting, polarization rotation and time delay. In the future, the EC-VCSEL will be expected to supply the fast and frequency-variable optical clock signals, which is essential for 3R signal regeneration. This research contributes to the acceleration of the all-optical 3R signal regeneration system.

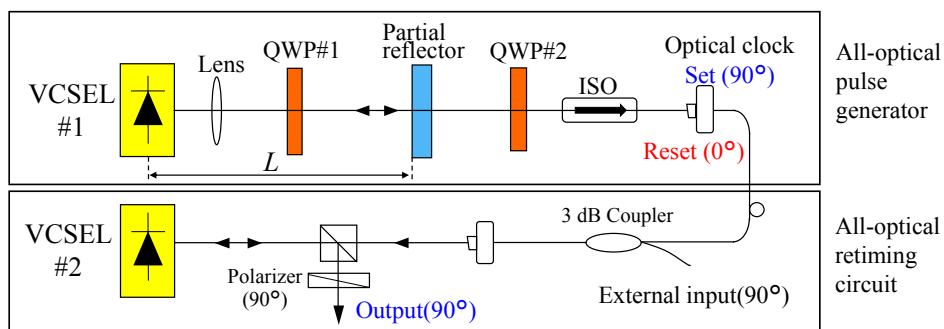


Fig. 6.3. All-optical signal regeneration system.

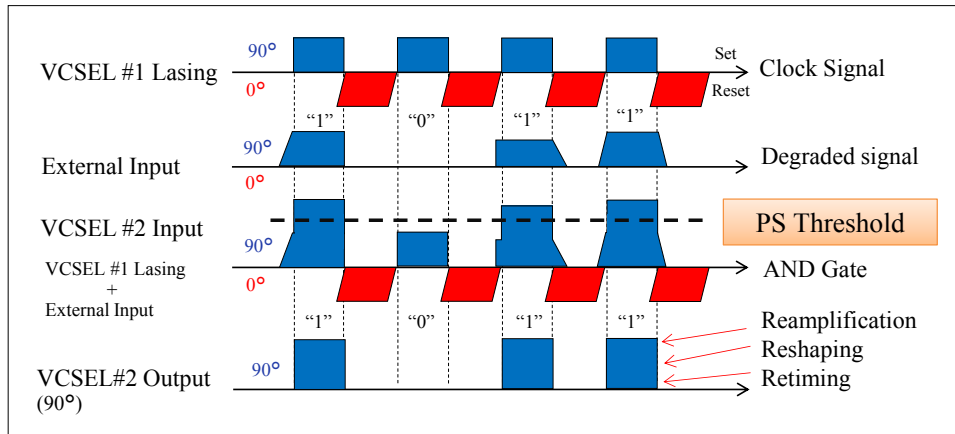


Fig. 6.4. All-optical 3R signal regeneration process. PS: polarization switching.

6.3 References

- [1] J. Sakaguchi, T. Katayama, and H. Kawaguchi, "High switching-speed operation of optical memory based on polarization bistable vertical-cavity surface-emitting laser," *IEEE J. Quantum Electron.*, vol. 46, no. 11, pp. 1526-1534, 2010.
- [2] E. K. Lau, X. Zhao, H. K. Sung, D. Parekh, C. Chang-Hasnain, and M. C. Wu, "Strong optical injection-locked semiconductor lasers demonstrating >100-GHz resonance frequencies and 80-GHz intrinsic bandwidths," *Opt. Express*, vol. 16, no. 9, pp. 6609-6618, 2008.

Acknowledgment

The research could not have been accomplished without the collaboration of many people, to whom I wish to express my greatest gratitude.

First and foremost I sincerely thank my academic supervisor Prof. Hitoshi Kawaguchi. It has been an honor to be his student. I appreciate all his contributions of time, ideas, and funding to make my study experience productive and stimulating. The enthusiasm he has for his research was contagious and motivational for me.

I would like to express my appreciation to Prof. Hisao Yanagi for his useful and insightful advice and encouragement, especially for his help on the matters related to my graduation.

I would like to thank Prof. Kiyomi Kakiuchi for taking care of my research related matters in the last half year.

I would like to thank Prof. Yukiharu Uraoka and Assoc. Prof. Takashi Tokuda, for their valuable and insightful comments and discussion, which were of great help on the fulfillment of this research.

A special thanks to Assist. Prof. Takeo Katayama who gave me guidance and support throughout my doctoral study, from the learning of instruments to the discussion and presentation of the results. I also got great help on Japanese language learning and daily life.

I would like to thank Dr. Kazuhiro Ikeda who has been an assistant professor in our lab for his help and encouragement on my research and life in the first two years of my study here.

I would like to thank Dr. S. Hattori from Mitsuboshi Diamond Industrial Co., LTD. for his help on the processing of the concave mirrors and the fabrication of the semi-spherical mirrors.

I would like to thank Dr. Daisuke Hayashi, who has been a post-doctoral researcher in our lab for his discussions and advices on my experiments and job hunting.

The members of the Kawaguchi lab have contributed immensely to my personal and professional time at NAIST. The group has been a source of friendships as well as good advice and collaboration. As a foreigner in Japan, I am grateful to the laboratory members: Dr. Yoshihiro Tsunemi, Dr. Nobuhide Yokota, and Mr. Masashi Kawabata et al. for their help on my research and life.

Finally, I would like to thank my beloved family, especially my wife for their support and encouragement throughout my doctoral study.

List of Publications

1. Academic journals

- [1] Tao Liu, Takeo Katayama, and Hitoshi Kawaguchi, “High-Frequency Self-modulation in Short-External-Cavity VCSEL with Concave Mirror,” *IEEE Photon. Technol. Lett.*, vol. 27, no. 3, pp. 280-283, Feb. 2015.

2. International conference

- [1] Tao Liu, Takeo Katayama, Hitoshi Kawaguchi, “Research on High Speed All-Optical Signal Regeneration System Using Polarization Bistable VCSELs,” The GIST-NAIST-NCTU Symposium, Nara, Japan, Nov. 21, 2013.
- [2] Tao Liu, Takeo Katayama, Hitoshi Kawaguchi, “High-Frequency Self-Modulation in Short-External-Cavity VCSEL with Semi-Spherical Mirror,” CLEO-PR, 26J1-2, Aug. 26, 2015.

3. Domestic conferences

- [1] 劉 濤, 片山 健夫, 河口 仁司, “凹面鏡外部共振器 VCSEL の高速偏光自己変調,” 2014 年電子情報通信学会総合大会, C-4-30, 新潟, 2014 年 3 月 20 日.
- [2] 劉 濤, 片山 健夫, 河口 仁司, “凹面鏡外部共振器 VCSEL による高速光パルス発生,” 2014 年電子情報通信学会ソサイエティ大会, C-4-25, 徳島, 2014 年 9 月 24 日.